EXPERIMENTAL APPARATUS

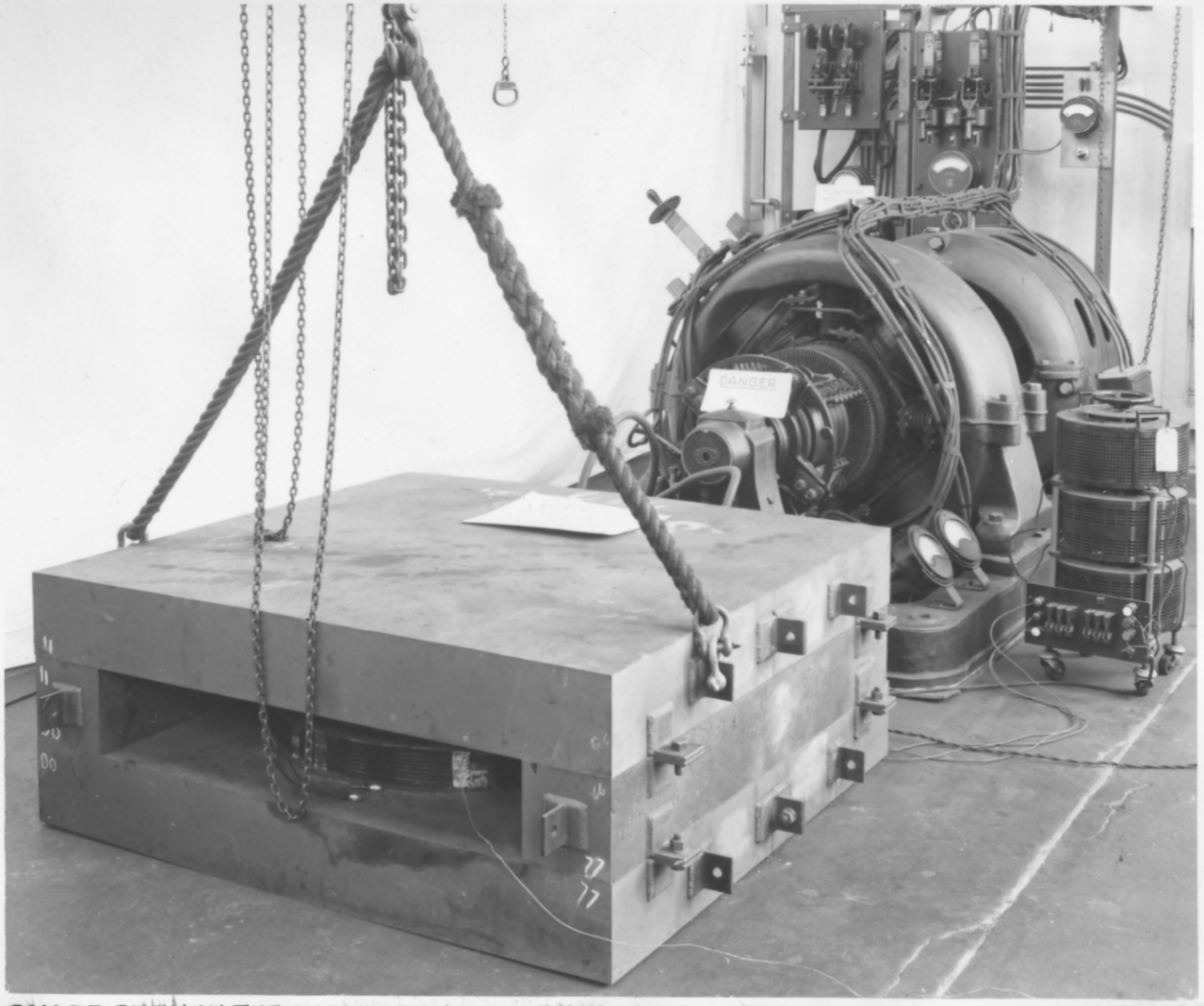

THE MAGNET CAN BE SEEN IN THE FOREGROUND, AND SOME OF THE LEADS TO THE SODIUM CONTAINER ENCLOSED IN IT. IN THE BACKGROUND CAN BE SEEN THE GENERATING SET, AND ON THE RIGHT THE TRANSFORMERS CONTROLLING THE HEATING OF THE SODIUM.

MAGNETOHYDRODYNAMIC WAVES

by

Antony Jameson.

SUMMARY.

The idea of magnetohydrodynamic waves was introduced by Alfven in 1942 and these waves have been postulated as the basis of various cosmic phenomena such as sunspots and magnetic variable stars. However, there has been a lack of any convincing experimental demonstration of the waves. Experiments with gases involved other interactions, and the only experiments with liquids, by Lundquist and later, under more favourable conditions, by Lehnert, failed to produce any really wavelike behaviour.

In this thesis the equations governing magnetohydrodynamic waves are examined in detail. Chapter 3 treats steady state situations. The effects of damping both by electric resistivity and by viscosity are taken into account. The presence of terms representing these raises the order of the equations so that the solution for a one-dimensional system has two modes, only one of which is wavelike, but either of which may be the more important. The solutions for two-dimensional and axisymmetric systems are obtained as eigenfunction series, in which the two modes are represented in the coefficient of each term. It is found that side wall

damping will dominate the situation if the fluid region is too narrow. It was this which prevented Lehnert from producing waves. Chapter 4 treats transient situations. The solution is found as a Laplace transform which can be inverted as a series quite simply if either viscous or resistive damping is absent, or if the two are equal. In these cases the same solutions can also be obtained directly as eigenfunction series.

On the basis of the theory developed it appeared that using the best available liquid conductor, sodium, with a field of .5 to 1.0 weber/m^2, and provided that the fluid region was not only about 15 cm deep but also quite wide, it should be possible to demonstrate convincing resonant phenomena in steady state situations, and propagation and reflection of transient waves. Chapter 5 describes experiments fulfilling these conditions in which resonant magnification of the transverse field by as much as 9 times at the centre of the fluid region was observed, and in which transient waves were seen to propagate through the sodium depth a number of times, being reflected back and forth.

PREFACE.

The work described in this thesis was done in the Department of Engineering at Cambridge between 1958 and 1961. I am indebted to Dr. J.A. Shercliff and Dr. M.D. Cowley for many useful discussions, and to Mr. G.E. Middleton for valuable advice on the design of the magnet. I am indebted also to the laboratory and workshop staff of the Department for their help with the apparatus. The work was financed by means of a contract with the U.K. Atomic Energy Authority, and the Atomic Energy Research Establishment, Harwell, assisted in the construction of apparatus. In particular my thanks are due to Mr. D.S. Lacey for supervising the construction at Harwell of the sodium container. During the first two years I received a maintenance grant from the Department of Scientific and Industrial Research.

The introductory sections as far as 2.2 are not original. The analysis in 3.2 and 3.3 had as its starting point an unpublished analysis by Dr. J.A. Shercliff. Section 3.6 is not original. The operation, described in 5.2, of filling the sodium container was directed by Mr. D.S. Lacey. Otherwise the work is original.

None of the thesis has been submitted at any other university.

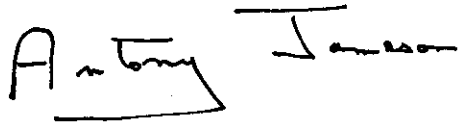

Trinity Hall. December, 1961.

CONTENTS

NOTATION.

Notation for general analysis:

t	time.
$\underline{E}$	electric field.
$\underline{B}$	magnetic field.
q	charge density.
$\underline{j}$	current density.
μ	magnetic constant.
ϵ	electric constant.
τ	resistivity.
$\lambda = \frac{\tau}{\mu}$	electric diffusivity.
$\underline{u}$	velocity.
p	pressure.
ρ	density.
ν	viscous diffusivity.

Notation for wave equations:

x,y,z or x,y,ϕ	coordinates.
B_0	fixed x component of $\underline{B}$.
B_1, u	variable z or ϕ components of $\underline{B}$, u.
$c = \frac{B_0}{(\mu\rho)^{\frac{1}{2}}}$	wave speed.
$h = \frac{B_1}{(\mu\rho)^{\frac{1}{2}}}$	
d	typical length.
$T = \frac{tc}{d}$	dimensionless time.

$X = \frac{x}{d}$, $Y = \frac{y}{d}$ dimensionless coordinates.

$\Lambda = \frac{\lambda}{cd}$, $\mathcal{N} = \frac{\nu}{cd}$ dimensionless damping parameters.

Notation for a one-dimensional system in a steady state:

d	half depth.
p	frequency.
$P = \frac{pd}{c}$	dimensionless frequency.
H, U	phasor representations of h, u.
k_1, k_2	roots for the two modes.
$K_1 = k_1 d$, $K_2 = k_2 d$	dimensionless roots.
r_1, r_2	multipliers for the two modes.
$Q = \frac{cd}{(\lambda\nu)^{\frac{1}{2}}} = \frac{1}{(\Lambda\mathcal{N})^{\frac{1}{2}}}$	
$\gamma = (\frac{\nu}{\lambda})^{\frac{1}{2}} = (\frac{\mathcal{N}}{\Lambda})^{\frac{1}{2}}$	
$\theta = \frac{(\lambda+\nu)p}{2c^2} = \frac{(\Lambda+\mathcal{N})P}{2}$	
I	power intake.
D	power dissipation.

Notation for a plane or cylindrical system in a steady state:

d, e	half depth, half width.
$E = \frac{e}{d}$	
y_1, y_2	inner radius, outer radius.
$C = \frac{y_2}{y_1}$	
$\mathfrak{D}(x)$, $\mathfrak{E}(y)$	eigenfunctions.

m, n	eigenvalues.
M, N	dimensionless eigenvalues.
$\bar{f}$	term in expansion of f.

$$L = \frac{J_1(ny_1)}{J_1(ny_2)} = \frac{Y_1(ny_1)}{Y_1(ny_2)}$$

$I = 1$ or $\frac{y_1}{y}$	boundary value.

$$Z = N - 1$$

For each term of the expansion the notation follows the one-dimensional analysis with in addition:

a	multiplier for each term.

$$\beta = \frac{(\lambda+\nu)n^2}{2p} = \frac{(\Lambda+\nu)N^2}{2P}$$

Notation for systems with conducting walls:

The notation follows the earlier notation with:

Suffices a,b	fluid and walls.
k, j	roots for fluid and walls.
a, b	multipliers for fluid and walls in eigenfunction expansions.
s	ratio deriving from the boundary condition for $\bar{f}$.

Notation for a one-dimensional system in a transient situation:

p	variable for Laplace transformation.
$\bar{f}$	Laplace transform of f.
$z = h - l$	

Otherwise the notation follows the notation for the steady state analysis except:

$$a = \frac{\lambda m^2}{2}$$

$$b = (c^2 m^2 - a^2)^{\frac{1}{2}}$$

$$\theta = \sin^{-1} \frac{\lambda m}{2c} = \sin^{-1} \frac{\Lambda M}{2}$$

Notation for a plane or cylindrical system in a transient situation:

The notation follows the notation for a one-dimensional system in a transient state with the same notation for expansion in eigenfunctions as was used for a plane or cylindrical system in a steady state.

REFERENCES.

1.	H. Alfven.	Arkiv Mat.Astron.Fysic., 29, 1942.
2.	S. Lundquist.	Phys.Rev., 76, 1949.
3.	B. Lehnert.	Phys.Rev., 94, 1954.
4.	H. Alfven.	Cosmical Electrodynamics, Oxford, 1950.
5.	T.G. Cowling.	Magnetohydrodynamics, Interscience, 1947.
6.	R. Courant and D. Hilbert.	Methods of Mathematical Physics, Volume I, Interscience, 1953.
7.	E.C. Titchmarsh.	Eigenfunction Expansions, Parts 1 and 2, Oxford, 1946 and 1958.
8.	H.S. Carslaw and J.C. Jaeger.	Conduction of Heat in Solids, Oxford, 1947.
9.	H.S. Carslaw and J.C. Jaeger.	Operational Methods in Applied Mathematics, Oxford, 1941.
10.	R.N. Lyon (Ed.).	Liquid Metals Handbook, Office of Naval Research, U.S.A.
11.	A.E. Knowlton (Ed.)	Standard Handbook for Electrical Engineers, McGraw Hill, 1949.
12.	F.W. Carter.	Journal Inst.El.Eng., 29, 1900.

References are given in the text by means of raised numbers.

CHAPTER 1.

PROLOGUE.

1.1 Magnetohydrodynamic waves.

The possibility of magnetohydrodynamic waves was first established by Alfven[1] in 1942. The stresses in a magnetic field can be resolved into a hydrostatic pressure $\frac{B^2}{2\mu}$ together with a tension $\frac{B^2}{\mu}$ along the lines of force. In an incompressible fluid the first can be balanced by the pressure of the fluid, leaving only the second. Also in a perfectly conducting fluid, motion of the fluid across the lines of force is prevented by the induced currents which such a motion would cause, so that the fluid and the lines of force move always together and we can think of the fluid mass as attached to the lines of force. These therefore are like stretched strings in which the ratio of tension to density is $\frac{B^2}{\mu\rho}$, and they are able to carry waves moving at a speed $\frac{B}{(\mu\rho)^{\frac{1}{2}}}$ like stretched strings. Such waves in a fluid which is not ideal will be damped by electric resistivity and viscosity. They can be generated by fluctuations in the fluid velocity at the boundaries caused by wall movement, or by fluctuations in the magnetic field at the boundaries caused by currents in conducting walls. These

currents can either be produced directly by application of a potential difference to walls insulated from the fluid, or induced by movement of the walls across the applied field.

1.2 Previous experiments.

There have been two attempts to produce these waves in liquids, the first by Lundquist[2], and the second by Lehnert[3]. There have also been some experiments with ionized gases. These are less suited to quantitative measurements, and here only waves in liquids will be discussed.

Lundquist used mercury in a cylindrical container, open at the top, figure 1.1. He oscillated a disc, ribbed to prevent loss of the motion by slip in a viscous boundary layer, at the bottom of the container, and measured the surface speeds at the top. At correct frequencies for a given field there should be resonance, and in an ideal undamped system the surface velocity should then tend to infinity. Because of the low conductivity of mercury he did not in fact succeed in obtaining any resonance at all.

In order to reduce the damping Lehnert used liquid sodium, which has five times the conductivity of mercury.

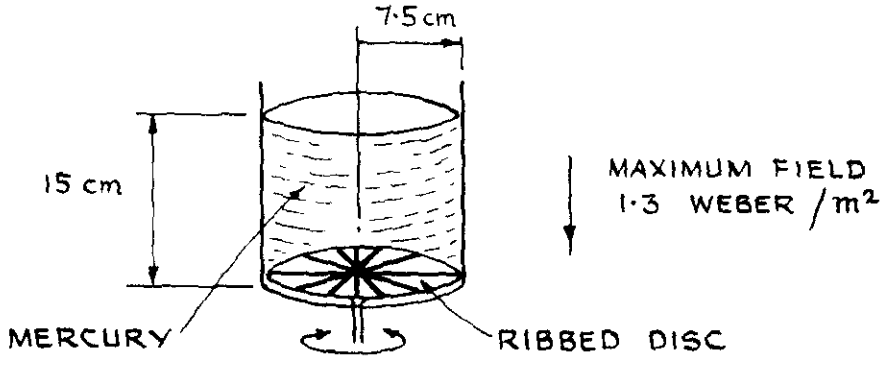

FIG. 1.1 LUNDQUIST'S EXPERIMENT.

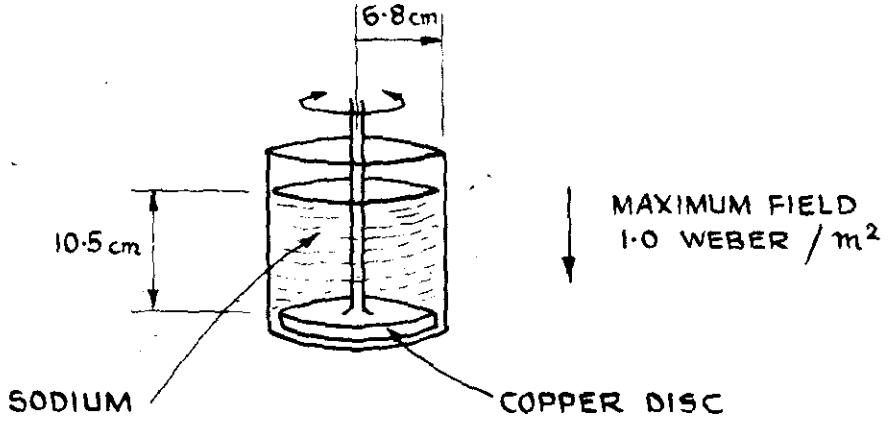

FIG. 1.2 LEHNERT'S EXPERIMENT.

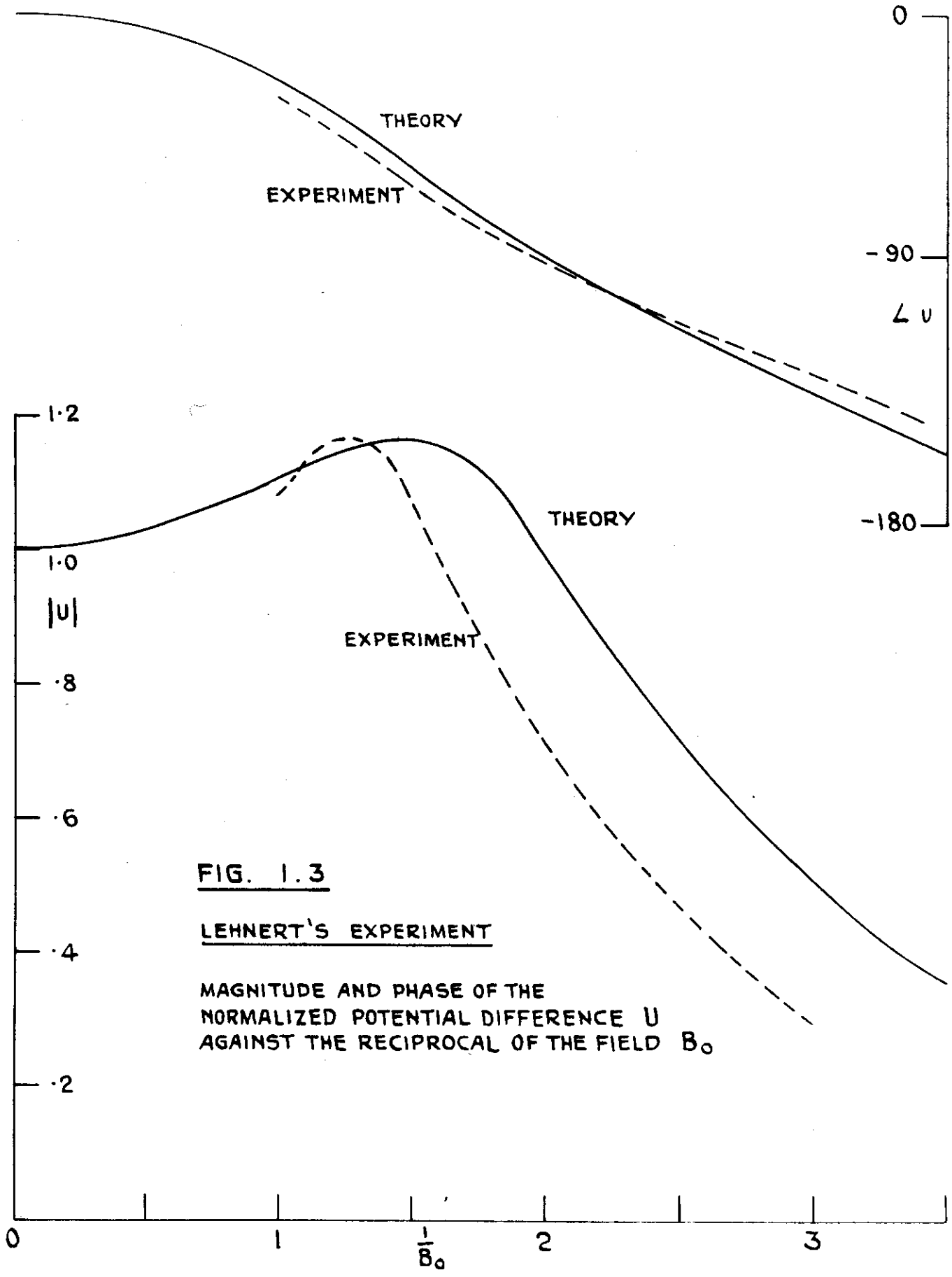

FIG. 1.3

LEHNERT'S EXPERIMENT

MAGNITUDE AND PHASE OF THE NORMALIZED POTENTIAL DIFFERENCE U AGAINST THE RECIPROCAL OF THE FIELD B_0

He also used a cylindrical container, open at the top, and oscillated a disc at the bottom, figure 1.2. But in this case the disc was of copper, and the excitation was chiefly by the induced currents flowing in it. He used a fixed frequency of 30 c/s and varied the field, and thus the resonant frequency of the system. He measured the potential difference between two probes on the surface induced by the fluid movement. His results are shown in figure 1.3. The maximum potential difference was only 1.15 times the potential difference at an infinite field intensity.

An examination of the wave equations makes it clear that the damping was chiefly due to the side walls. Lundquist[2] was aware of the importance of side wall damping, but Lehnert[3] makes no comment on it. Also by varying the field with the frequency fixed the field at resonance was only about half the maximum available field so that conditions for wave formation were not as favourable as they might have been.

1.3 The present work.

When the author joined the magnetohydrodynamics group at the Cambridge University Engineering Department

in 1952 there had thus been no experimental demonstration of well developed waves under controlled quantitative conditions, and a further investigation seemed worthwhile. In the present work, started after discussions with Dr. Shercliff, who was interested in the possibility of an experiment using electric excitation, the theoretical behaviour of the waves in both steady state and transient situations is analysed in Chapters 2-4. Chapter 5 discusses the design of an apparatus to produce quite well developed waves, and presents the results of steady state and transient experiments with such an apparatus.

CHAPTER 2.

PRELIMINARY THEORY.

2.1 The wave equations.

Derivations of the wave equations can be found in standard works[4,5]. The development for plane and axisymmetric systems is here summarized.

We start with the usual equations of magnetohydrodynamics, in which the electric force $q\,\underline{E}$ and the displacement current $\epsilon \frac{\partial \underline{E}}{\partial t}$ are assumed negligible. The equations for an incompressible fluid are then

$$\nabla \times \underline{E} = -\frac{\partial \underline{B}}{\partial t}$$

$$\nabla \cdot \underline{E} = \frac{q}{\epsilon}$$

$$\nabla \times \underline{B} = \mu \underline{j}$$

$$\nabla \cdot \underline{B} = 0$$

$$\tau \underline{j} = \underline{E} + \underline{u} \times \underline{B}$$

$$\frac{d\underline{u}}{dt} = \frac{\underline{j} \times \underline{B}}{\rho} - \frac{\nabla p}{\rho} + \nu \triangle \underline{u}$$

$$\nabla \cdot \underline{u} = 0$$

From these

$$\frac{\partial \underline{B}}{\partial t} = \nabla \times (\underline{u} \times \underline{B}) + \lambda \triangle \underline{B}$$

$$= \underline{B} \cdot \nabla \underline{u} - \underline{u} \cdot \nabla \underline{B} + \lambda \triangle \underline{B},$$

$$\lambda = \frac{\tau}{\mu}$$

$$\frac{\partial \underline{u}}{\partial t} + \underline{u} \cdot \nabla \underline{u} = \frac{1}{\mu\rho} (\nabla \times \underline{B}) \times \underline{B} - \frac{\nabla p}{\rho} + \nu \triangle \underline{u}$$

$$= \frac{1}{\mu\rho} \underline{B} \cdot \nabla \underline{B} - \frac{\nabla P}{\rho} + \nu \triangle \underline{u} ,$$

$$P = p + \frac{B^2}{2\mu}$$

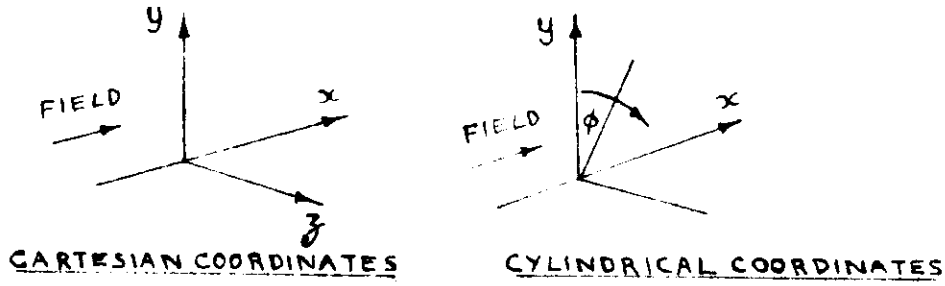

Fig.2.1

Take Cartesian coordinates x, y, z or cylindrical coordinates x, y, ϕ where ϕ is measured about the x axis, and assume either that the system does not vary in the z direction, or that it is axially symmetric about the x axis. Assume also that the only components of $\underline{B}$ and $\underline{u}$ which are not zero are a fixed x component of $\underline{B}$, B_0, and variable z or ϕ components of $\underline{B}$ and $\underline{u}$, B_1 and u. Then in the first case the equations reduce to

$$(\frac{\partial}{\partial t} - \lambda \triangle) B_1 = B_0 \frac{\partial u}{\partial x}$$

$$(\frac{\partial}{\partial t} - \nu \triangle) u = \frac{B_0}{\mu\rho} \frac{\partial B_1}{\partial x}$$

$$\frac{\partial P}{\partial x} = 0$$

$$\frac{\partial P}{\partial y} = 0$$

while in the second case they reduce to the same first three equations but with

$$\frac{B_1^2}{4\pi\rho y} + \frac{\partial P}{\partial y} = \frac{u^2}{y} .$$

In the second case differentiating the last two of the four equations with respect to y and x gives

$$\frac{\partial}{\partial x}\left(\frac{u^2 - \frac{B_1^2}{4\pi\rho}}{y}\right) = 0 .$$

This does not necessarily hold for a solution of the first two equations. Our assumption that it is possible for the x and y components of $\underline{B}$ and $\underline{u}$ to vanish is thus not valid, but if we assume B_1 and u are small enough for their squares to be neglected a solution of the first two equations still represents a good approximation of the true situation. When $\lambda = \nu = 0$ these two equations become the classical wave equations for a wave speed

$$c = \frac{B_0}{(4\pi\rho)^{\frac{1}{2}}}$$

If we replace B_1 by

$$h = \frac{B_1}{(4\pi\rho)^{\frac{1}{2}}}$$

so that both variables have the dimensions of velocity, the pair appears in the more symmetric form

$$(\frac{\partial}{\partial t} - \lambda\Delta)h = c\frac{\partial u}{\partial x}$$

$$(\frac{\partial}{\partial t} - \nu\Delta)u = c\frac{\partial h}{\partial x}$$

2.2 Boundary conditions.

At a boundary between two resistive media of the same permeability and dielectric constant the tangential component of $\underline{E}$ and the tangential and normal components of $\underline{B}$ and $\underline{u}$ are continuous. The assumptions of 2.1 imply continuity of the normal components of $\underline{B}$ and $\underline{u}$, and since

$$\underline{E} = \tau\underline{j} - \underline{u} \times \underline{B}, \qquad \tau\underline{j} = \nabla \times \underline{B}$$

the remaining conditions are satisfied if on a wall $x = a$ if

$\lambda\frac{\partial h}{\partial x} + cu$, h and u are continuous

and on a wall $y = a$ if

$\lambda\frac{\partial h}{\partial y}$, h and u are continuous.

If one of the media is inviscid, there may be a discontinuity of u. If one of the media is a perfect conductor a current sheet may form with a discontinuity of h across it. If one of the media is a non conductor so that λ is infinite and $\underline{j}$ zero, the condition for $\underline{E}$ does not apply.

Finally we note that since

$$\nabla \times \underline{B} = \mu \underline{j}.$$

B_1 in a plane, or $y B_1$ in a cylindrical system is a stream function for μj, and therefore constant at a non-conducting surface.

2.3 Limiting cases.

When ν or $\lambda \to \infty$, Δu or $\Delta h \to 0$, since the other terms remain finite. But a function which satisfies Laplace's equation and is constant on the boundaries is constant everywhere, so that in these cases if u or h is constant on the boundaries, $\frac{\partial u}{\partial x}$ or $\frac{\partial h}{\partial x} \to 0$, and the equations reduce to

$$(\frac{\partial}{\partial t} - \lambda\Delta)h = 0$$

or

$$(\frac{\partial}{\partial t} - \nu\Delta)u = 0$$

The first of these is the equation for the skin effect in a conducting solid, the second the equation for a velocity boundary layer in a non-conducting liquid.

When ν or $\lambda = 0$ the equations

$$(\frac{\partial}{\partial t} - \lambda\Delta)h = c\frac{\partial u}{\partial x}$$

$$\frac{\partial u}{\partial t} = c\frac{\partial h}{\partial x}$$

or

$$\frac{\partial h}{\partial t} = c\frac{\partial u}{\partial x}$$

$$(\frac{\partial}{\partial t} - \nu\Delta)\, u = c\frac{\partial h}{\partial x}$$

reduce to

$$(\frac{\partial^2}{\partial t^2} - \lambda\frac{\partial}{\partial t}\Delta - c^2\frac{\partial^2}{\partial x^2})h = (\frac{\partial^2}{\partial t^2} - \lambda\frac{\partial}{\partial t}\Delta - c^2\frac{\partial^2}{\partial x^2})u = 0$$

or

$$(\frac{\partial^2}{\partial t^2} - \nu\frac{\partial}{\partial t}\Delta - c^2\frac{\partial^2}{\partial x^2})h = (\frac{\partial^2}{\partial t^2} - \nu\frac{\partial}{\partial t}\Delta - c^2\frac{\partial^2}{\partial x^2})u = 0$$

If we solve for h and u independently each from their own boundary conditions the equations connecting them could fail. But if $\nu = 0$ u is indeterminate at the boundary because free slip is possible, and if $\lambda = 0$ h is indeterminate at the boundary, because a current sheet can form along the wall — a current sheet across the field involves an infinite force density from the magnetic force $\underline{j} \times \underline{B}$, but at a wall slip would introduce an infinite viscous stress, so this is possible. In the first case we therefore solve for h and determine u from h, whereas in the second we solve for u and determine h from u.

2.4 Dimensionless form of the equations - damping terms.

If d is a typical length of the system the equations can be put in dimensionless form by the

substitutions

$$X = \frac{x}{d}\ ,\quad Y = \frac{y}{d}\ ,\quad T = \frac{to}{d}\ ,\quad \Lambda = \frac{\lambda}{od}\ ,\quad \mathcal{N} = \frac{\nu}{od}\ ,$$

capitals representing the dimensionless variables.

The transformed equations are

$$(\frac{\partial}{\partial T} - \Lambda\Delta)h = \frac{\partial u}{\partial X}$$

$$(\frac{\partial}{\partial T} - \mathcal{N}\Delta)u = \frac{\partial h}{\partial X}$$

At a boundary $X = A$

$\Lambda\frac{\partial h}{\partial X} + u$, h and u are continuous,

at a boundary $Y = A$

$\Lambda\frac{\partial h}{\partial Y}$, h and u are continuous.

The properties of a one dimensional system are thus entirely determined by the damping terms Λ and $\mathcal{N}$. Taking the original brackets $(\frac{\partial}{\partial t} - \lambda\Delta)h$ and $(\frac{\partial}{\partial t} - \nu\Delta)u$ with $\frac{d}{c}$ as the typical time, we see that they represent the ratios of the damping to the inertial terms in each. They are the reciprocals of the magnetic and viscous Reynolds numbers based on the wave speed, and the parameter $\frac{1}{\Lambda}$ was introduced by Lundquist as a measure of the electric quality of the system.

2.5 General properties of solutions.

Since differentiation converts an even function to an odd function, or an odd one to an even one, a solution

for h even in x must be balanced by a solution for u odd in x, and a solution odd in x must be balanced by a solution even in x. Therefore if the boundary conditions for h and u are even and odd respectively, an odd solution for h must represent a transient, and will die out, so in general the solution will be of the same type as the boundary conditions.

For a steady state, assuming

$$h = H e^{ipt}, \quad u = U e^{ipt},$$

the equations reduce to

$$(ip - \lambda \Delta) H = c \frac{\partial U}{\partial x}$$

$$(ip - \nu \Delta) U = c \frac{\partial H}{\partial x}$$

Combining these

$$((ip - \lambda \Delta)(ip - \nu \Delta) - c^2 \frac{\partial^2}{\partial x^2}) H = 0$$

Suppose that $H = X(x)\ Y(y)$.

Then for a plane system we get

$$p^2 XY + ip(\lambda+\nu)(X''Y+XY'') - \lambda\nu(X''''Y+2X''Y''+XY'''') + c^2 X''Y = 0$$

Now if

$$Y'' = -n^2 Y, \quad Y'''' = -n^2 Y'' = n^4 Y, \quad n \text{ a constant},$$

we get on dividing by y

$$p^2X + ip(\lambda+\nu)(X''-n^2X) - \lambda\nu(X''''-2n^2X''+n^4X) + c^2X'' = 0$$

and the variables are separated.

If the variables are replaced by variables which vanish at the walls it is now possible to find a solution satisfying the boundary conditions on both H and U as a series of eigenfunctions because the nature of the y variation terms is the same for both.

If we put

$$X'' = -m^2X$$

we can again separate the variables. But in this case the eigenfunctions would have to satisfy two boundary conditions at each end because of the cross derivative terms between H and U, and this is impossible. An expansion in eigenfunctions of x becomes possible only if ν or $\lambda = 0$ so that one boundary condition is relaxed.

For transient situations from which t has not been eliminated an attempt to separate both x and y in this simple way thus breaks down in the most general case, and we cannot expect to find such simple solutions.

When $\lambda = \nu$ the equations

$$\left(\frac{\partial}{\partial t} - \nu\Delta\right) h = c\frac{\partial u}{\partial x}$$

$$\left(\frac{\partial}{\partial t} - \lambda\Delta\right) u = c\frac{\partial h}{\partial x}$$

can be expressed as two independent equations by the substitutions

$$h + u = v, \qquad h - u = w$$

which give

$$\left(\frac{\partial}{\partial t} - c\frac{\partial}{\partial x} - \lambda\Delta\right) v = 0$$

$$\left(\frac{\partial}{\partial t} + c\frac{\partial}{\partial x} - \lambda\Delta\right) w = 0$$

The system is thus reduced from a fourth order to a second order system and expansion is now possible in appropriate eigenfunctions of x or y.

CHAPTER 3.

STEADY STATE THEORY.

3.1 Separation of the different aspects of the waves.

The behaviour of the waves is more easily understood if the different underlying factors are isolated. The equations will here be studied first in steady state situations and secondly in transient situations. In each case one-dimensional situations will first be examined to elucidate the basic behaviour and the effect of side walls will be examined subsequently.

3.2 Half infinite system.

Consider now the general case of a half infinite system in a steady state

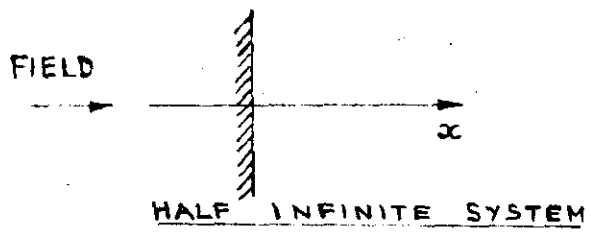

Fig. 3.1

If H and U are the phasor representations of h and u the equations are

$$(ip - \lambda\frac{\partial^2}{\partial x^2})H = c\frac{\partial U}{\partial x}$$

$$(ip - \nu\frac{\partial^2}{\partial x^2})U = c\frac{\partial H}{\partial x}$$

These are satisfied by $H = r\,e^{ikx}$, $U = e^{ikx}$ if

$$(ip + \lambda k^2)r = ick$$

$$ip + \nu k^2 = ick\, r$$

$$(ip+\lambda k^2)(ip+\nu k^2) + c^2k^2 = \lambda\nu k^4 + (c^2+i(\lambda+\nu)p)k^2 - p^2 = 0$$

$$k^2 = -\alpha \pm (\alpha^2 + \beta)^{\frac{1}{2}}$$

$$2\alpha = \frac{c^2 + i(\lambda+\nu)p}{\lambda\nu}, \qquad \beta = \frac{p^2}{\lambda\nu}$$

For each value of k^2

$$r = \frac{ick}{ip + \lambda k^2} = \frac{ip + \nu k^2}{ick}$$

$$r^2 = \frac{ip + \nu k^2}{ip + \lambda k^2}$$

Representative boundary conditions for magnetic and mechanical excitation are

$H = 1$, $U = 0$ at the wall (1).

and

$H = 0$, $U = 1$ at the wall (2).

These can be satisfied by a combination of terms involving the two roots for k^2. The solutions for cases (1) and (2) are

$$H = \frac{r_1 e^{ik_1x} - r_2 e^{ik_2x}}{r_1 - r_2}, \qquad U = \frac{e^{ik_1x} - e^{ik_2x}}{r_1 - r_2}$$

and

$$H = \frac{e^{ik_1x} - e^{ik_2x}}{\frac{1}{r_1} - \frac{1}{r_2}}, \quad U = \frac{\frac{e^{ik_1x}}{r_1} - \frac{e^{ik_2x}}{r_2}}{\frac{1}{r_1} - \frac{1}{r_2}}$$

where k_1 and k_2 must be given signs such that $H, U \to 0$ at ∞.

In a case where $\frac{\lambda p}{c^2}, \frac{\nu p}{c^2} \ll 1$,

$$\frac{\beta}{a^2} \ll 1$$

and

$$k_2^2 \doteq -2a = -\frac{c^2 + i(\lambda+\nu)p}{\lambda\nu}$$

$$k_1^2 \doteq \frac{\beta}{2a} = \frac{p^2}{c^2 + i(\lambda+\nu)p}$$

We cannot ignore $\frac{\lambda p}{c^2}, \frac{\nu p}{c^2}$ compared with 1 in k_1, k_2, although they are small, because x is unbounded, and $\theta x \to \infty$ with x however small θ may be.

To make $H, U \to 0$ at ∞ we must take

$$k_1 = -\left(\frac{p^2}{c^2 + i(\lambda+\nu)p}\right)^{\frac{1}{2}}, \quad k_2 = i\left(\frac{c^2 + i(\lambda+\nu)p}{\lambda\nu}\right)^{\frac{1}{2}}$$

Also

$$r_1^2 = \frac{ip + \nu k_1^2}{ip + \lambda k_1^2} = \frac{c^2 + i\lambda p}{c^2 + i\nu p}$$

$$r_2^2 = \frac{ip + \nu k_2^2}{ip + \lambda k_2^2} = \frac{c^2 + i\nu p}{c^2 + i\lambda p}\frac{\nu}{\lambda}$$

Here $\frac{\lambda p}{c^2}$, $\frac{\nu p}{c^2}$ may be ignored compared with 1, so allowing for the correct signs of k_1, k_2

$$r_1 \doteq -1, \quad r_2 \doteq \left(\frac{\nu}{\lambda}\right)^{\frac{1}{2}}$$

$$r_1 - r_2 \doteq -\frac{\lambda^{\frac{1}{2}} + \nu^{\frac{1}{2}}}{\lambda^{\frac{1}{2}}}, \quad \frac{1}{r_1} - \frac{1}{r_2} \doteq -\frac{\lambda^{\frac{1}{2}} + \nu^{\frac{1}{2}}}{\nu^{\frac{1}{2}}}$$

With these values the solutions for cases (1) and (2), magnetic and viscous excitation, are

$$H = \frac{\lambda^{\frac{1}{2}} e^{ik_1 x} + \nu^{\frac{1}{2}} e^{ik_2 x}}{\lambda^{\frac{1}{2}} + \nu^{\frac{1}{2}}}, \quad U = -\frac{\lambda^{\frac{1}{2}} e^{ik_1 x} - \lambda^{\frac{1}{2}} e^{ik_2 x}}{\lambda^{\frac{1}{2}} + \nu^{\frac{1}{2}}}$$

and

$$H = -\frac{\nu^{\frac{1}{2}} e^{ik_1 x} - \nu^{\frac{1}{2}} e^{ik_2 x}}{\lambda^{\frac{1}{2}} + \nu^{\frac{1}{2}}}, \quad U = \frac{\nu^{\frac{1}{2}} e^{ik_1 x} + \lambda^{\frac{1}{2}} e^{ik_2 x}}{\lambda^{\frac{1}{2}} + \nu^{\frac{1}{2}}}$$

The terms corresponding to k_1 represent waves which penetrate some distance into space, while those corresponding to k_2 represent a rapidly diminishing disturbance confined to a boundary layer. To obtain waves we must therefore use magnetic excitation if $\lambda > \nu$, mechanical excitation if $\nu > \lambda$.

3.3 Confined one-dimensional systems.

For resonance effects the system must be confined.

Consider a system with walls at $\pm d$.

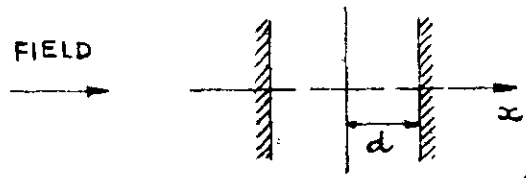

ONE - DIMENSIONAL SYSTEM
Fig. 3.2

If $H = 1$, $U = 0$ at the walls, H will be even, U odd.

If $H = 0$, $U = 1$ at the walls, H will be odd, U even.

In case (1) put $H = r \cos kx$, $U = \sin kx$.

In case (2) put $H = r \sin kx$, $U = -\cos kx$.

In either case the equations are satisfied if

$$(ip + \lambda k^2)r = \sigma k$$

$$ip + \nu k^2 = -\sigma k r$$

k_1^2, k_2^2 take the same values as before but

$$r^2 = -\frac{ip + \nu k^2}{ip + \lambda k^2}$$

For cases (1) and (2) we now have

$$H = \frac{r_1 \dfrac{\cos k_1 x}{\sin k_1 d} - r_2 \dfrac{\cos k_2 x}{\sin k_2 d}}{r_1 \cot k_1 d - r_2 \cot k_2 d}, \quad U = \frac{\dfrac{\sin k_1 x}{\sin k_1 d} - \dfrac{\sin k_2 x}{\sin k_2 d}}{r_1 \cot k_1 d - r_2 \cot k_2 d}$$

and

$$H = \frac{\dfrac{\sin k_1 x}{\sin k_1 d} - \dfrac{\sin k_2 x}{\sin k_2 d}}{\dfrac{\cot k_1 d}{r_1} - \dfrac{\cot k_2 d}{r_2}}, \quad U = \frac{\dfrac{\cos k_1 x}{r_1 \sin k_1 d} - \dfrac{\cos k_2 x}{r_2 \sin k_2 d}}{\dfrac{\cot k_1 d}{r_1} - \dfrac{\cot k_2 d}{r_2}}$$

Using d as a typical length these results can be put in dimensionless form.

With

$$X = \frac{x}{d}\,, \quad P = \frac{pd}{c}\,, \quad \wedge = \frac{\lambda}{cd}\,, \quad \sim = \frac{\nu}{cd}\,, \quad K = kd$$

capitals representing the dimensionless variables, the solution for case (1), magnetic excitation, is

$$H = \frac{r_1 \dfrac{\cos K_1 X}{\sin K_1} - r_2 \dfrac{\cos K_2 X}{\sin K_2}}{r_1 \cot K_1 - r_2 \cot K_2}\,, \quad U = \frac{\dfrac{\sin K_1 X}{\sin K_1} - \dfrac{\sin K_2 X}{\sin K_2}}{r_1 \cot K_1 - r_2 \cot K_2}\,,$$

$$K^2 = -\alpha \pm (\alpha^2 + \beta)^{\frac{1}{2}}\,,$$

$$2\alpha = \frac{1 + i(\wedge + \sim)P}{\wedge \sim}\,, \qquad \beta = \frac{P^2}{\wedge \sim}\,,$$

$$r^2 = \frac{iP + \sim K^2}{iP + \wedge K^2}\,.$$

The situation is completely determined by P, $\wedge$ and $\sim$.

The previous analysis now applies if $\wedge P$, $\sim P \ll 1$, giving

$$K_1 = \pm \left(\frac{P^2}{1 + i(\wedge + \sim)P}\right)^{\frac{1}{2}}\,, \quad K_2 = \pm i\left(\frac{1 + i(\wedge + \sim)P}{\wedge \sim}\right)^{\frac{1}{2}}$$

the signs being no longer important, and

$$r_1^2 = -\frac{1 + i\wedge P}{1 + i\sim P}\,, \qquad r_2^2 = -\frac{1 + i\sim P}{1 + i\wedge P}\,\frac{\sim}{\wedge}$$

$$r_1 = \pm i \qquad\qquad r_2 = \pm i\left(\frac{\sim}{\wedge}\right)^{\frac{1}{2}} = \pm i\left(\frac{\nu}{\lambda}\right)^{\frac{1}{2}}$$

With $(\frac{1}{\Lambda N})^{\frac{1}{2}} \gg 1$

$$2 \cos K_2 \doteq -2i \sin K_2 \doteq e^{-iK_2},$$

$$\cot K_2 \doteq -i$$

and with X +ve and near 1

$$\frac{\cos K_2 X}{\sin K_2} \doteq -i e^{iK_2 X'}, \quad \frac{\sin K_2 X}{\sin K_2} \doteq e^{iK_2 X'}, \quad X' = 1 - X$$

Then for case (1)

$$H \doteq \frac{\frac{\cos K_1 X}{\sin K_1} - (\frac{N}{\Lambda})^{\frac{1}{2}} e^{iK_2 X'}}{i \cot K_1 - (\frac{N}{\Lambda})^{\frac{1}{2}}}, \quad U \doteq -\frac{\frac{\sin K_1 X}{\sin K_1} - e^{iK_2 X'}}{i \cot K_1 - (\frac{N}{\Lambda})^{\frac{1}{2}}}$$

Put

$$Q = (\frac{1}{\Lambda N})^{\frac{1}{2}}, \quad \gamma = (\frac{N}{\Lambda})^{\frac{1}{2}}, \quad 2\theta = (\Lambda + N)P$$

$$K_1 \doteq P(1 - i\theta), \quad K_2 \doteq iQ(1 + i\theta)$$

$$\cos K_1 \doteq \cos P \mathrm{ch}\theta P + i \sin P \mathrm{sh}\theta P, \quad \sin K_1 \doteq \sin P \mathrm{ch}\theta P - i \cos P \mathrm{sh}\theta P$$

Then the wave terms are

$$\frac{i \cos P(1 - i\theta)X}{i A \cos P - B \sin P}, \quad -\frac{\sin P(1 - i\theta)X}{i A \cos P - B \sin P},$$

where

$$A = \mathrm{ch}\theta P + \gamma \mathrm{sh}\theta P, \qquad B = \gamma \mathrm{ch}\theta P + \mathrm{sh}\theta P$$

or if $P \sim 1$

$$A \doteq 1 + \gamma\theta P, \qquad B \doteq \gamma + \theta P.$$

$$A^2 \cos P + B^2 \sin^2 P = \frac{A^2+B^2}{2} + \frac{A^2-B^2}{2} \cos^2 P$$

and is least when $\cos P = 0$ if $A > B$, $\gamma < 1$, and when $\sin P = 0$ if $A < B$, $\gamma > 1$.

When $\cos P = 0$, $\sin P = \pm 1$,

$$\cos K_1 = \pm i\theta P, \quad \sin K_1 = \pm 1$$

and the solution for case (1) is

$$H = \frac{\mp i \cos P(1-i\theta)X + \gamma e^{-Q(1+i\theta)X'}}{\theta P + \gamma}, \quad U = \frac{\pm \sin P(1-i\theta)X - e^{-Q(1+i\theta)X'}}{\theta P + \gamma}$$

When $\sin P = 0$, $\cos P = \pm 1$,

$$\cos K_1 = \pm 1, \quad \sin K_1 = \mp i\theta P$$

and the solution for case (1) is

$$H = \frac{\pm \cos P(1-i\theta)X + \gamma\theta P e^{-Q(1+i\theta)X'}}{1 + \gamma\theta P}, \quad U = \frac{\mp i \sin P(1-i\theta)X - \theta P e^{Q(1+i\theta)X'}}{1 + \gamma\theta P}$$

These are the resonant conditions for cases in which γ > or < 1. Magnification is only possible if $\gamma < 1$, $\lambda > \nu$, resonance then occurring when $P = \frac{\pi}{2}, \frac{3\pi}{2} \ldots\ldots$ If $\nu > \lambda$ resonance is exhibited by a reduction in the diminution of H which takes place when $P = \pi, 2\pi \ldots\ldots$

For the alternative case, mechanical excitation, the solution is the same with H and U, and λ and ν interchanged, magnification now only being possible if $\nu > \lambda$.

When ν or $\lambda = 0$ the second mode disappears, leaving only the wave mode. When $\nu = 0$ the solution for magnetic excitation reduces to

$$H = \frac{\cos KX}{\cos K}, \quad U = \frac{iK}{P}\frac{\sin KX}{\cos K}$$

$$K^2 = \frac{P^2}{1 + i\wedge P}$$

$$K = P(1-i\theta), \quad P = 2\theta.$$

When $\lambda = \nu$ there is also a simplification. In this case

$$\alpha = \frac{1}{2\wedge^2} + \frac{iP}{\wedge}, \quad \beta = \frac{P^2}{\wedge^2}, \quad (\alpha^2+\beta^2)^{\frac{1}{2}} = \frac{1}{\wedge}\left(\left(\frac{1}{2\wedge}\right)^2 + \frac{iP}{\wedge}\right)^{\frac{1}{2}}$$

$$K^2 = -\frac{1}{2\wedge^2} - \frac{iP}{\wedge} \pm \frac{1}{\wedge}\left(\left(\frac{1}{2\wedge}\right)^2 + \frac{iP}{\wedge}\right)^{\frac{1}{2}} = -\left(\frac{1}{2\wedge} \pm \left(\left(\frac{1}{2\wedge}\right)^2 + \frac{iP}{\wedge}\right)\right)^2$$

$$K = i\left(\frac{1}{2\wedge} \pm \left(\left(\frac{1}{2\wedge}\right)^2 + \frac{iP}{\wedge}\right)^{\frac{1}{2}}\right), \quad K_2 - K_1 = 2i\left(\left(\frac{1}{2\wedge}\right)^2 + \frac{iP}{\wedge}\right)^{\frac{1}{2}}$$

$$r_1 = r_2 = -i$$

and for magnetic excitation

$$H = \frac{\sin K_2 \cos K_1 X - \sin K_1 \cos K_2 X}{\sin(K_2 - K_1)}, \quad U = i\,\frac{\sin K_2 \sin K_1 X - \sin K_1 \sin K_2 X}{\sin(K_2 - K_1)}$$

When $\wedge P \ll 1$

$$K_2 = \frac{i}{\wedge} - P, \quad K_1 = \frac{P}{1 + i\wedge P}$$

$$K_2 - K_1 = \frac{i}{\wedge} - 2P$$

$$\frac{\sin K_2}{\sin(K_2 - K_1)} = \frac{e^{\left(\frac{1}{\wedge} + iP\right)}}{e^{\left(\frac{1}{\wedge} + 2iP\right)}} = e^{-iP}$$

This simplification corresponds to the reduction of order in the equations where $\lambda = \nu$ (2.5). There is no

resonance, there being a steady phase change with frequency and no magnification.

The results of numerical calculations are given in Figures 3.3 - 3.6. These and all later numerical calculations were conveniently carried out with the computer at the Mathematical Laboratory (Appendix 1). The calculations are for magnetic excitation, H being taken as 1 at the wall, the results for mechanical excitation being obtained by replacing H by U and γ by $\frac{1}{\gamma}$. Figures 3.3 and 3.4 show the field H at the centre against the dimensionless frequency P at different values of γ for $\Lambda + N = .01$ and .1. The absence of resonance when $\lambda = \nu$ is apparent, as is the absence of magnification when $\nu > \lambda$ and the displacement of resonant frequency. Figures 3.5 and 3.6 show the amplification at the fundamental and harmonic frequencies $P = \frac{\pi}{2}$ and $\frac{3\pi}{2}$ against variation of $\Lambda + N$ and γ. The amplification may be limited either by the value of $\Lambda + N$ (the curves for diminishing γ then asymptotically approaching the curve for $\gamma = 0$ when $\gamma \ll \Lambda + N$) or by the value of γ, the curve for each value of peeling off to the right and approaching an amplification

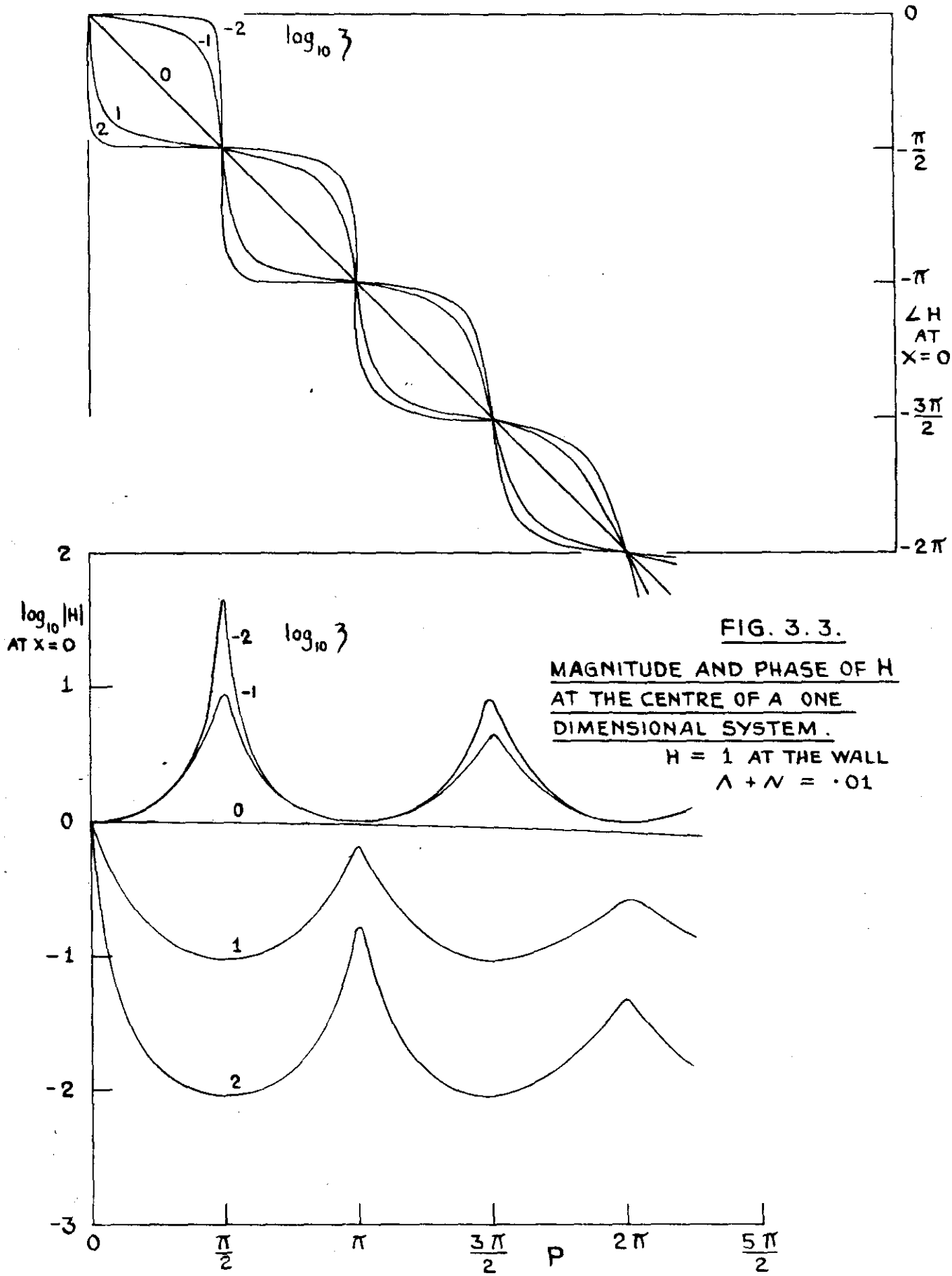

FIG. 3.3.

MAGNITUDE AND PHASE OF H AT THE CENTRE OF A ONE DIMENSIONAL SYSTEM.

H = 1 AT THE WALL

$\Lambda + N = \cdot 01$

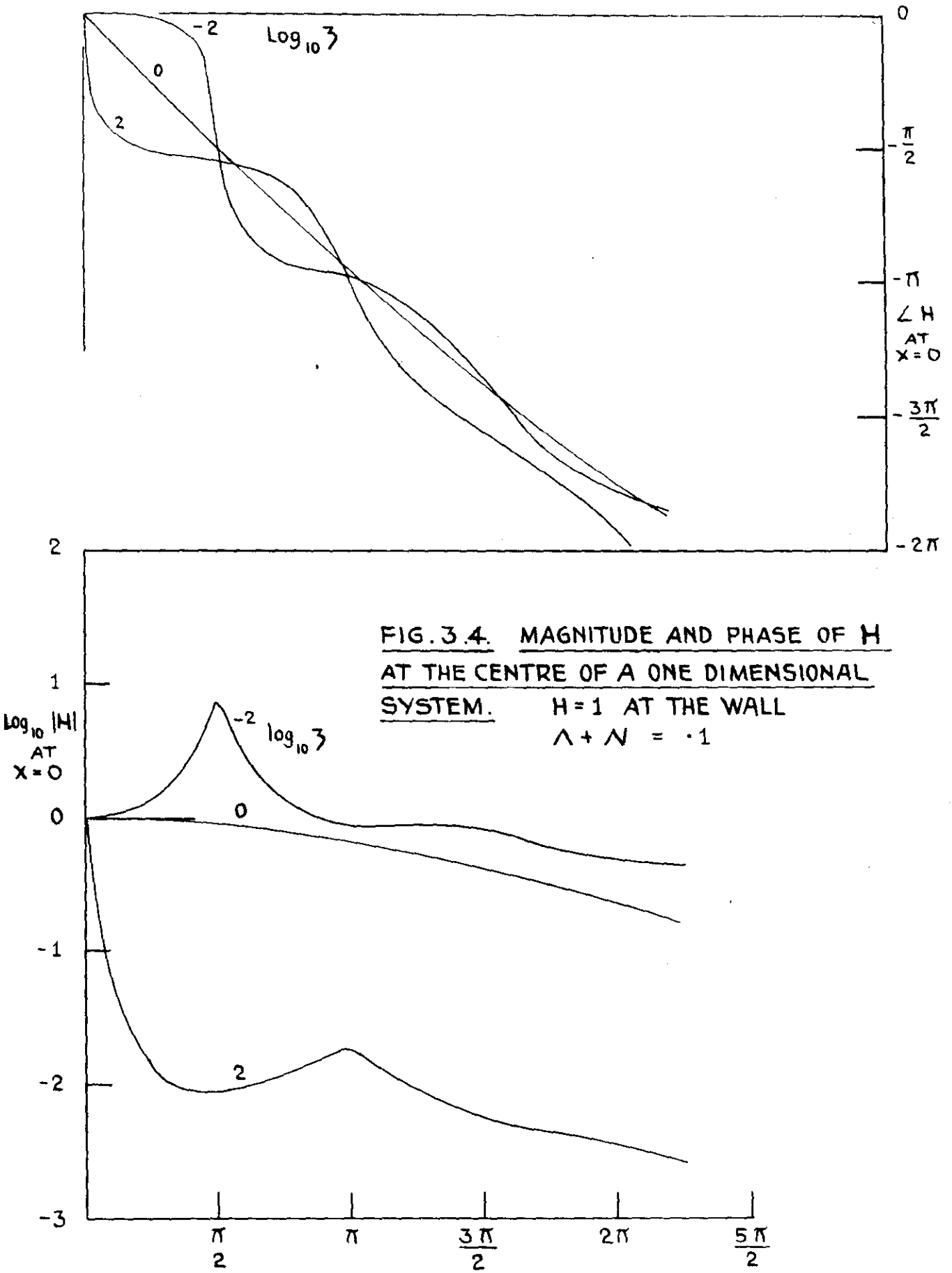

FIG. 3.4. MAGNITUDE AND PHASE OF H AT THE CENTRE OF A ONE DIMENSIONAL SYSTEM. H = 1 AT THE WALL
$\Lambda + N = \cdot 1$

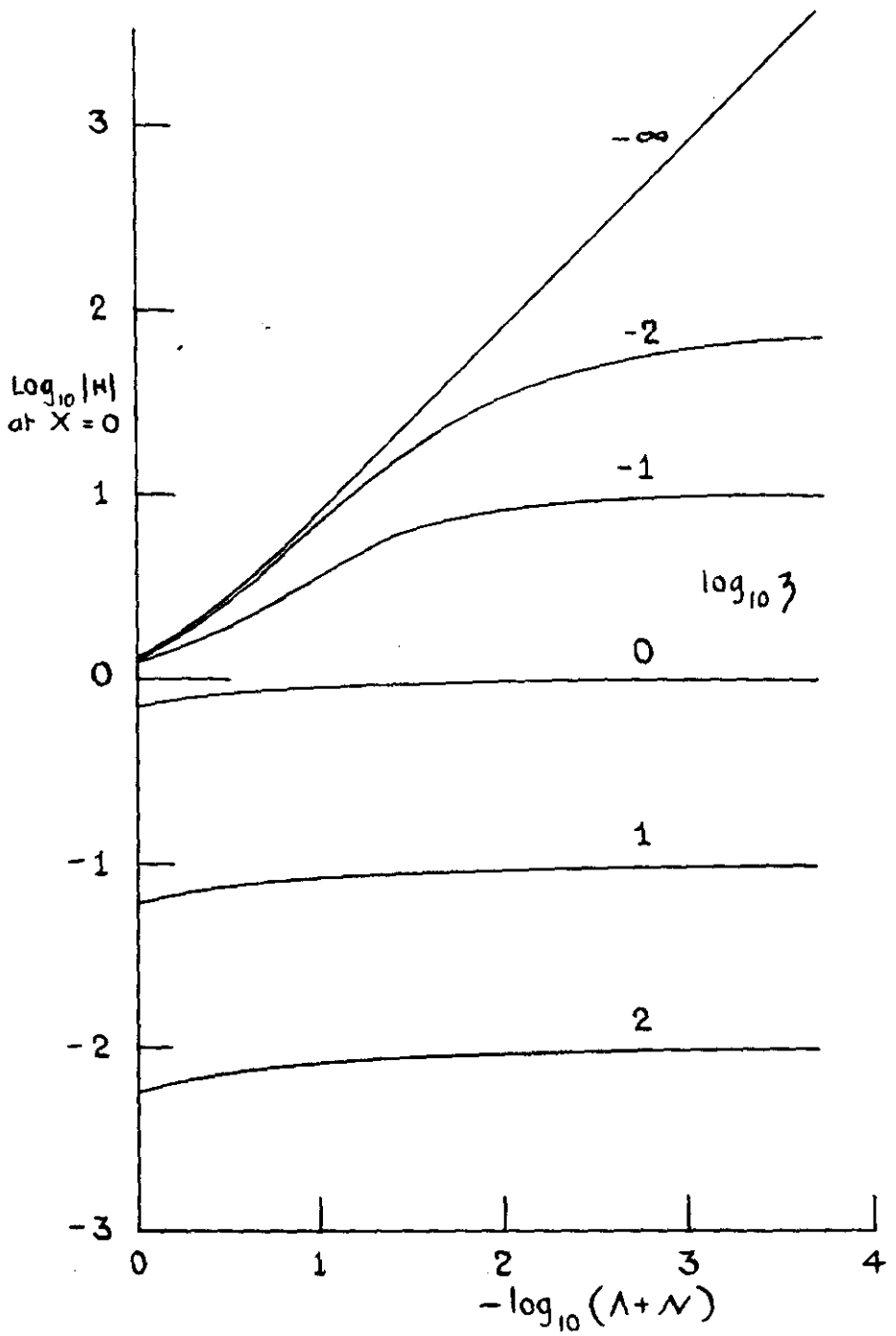

FIG. 3.5 MAGNITUDE OF H AT THE CENTRE OF A ONE DIMENSIONAL SYSTEM AT THE FUNDAMENTAL RESONANCE : $P = \frac{\pi}{2}$

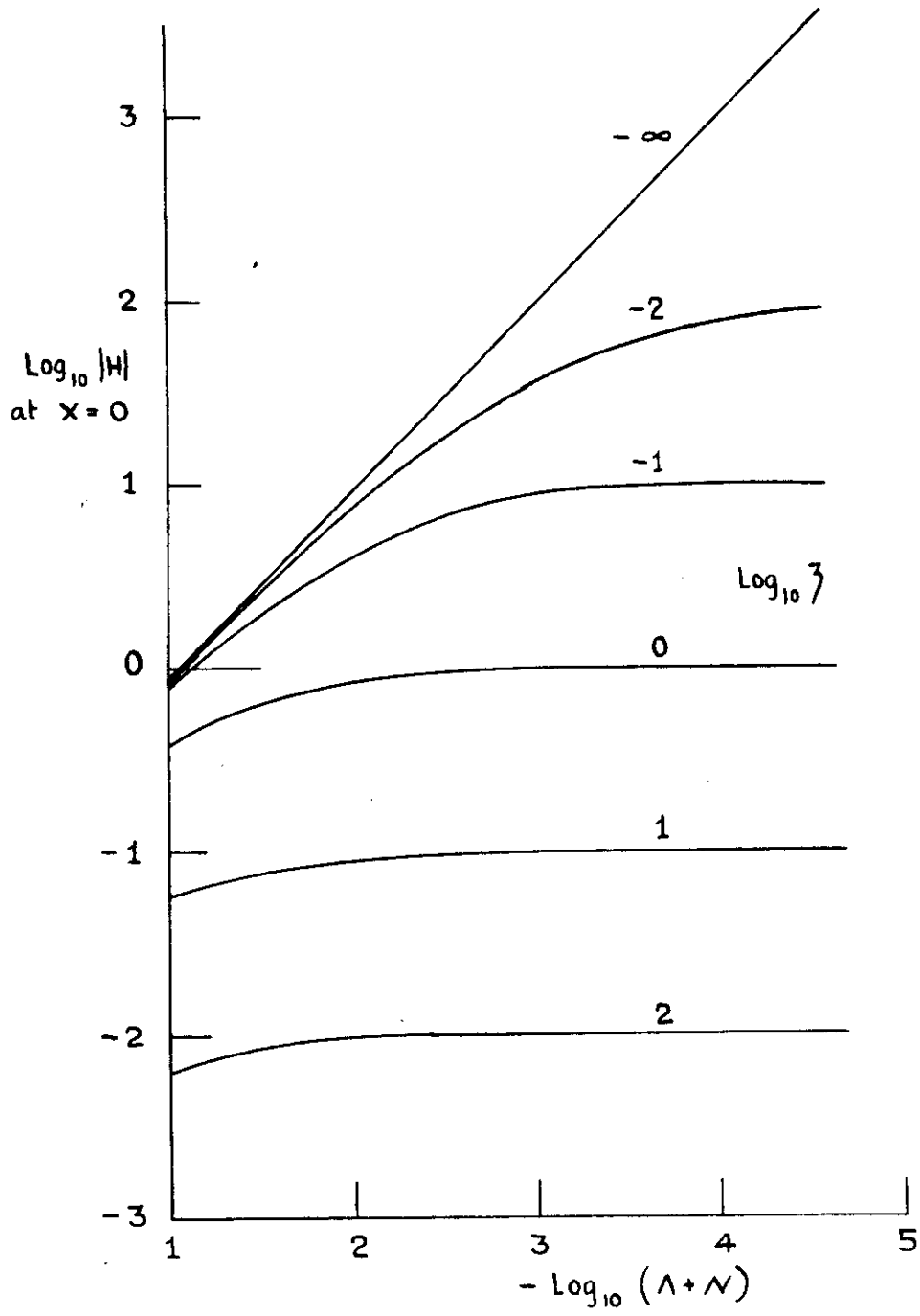

FIG. 3.6 MAGNITUDE OF H AT THE CENTRE OF A ONE DIMENSIONAL SYSTEM AT THE FIRST HARMONIC RESONANCE : $P = \frac{3\pi}{2}$

of $\frac{1}{\gamma}$ when $\Lambda+\nu < \gamma$. From the second figure it can be seen that a harmonic resonance with magnification is only possible if $\Lambda+\nu \sim .05$ or less.

The available liquid conductors are liquid metals for which $\gamma \sim 10^{-2}$ or less, so that for magnification magnetic excitation must be used. Lundquist's method is equivalent to this, since the fluid trapped in the ribs of the oscillating disc had the same effect as a conducting disc. When the total damping is sufficiently small, however, the effect of viscosity can nevertheless not be ignored, because of the way in which it affects the excitation, finally limiting the performance.

3.4 Power intake and dissipation.

The distribution of power between the modes corresponding to k_1 and k_2, and the electric and viscous action of the fluid, is interesting.

If the excitation is magnetic, power is taken in by the potential difference acting on the wall current. The flux for one half is $(\mu\rho)^{\frac{1}{2}} \int_0^d h\, dx$, the e.m.f. $-(\mu\rho)^{\frac{1}{2}} \int_0^d \frac{\partial h}{\partial t}\, dx$. Also the current for $h = 1$ at the boundary is $(\frac{\rho}{\mu})^{\frac{1}{2}}$, so the intake of power for one wall is

$$I = -\rho \int_0^d \frac{\partial h}{\partial t}\, dx.$$

If the excitation is mechanical, power is taken in by the viscous force on the moving wall. The force is $\rho\nu(\frac{\partial u}{\partial x})_{x=d}$

so with $u = 1$ at the wall, the intake for one wall is

$$I = \rho\nu\left(\frac{\partial u}{\partial x}\right)_{x=d}$$

Also if H and U are the phasor representations of h and u, the mean intake with magnetic excitation is

$$I_{mean} = \mathrm{Re}\ \frac{i\rho\omega}{2}\int_0^d H dx = \mathrm{Re}\ \frac{i\rho\omega P}{2}\int_0^1 H dX$$

and the mean intake with mechanical excitation is

$$I_{mean} = \mathrm{Re}\ \frac{\rho\nu}{2}\left(\frac{\partial U}{\partial x}\right)_{x=d} = \mathrm{Re}\ \frac{\rho\omega\lambda}{2}\left(\frac{\partial U}{\partial X}\right)_{X=1}$$

Now we note that

$$2\theta = (\lambda+\lambda)P = (\lambda\lambda)^{\frac{1}{2}}P\left(\left(\frac{\lambda}{\lambda}\right)^{\frac{1}{2}} + \left(\frac{\lambda}{\lambda}\right)^{\frac{1}{2}}\right) = \frac{P}{Q}\left(\frac{1}{\eta}+\eta\right)$$

and therefore for all values of

$$\frac{\eta Q}{P},\ \frac{Q}{P},\ \frac{Q}{\eta P} \neq \frac{1}{2\theta}$$

Here with $H = 1$ at the boundary

$$\int_0^1 H dX = \frac{\frac{r_1}{K_1} - \frac{r_2}{K_2}}{r_1 \cot K_1 - r_2 \cot K_2} = \frac{i\left(\frac{1+i\theta}{P} + i\eta\left(\frac{1-i\theta}{Q}\right)\right)}{i\cot P(1-i\theta) - \eta}$$

Therefore to the first order,

when $\cos P = 0$, $\cot P(1-i\theta) \doteq i\theta P$,

$$I_{mean} \doteq \frac{\rho\omega}{2(\theta P+\eta)}$$

and when $\sin P = 0$, $\cot P\,(1-i\theta) = \frac{i}{\theta P}$,

$$I_{mean} = \frac{\rho c}{2(\frac{1}{\theta P} + \gamma)}$$

The power is taken in largely by the mode corresponding to K_1, the wave mode.

Also with $U = 1$ at the boundary

$$\left(\frac{\partial U}{\partial X}\right)_{X=1} = \frac{\frac{K_1}{r_1} - \frac{K_2}{r_2}}{\frac{\cot K_1}{r_1} - \frac{\cot K_2}{r_2}} = \frac{iP(1-i\theta) - \frac{Q}{\gamma}(1+i\theta)}{i\cot P(1-i\theta) - \frac{1}{\gamma}}$$

so when $\cos P = 0$

$$I_{mean} = \frac{\rho c N Q}{2\gamma(\theta P + \frac{1}{\gamma})} = \frac{\rho c}{2(\theta P + \frac{1}{\gamma})}$$

and when $\sin P = 0$

$$I_{mean} = \frac{\rho c}{2(\frac{1}{\theta P} + \frac{1}{\gamma})}$$

The intake of power is thus the same as with magnetic excitation, $\frac{1}{\gamma}$ replacing γ , but it is now largely by the mode corresponding to K_2, the boundary layer mode.

The power is dissipated partly by electric resistivity, partly by viscosity. The electric dissipation for one

half is

$$D_\lambda = \tau \int_0^d j^2 \, dx$$

so here with a current $(\frac{\rho}{\mu})^{\frac{1}{2}} \frac{\partial h}{\partial x}$

$$D_\lambda = \rho\lambda \int_0^d (\frac{\partial h}{\partial x})^2 \, dx$$

The viscous dissipation is

$$D_\nu = 2\rho\nu \int_0^d \sum_{ab} e_{ab}^2 \, dx, \quad e_{ab} = \tfrac{1}{2}(\frac{\partial u_a}{\partial x_b} + \frac{\partial u_b}{\partial x_a})$$

which reduces to

$$D_\nu = \rho\nu \int_0^d (\frac{\partial u}{\partial x})^2 \, dx$$

Then if H, U are the phasor representations of h, u,

$$D_{\lambda mean} = \frac{\rho\lambda}{2} \int_0^d \left|\frac{\partial H}{\partial x}\right|^2 dx = \frac{\rho q \Lambda}{2} \int_0^1 \left|\frac{\partial H}{\partial X}\right|^2 dX$$

$$D_{\nu mean} = \frac{\rho\nu}{2} \int_0^d \left|\frac{\partial U}{\partial x}\right|^2 dx = \frac{\rho c \mathcal{N}}{2} \int_0^1 \left|\frac{\partial U}{\partial X}\right|^2 dX$$

Now for magnetic excitation

$$\frac{\partial H}{\partial X} = - \frac{r_1 K_1 \frac{\sin K_1 X}{\sin K_1} - r_2 K_2 \frac{\sin K_1 X}{\sin K_2}}{r_1 \cot K_1 - r_2 \cot K_2} = \frac{A}{B} \text{ say,}$$

$$\left|\frac{\partial H}{\partial X}\right|^2 = \frac{|A|^2}{|B|^2} .$$

$$A \propto P(i+\theta)\,\frac{\sin P(1-i\theta)X}{\sin P(1-i\theta)} + \gamma Q e^{-Q(1+i\theta)X'},\quad X' = 1-X,\ X \text{ + ve}$$

When $\cos P = 0$, $\sin P(1-i\theta) \propto 1$,

$$A \propto P(i+\theta)(\sin PX - i\theta PX\cos PX) + \gamma Q e^{-QX'}(\cos\theta QX' - i\sin\theta QX')$$

$$\propto \gamma Q e^{-QX'}\cos\theta QX' + i(P\sin PX - \gamma Q e^{-QX'}\sin\theta QX')$$

$$|A|^2 \propto P^2\sin^2 PX' + \gamma^2 Q^2 e^{-2QX'} - 2\gamma PQ e^{-QX'}\sin PX\sin\theta QX'$$

When $\sin P = 0$, $\sin P(1-i\theta) \propto i\theta P$,

$$A \propto \left(\frac{1}{\theta} - i\right)(\sin PX - i\theta PX\cos PX) + \gamma Q e^{-QX'}(\cos\theta QX' - i\sin\theta QX')$$

$$\propto \frac{1}{\theta}\sin PX + \gamma Q e^{-QX'}\cos\theta QX' - i(\sin pX + pX\cos PX + \gamma Q e^{-QX'}\sin\theta QX')$$

$$|A|^2 \propto \frac{1}{\theta^2}\sin^2 PX + \gamma^2 Q^2 e^{-2QX'} + 2PQe^{-QX'}\left(\frac{1}{\theta}\sin PX\cos\theta QX' + \sin PX\sin\theta QX' + PX\cos PX\sin\theta QX'\right)$$

Integration with respect to X from 0 to 1 of the first two terms neglecting e^{-2Q}, gives

$$\tfrac{1}{2}(P^2 + \gamma^2 Q),$$

when $\cos P = 0$, and

$$\tfrac{1}{2}\left(\frac{1}{\theta^2} + \gamma^2 Q\right)$$

when $\sin P = 0$.

Also the integrals of the remaining terms because either

$$\cos P = 0, \quad |\cos PX'| < PX'$$

or

$$\sin P = 0, \qquad |\sin PX'| < PX'$$

or

$$|\sin \theta QX'| < \theta QX' ,$$

are less than factors of $\int_0^1 X' e^{-QX'} dX'$, but

$$\int_0^1 X' e^{QX'} dX' = \left(\frac{X'}{Q} e^{-QX'} \right)_1^0 + \frac{1}{Q} \int_0^1 e^{-QX'} dX'$$

$$= \left(\left(\frac{X'}{Q} + \frac{1}{Q^2} \right) e^{-QX'} \right)_1^0 < \frac{1}{Q^2} < \frac{\theta^2}{P^2}$$

and accordingly they can be neglected.

The dissipation is thus to this order of accuracy, the sum of the dissipation corresponding to each term alone.

Finally when $\cos P = 0$

$$|B| \doteq \theta P + \gamma ,$$

therefore

$$D_{\lambda \text{mean}} \doteq \frac{\rho c \Lambda}{4} \frac{P^2 + \gamma^2 Q}{(\theta P + \gamma)^2} = \frac{\rho c}{4} \frac{\Lambda P^2 + \gamma}{(\theta P + \gamma)^2}$$

and when $\sin P = 0$

$$|B| \doteq \frac{1}{\theta P} + \gamma ,$$

therefore

$$D_{\lambda \text{mean}} \doteq \frac{\rho c \Lambda}{4} \frac{\frac{1}{\theta^2} + \gamma^2 Q}{(\frac{1}{\theta P} + \gamma)^2} = \frac{\rho c}{4} \frac{\frac{\Lambda}{\theta^2} + \gamma}{(\frac{1}{\theta P} + \gamma)^2}$$

Also

$$\frac{\partial U}{\partial X} = \frac{\frac{K_1 \cos K_1 X}{\sin K_1} - \frac{K_2 \cos K_2 X}{\sin K_2}}{r_1 \cot K_1 - r_2 \cot K_2}$$

and a similar analysis again shows that we can evaluate $\int_0^1 \left|\frac{\partial U}{\partial X}\right|^2 dX$ as the sum of the integrals of the squares of the two terms separately, ignoring the cross terms.

We obtain

$$D_{\nu\,\text{mean}} \doteq \frac{\rho c \mathcal{N}}{4} \frac{P^2 + Q}{(\theta P + \eta)^2} = \frac{\rho c}{4} \frac{\mathcal{N} P^2 + \eta}{(\theta P + \eta)^2}$$

when $\cos P = 0$, and

$$D_{\nu\,\text{mean}} \doteq \frac{\rho c \mathcal{N}}{4} \frac{\frac{1}{\theta^2} + Q}{(\frac{1}{\theta P} + \eta)^2} = \frac{\rho c}{4} \frac{\frac{\mathcal{N}}{\theta^2} + \eta}{(\frac{1}{\theta P} + \eta)^2}$$

when $\sin P = 0$.

For the wave mode electric or viscous dissipation is thus more important according as $\lambda >$ or $< \nu$, whereas for the boundary layer mode they are equal. When $\cos P = 0$ the total dissipation corresponding to the wave and boundary layer modes is

$$\frac{\rho c}{4} \frac{(\Lambda + \mathcal{N}) P^2}{(\theta P + \eta)^2} = \frac{\rho c}{2} \frac{\theta P}{(\theta P + \eta)^2} \quad \text{and} \quad \frac{\rho c}{2} \frac{\eta}{(\theta P + \eta)^2},$$

and when $\sin P = 0$ the dissipation for the two modes is

$$\frac{\rho c}{4} \frac{\frac{\Lambda + \mathcal{N}}{\theta^2}}{(\frac{1}{\theta P} + \eta)^2} = \frac{\rho c}{2} \frac{\frac{1}{\theta P}}{(\frac{1}{\theta P} + \eta)^2} \quad \text{and} \quad \frac{\rho c}{2} \frac{\eta}{(\frac{1}{\theta P} + \eta)^2}.$$

The wave or boundary layer mode is thus more important according as θP or $\frac{1}{\theta P} >$ or $< \eta$.

A check on the power balance gives

$$D = \frac{\rho c}{2(\theta P + \gamma)} = I$$

when $\cos P = 0$ and

$$D = \frac{c}{2(\frac{1}{\theta P} + \gamma)} = I$$

when $\sin P = 0$.

When $\lambda = \nu$ the power dissipated in the wave mode is always $\frac{\theta P}{(\theta P+1)^2}$, corresponding to the constant amplitude of this mode. The change in power intake as the frequency changes is balanced by the change in dissipation in the boundary layer mode, corresponding to the change in its amplitude required to make up the boundary value as nodes or antinodes of the wave mode pass the boundary. As $\lambda \to 0$ the steepness of the boundary layer determined by $Q = \frac{1}{\Lambda}$ increases so that the power dissipated is constant, and there is no increase in amplitude. This result does not correspond to the solution for $\lambda = 0$, which would be infinite at resonance, because the introduction of the Δ terms changes the order of the equations.

When the excitation is mechanical and $\lambda = 0$ there is an apparent breakdown in the power balance because the power intake would normally be mainly by the boundary layer mode which no longer exists. However the calculation of power intake from the velocity gradient at the wall breaks down in this case, because there is a current sheet at the wall with an infinite $\underline{j} \times \underline{B}$ force, making the viscous

force indeterminate. If we consider what happens to the solution

$$H = \frac{\frac{\sinh K_1 X}{\sinh K_1} - \frac{\sinh K_2 X}{\sinh K_2}}{\frac{\coth K_1}{r_1} - \frac{\coth K_2}{r_2}}, \qquad U = \frac{\frac{\cosh K_1 X}{r_1 \cosh K_1} - \frac{\cosh K_2 X}{r_2 \cosh K_2}}{\frac{\coth K_1}{r_1} - \frac{\coth K_2}{r_2}}$$

for a case in which $\lambda \neq 0$, when $\lambda \to 0$, we see that the velocity boundary layer diminishes in magnitude because of the factor $\frac{1}{r_2} = \frac{1}{\eta}$, but increases in steepness since $K_2 = iQ(1+i\theta) \to \infty$, so that it can still account for the required intake of power, while the current sheet appears as the limit of the magnetic boundary layer which has no factor $\frac{1}{r_2}$.

3.5 <u>The effect of side walls in an ideal case</u>.

The effect of side walls must now be considered. Take a plane system with walls at $x = \pm d$, $y = \pm e$, or a cylindrical system with walls at $x = \pm d$, $y = y_1, y_2$.

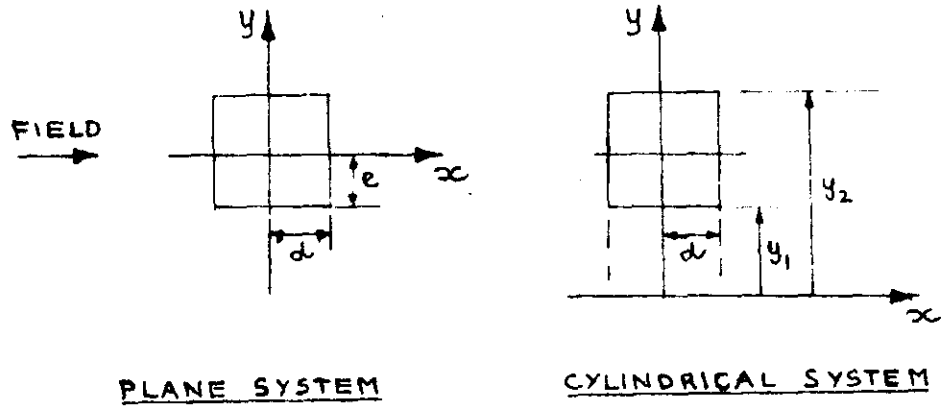

PLANE SYSTEM CYLINDRICAL SYSTEM

Fig.3.7

With an ideal fluid for which $\lambda = \nu = 0$

$$ipH = c\frac{\partial U}{\partial x}, \qquad ipU = c\frac{\partial H}{\partial x}$$

$$(p^2 + c^2\frac{\partial^2}{\partial x^2})H = (p^2 + c^2\frac{\partial^2}{\partial x^2})U = 0$$

The boundary conditions for magnetic excitation by a wall current can be taken as

$h = 1$ in a plane case,

$h = \frac{y_1}{y}$ in a cylindrical case,

because h_1 or yB_1 is a stream function for $p = i$ (2.2) and true in constant at the wall, this corresponding to no disturbance outside the system.

The equations being independent of y the solution is the same as without side walls, simply

$$H = \frac{\cos\frac{px}{c}}{\cos\frac{pd}{c}} \quad \text{or} \quad \frac{y_1}{y}\frac{\cos\frac{px}{c}}{\cos\frac{pd}{c}}$$

The boundary conditions on each side wall are met by the formation of a current sheet from the coalescence of the cross currents corresponding to the variation in h. That this sheet is just strong enough to balance the difference in h between inside and outside follows from the stream function property of h. Such sheets do not form on the end walls because they would imply infinite $\underline{j} \times \underline{B}$ forces.

For an aribtrary section similar considerations apply; d is now a function of y, and because of the stream function property currents corresponding to x and y variation of h cancel at the walls except on portions parallel to the field, where sheets form. When $\lambda, \nu \neq 0$ neither current sheets nor velocity discontinuities are possible at the side walls and the side wall effects must penetrate into the fluid. In order to obtain wave behaviour it will be essential that the walls be sufficiently separated.

3.6 Eigenfunction expansions.

The detailed analysis when $\lambda, \nu \neq 0$ can either be numerical, or where it is possible to separate the variables, by expansion in eigenfunctions. The eigenfunction method can give a picture of the behaviour without the need for a separate calculation for each different case. Detailed treatments of the method can be found in works on partial differential equations[6,7].

Here the terms involving y variation are the Δ terms, where for a plane or cylindrical case

$$\Delta \equiv \frac{\partial^2}{\partial x^2} + \frac{\partial^2}{\partial y^2} \quad \text{or} \quad \frac{\partial^2}{\partial x^2} + \frac{\partial^2}{\partial y^2} + \frac{1}{y}\frac{\partial}{\partial y} - \frac{1}{y^2}$$

and the variable y can be separated by expressing the

solution as an expansion of functions satisfying

$$\mathcal{E}'' = -n^2\mathcal{E} \quad \text{or} \quad \mathcal{E}'' + \frac{\mathcal{E}'}{y} - \frac{\mathcal{E}}{y^2} = -n^2\mathcal{E}$$

Functions satisfying these and satisfying boundary conditions at two values y_1, y_2 of y, exist only for particular eigenvalues n, and it is possible to express the most general solution for a geometry with parallel walls as an expansion of the eigenfunctions corresponding to these values because of the orthogonality property,

$$\int_{y_1}^{y_2} A\,\mathcal{E}_\delta\,\mathcal{E}_\epsilon \, dy = 0,$$

$\delta \neq \epsilon$, A a function depending on the equation satisfied by

for eigenfunctions $\mathcal{E}_\delta, \mathcal{E}_\epsilon$ of separate eigenvalues n_δ, n_ϵ, which allows the most general condition $f = f(y)$ to be satisfied on a boundary x = constant, provided this is put in a form consistent with the conditions satisfied by $\mathcal{E}$ at y_1, y_2. Thus to represent f by an expansion

$$f = \sum \bar{f}_\epsilon \mathcal{E}_\epsilon$$

we multiply by $A\,\mathcal{E}_\epsilon$ and integrate to obtain, because of the orthogonality property,

$$\bar{f}_\epsilon = \frac{\int_{y_1}^{y_2} A\,\mathcal{E}_\epsilon f \, dy}{\int_{y_1}^{y_2} A\,\mathcal{E}_\epsilon^{\,2} \, dy}$$

The orthogonality property follows directly from the equation satisfied by ϵ.

The general equation

$$\epsilon'' + a\epsilon' + b\epsilon = -n^2\epsilon$$

multiplied by A such that

$$A' = Aa,$$

becomes

$$(A\epsilon')' + B\epsilon = -n^2 A\epsilon, \quad B = Ab.$$

Now multiplying

$$(A\epsilon_\delta')' + B\epsilon_\delta = -n_\delta^2 A\epsilon_\delta$$

$$(A\epsilon_\epsilon')' + B\epsilon_\epsilon = -n_\epsilon^2 A\epsilon_\epsilon$$

by ϵ_ϵ and ϵ_δ, subtracting and integrating,

$$\int((A\epsilon_\delta')'\epsilon_\epsilon - (A\epsilon_\epsilon')'\epsilon_\delta)dx = (n_\delta^2 - n_\epsilon^2)\int A\epsilon_\delta\epsilon_\epsilon \, dx$$

Then integrating by parts the first term vanishes if any linear combination of ϵ and ϵ' vanishes at y_1 and y_2. The question of convergence is covered in the standard works[6,7].

The method can only work for geometries for which separation is possible after the equations have been expressed in terms of variables constant at the boundaries, since the orthogonality property refers to a given pair

of limits of the variable in terms of which the expansion is carried out.

Here expansion is possible with rectangular sections, and in the plane and cylindrical cases the appropriate eigenfunctions are

$$\mathcal{E}(y) = \cos ny \quad \text{or} \quad \sin ny,$$

$$n \text{ such that } \mathcal{E}(e) = 0, \quad n_\epsilon = \frac{\epsilon\pi}{2e}$$

or

$$\mathcal{E}(y) = J_1(ny)\, Y_1(ny_1) - Y_1(ny)\, J_1(ny_1),$$

$$n \text{ such that } \mathcal{E}(y_2) = 0.$$

In the first case, if the solution is symmetric about the x axis, the coefficients of the sine terms vanish, leaving a cosine series. Also

$$A = 1, \qquad \int_{-e}^{e} A\mathcal{E}^2\, dy = e$$

In the second case

$$A = y$$

and to evaluate $\int_{y_1}^{y_2} A\mathcal{E}^2\, dy$ we note[8] that the equation for $\mathcal{E}$ multiplied by $2y\mathcal{E}'$ is

$$((y\mathcal{E}')^2)' + (\mathcal{E}^2)' = -2n^2y^2(\mathcal{E}^2)'$$

whence integrating by parts with $\epsilon = 0$ at y_1, y_2

$$\left((y\epsilon')^2\right)_{y_1}^{y_2} = 2n^2 \int_{y_1}^{y_2} y\epsilon^2 \, dy \quad .$$

Now

$$y_1 \epsilon'(y_1) = ny_1(J_1'(ny_1)Y_1(ny_1) - Y_1'(ny_1)J_1(ny_1)) = -\frac{2}{\pi}$$

$$y_2 \epsilon'(y_2) = ny_2(J_1'(ny_1)Y_1(ny_1) - Y_1'(ny_2)J_1(ny_1)).$$

But since n is a zero of (y_2)

$$\frac{J_1(ny_1)}{J_1(ny_2)} = \frac{Y_1(ny_1)}{Y_1(ry_2)} = L \quad \text{say},$$

$$y_2 \epsilon'(y_2) = -\frac{2L}{\pi} .$$

Thus

$$\int_{y_1}^{y_2} y\epsilon^2 \, dy = \frac{2}{n^2\pi^2}(L^2 - 1)$$

3.7 <u>General case of a plane or cylindrical system</u>.

It is now possible to solve the general steady state case for which

$$(ip - \lambda\Delta)H = c\frac{\partial U}{\partial x} ,$$

$$(ip - \nu\Delta)U = c\frac{\partial H}{\partial x} ,$$

$$\Delta \equiv \frac{\partial^2}{\partial x^2} + \frac{\partial^2}{\partial y^2} \quad \text{or} \quad \frac{\partial^2}{\partial x^2} + \frac{\partial^2}{\partial y^2} + \frac{1}{y}\frac{\partial}{\partial y} - \frac{1}{y^2}$$

Where

$$H = I, \quad I = 1 \quad \text{or} \quad \frac{y_1}{y}, \quad U = 0 \quad \text{at the walls}$$

put

$$H = I + Z, \quad Z = 0 \quad \text{at the walls}$$

and where $\epsilon(y)$ are the appropriate eigenfunctions, let

$$I = \Sigma \bar{I}_\epsilon \epsilon_\epsilon, \quad Z = \Sigma \bar{Z}_\epsilon \epsilon_\epsilon, \quad U = \Sigma \bar{U}_\epsilon \epsilon_\epsilon$$

Then the original equations are satisfied if

$$(ip + \lambda n^2 - \lambda \frac{\partial^2}{\partial x^2}) \bar{Z} = c\frac{\partial \bar{U}}{\partial x} - ip\bar{I}$$

$$(ip + \nu n^2 - \nu \frac{\partial^2}{\partial x^2}) \bar{U} = c\frac{\partial \bar{Z}}{\partial x}$$

$\bar{Z} = \bar{U} = 0$ when $x = \pm d$.

These have a particular integral

$$\bar{Z} = -\frac{ip\bar{I}}{ip+\lambda n^2}, \quad \bar{U} = 0.$$

The equations for the complementary functions are just the one dimencional equations with $ip+\lambda n^2$, $ip+\nu n^2$ replacing ip.

We obtain

$$\bar{Z} = a\bar{I}\left(\frac{\frac{r_1 \cos k_1 x}{\sin k_1 d} - \frac{r_2 \cos k_2 x}{\sin k_2 d}}{r_1 \cot k_1 d - r_2 \cot k_2 d} - 1\right),$$

$$\bar{U} = a\bar{I}\left(\frac{\frac{\sin k_1 x}{\sin k_1 d} - \frac{\sin k_2 x}{\sin k_2 d}}{r_1 \cot k_1 d - r_2 \cot k_2 d}\right),$$

$$a = \frac{ip}{ip + \lambda n^2}$$

$$k^2 = -\alpha \pm (\alpha^2 + \beta)^{\frac{1}{2}}$$

$$2\alpha = \frac{\varrho^2 + \lambda(ip + \nu n^2) + \nu(ip + \lambda n^2)}{\lambda\nu} = \frac{\varrho^2 + i(\lambda + \nu)p + 2\lambda\nu n^2}{\lambda\nu}$$

$$\beta = -\frac{(ip + \lambda n^2)(ip + \nu n^2)}{\lambda\nu} = \frac{p^2 - i(\lambda + \nu)pn^2 - \lambda\nu n^4}{\lambda\nu}$$

$$r^2 = -\frac{ip + \nu n^2 + \nu k^2}{ip + \lambda n^2 + \lambda k^2}$$

In a plane case

$$I = 1, \quad \bar{I}_1 = \frac{4}{\pi}, \quad \bar{I}_2 = 0, \quad \bar{I}_3 = -\frac{4}{3\pi} \ldots\ldots$$

In a cylindrical case

$$I = \frac{y_1}{y}, \quad \bar{I} = \frac{\pi^2 n^2}{(L^2 - 1)} \int_{y_1}^{y_2} y_1 \epsilon \, dy$$

$$\int_{y_1}^{y_2} \epsilon \, dy = \frac{1}{n} \left(Y_o(ny) J_1(ny_1) - J_o(ny) Y_1(ny_1) \right)_{y_1}^{y_2}$$

Also

$$Y_o(ny_1) J_1(ny_1) + J_o(ny_1) Y_1(ny_1) = \frac{2}{\pi n y_1} ,$$

$$\frac{J_1(ny_1)}{J_1(ny_2)} = \frac{Y_1(ny_1)}{Y_1(ny_2)} = L,$$

whence

$$\bar{Y} = \frac{\pi y_1}{L^2 - 1} \left(\frac{L}{y_2} - \frac{1}{y_1} \right) = \pi \frac{\frac{L}{C} - 1}{L^2 - 1} , \quad C = \frac{y_2}{y_1} .$$

Using the dimensionless variables

$$X = \frac{x}{d} , \quad Y = \frac{y}{d} , \quad P = \frac{pd}{c} , \quad \Lambda = \frac{\lambda}{cd} , \quad \mathrm{N} = \frac{\nu}{cd} ,$$

$$N = nd, \quad K = kd,$$

we now have, where $N \sim 1$, ΛP, $\mathrm{N} P \ll 1$,

$$K_1^2 \doteq \frac{P^2 - i(\Lambda + \mathrm{N}) P N^2 - \Lambda \mathrm{N} N^4}{1 + i(\Lambda + \mathrm{N}) P + 2 \Lambda \mathrm{N} N^2} , \quad K_2^2 \doteq - \frac{1 + i(\Lambda + \mathrm{N}) P + 2 \Lambda \mathrm{N} N^2}{\Lambda \mathrm{N}}$$

$$r_1^2 \doteq - \frac{1 + i \Lambda P + \Lambda \mathrm{N} N^2}{1 + i \mathrm{N} P + \Lambda \mathrm{N} N^2} , \quad r_2^2 \doteq - \frac{1 + i \mathrm{N} P + \Lambda \mathrm{N} N^2}{1 + i \Lambda P + \Lambda \mathrm{N} N^2} \frac{\mathrm{N}}{\Lambda}$$

or with second order error

$$K_1 = P \left(\frac{1 - i(\Lambda + \mathrm{N}) \frac{N^2}{P}}{1 + i(\Lambda + \mathrm{N}) P} \right)^{\frac{1}{2}} , \quad K_2 = i \left(\frac{1 + i(\Lambda + \mathrm{N}) P}{\Lambda \mathrm{N}} \right)^{\frac{1}{2}}$$

and with first order error

$$r_1 = -i, \quad r_2 = -i \left(\frac{\mathrm{N}}{\Lambda} \right)^{\frac{1}{2}}$$

Also

$$a = \frac{iP}{iP+\Lambda N^2}$$

or with first order error

$$a = 1.$$

Then putting

$$Q = \frac{1}{(\Lambda N)^{\frac{1}{2}}}, \quad \gamma = \left(\frac{N}{\Lambda}\right)^{\frac{1}{2}}, \quad 2\theta = (\Lambda+N)P, \quad 2\beta = (\Lambda+N)\frac{N^2}{P},$$

$$K_1 \doteq P(1 - i(\theta+\beta)), \qquad K_2 \doteq iQ(1+i\theta)$$

the one-dimensional analysis holds with $\theta+\beta$ replacing θ in K_1.

The amplitude of the wave term of $\bar{Z}$ at resonance assuming $\gamma < 1$, will be

$$\frac{I}{(\theta+\beta)P+\gamma}$$

At the fundamental resonance $P = \frac{\pi}{2}$.

For a plane case for which $\frac{e}{d} = E$, $N = \frac{\epsilon\pi}{2E}$, then also

$$\beta = \frac{\epsilon^2\theta}{E^2}.$$

Thus if $\gamma \sim \theta$, $E \sim 1$, the first term of the expansion will be dominant because of the rapid increase in β, and the profile along the y axis will approximate to a sine wave. If on the other hand $\gamma \gg \theta$, or $E \gg 1$, each of the

earlier terms will be nearly the same multiple of $\bar{I}$, so they will add up to a multiple of I. Except for boundary layers near the walls, where the higher terms become important, the profile will therefore be flat. Also, if $\gamma \sim \theta$, the amplitude will fall off rapidly if E falls below one, by virtue of the factors

$$1 + \frac{1}{E^2}, \quad 1 + \frac{9}{E^2} \ldots\ldots$$

In the case of a cylindrical system, when $y_1 \to 0$ the terms of the solution involving the Neumann function Y_1 disappear because $Y_1(ny_1) \to \infty$ at 0, and when $y_1 \to \infty$ the solution $\to$ the solution for a plane system. Now the zeros n of $J_1(ny_2)$ aproach $\frac{(\epsilon + \frac{1}{4})\pi}{y_2}$ asymptotically from below, and for a plane system the zeros are $\frac{\epsilon\pi}{y_2 - y_1}$. Thus in general n lies at a point between $\frac{\epsilon\pi}{y_2 - y_1}$ and $\frac{(\epsilon + \frac{1}{4})\pi}{y_2 - y_1}$ which depends on $\frac{y_2}{y_1}$.

The remarks on side wall damping for a plane system therefore apply equally to a cylindrical system, with n slightly greater than before.

When ν or $\lambda = 0$ some of the characteristics of the behaviour are easier to distinguish.

With $\nu = 0$ the equations for a plane case reduce to

$$(ip - (\lambda + \frac{c^2}{ip}) \frac{\partial^2}{\partial x^2} - \lambda \frac{\partial^2}{\partial y^2})H = 0$$

The solution becomes

$$\bar{Z} = a\bar{I}\left(\frac{\cos kx}{\cos kd} - 1\right)$$

$$a = \frac{ip}{ip + \lambda n^2}, \qquad k^2 = \frac{p^2 - i\lambda n^2 p}{c^2 + i\lambda p}$$

Since, however, there is no longer a boundary condition U, it become possible to separate the variable x, and to obtain an alternative picture of the solution as an expansion in eigenfunctions of x which can now meet the necessary boundary conditions. This will emphasize the different characteristics of the behaviour.

The required functions are

$\mathfrak{D}(x) = \cos mx$ or $\sin mx$,

m a zero of $\cos md$ or $\sin md$,

satisfying

$$\mathfrak{D}'' = -m^2\mathfrak{D}$$

If the system is symmetrical about $y = 0$ the sine terms will vanish.

We now put for a plane case

$$H = I + Z, \quad I = \Sigma \bar{I}_\delta \mathfrak{D}_\delta, \quad Z = \Sigma \bar{Z}_\delta \mathfrak{D}_\delta$$

where

$$\bar{I}_1 = \frac{4}{\pi}, \quad \bar{I}_2 = 0, \quad \bar{I}_3 = -\frac{4}{3\pi}, \quad \ldots\ldots$$

Then the equations are satisfied if

$$(ip + (\lambda + \frac{c^2}{ip})m^2 - \lambda \frac{\partial^2}{\partial y^2})\bar{Z} = - ip\bar{I}$$

$$\bar{Z} = - a\bar{I}(1 - \frac{\cosh ky}{\cosh ke}) ,$$

$$a = \frac{ip}{ip + \lambda m^2 + \frac{c^2 m^2}{ip}} , \quad k^2 = \frac{ip}{\lambda} + m^2 + \frac{c^2 m^2}{i\lambda p}$$

When $p = cm_1, cm_3, \ldots\ldots$

$$a_1 = \frac{c}{\lambda m_1} , \quad a_3 = \frac{c}{\lambda m_3} \quad \ldots\ldots$$

whereas normally, since $\frac{p}{\lambda}$, $\frac{c^2 m^2}{\lambda p} \gg m^2$ for the lower values of m, a is much smaller. The resonance is thus revealed in an increase of the multiplier of the relevant term.

Also for these values of p

$$k_1 = m_1, \quad k_3 = m_3 \quad \ldots\ldots$$

whereas normally k is much greater.

The region of y variation $\sim \frac{1}{k}$. Thus normally this region is a thin layer near the wall, but at resonance it expands to a width $\sim \frac{d}{\delta}$, δ depending on which resonance.

A second alternative is a double expansion

$$H = I + Z, \quad I = \Sigma \bar{I}_{\delta\epsilon} \mathfrak{D}_\delta \mathfrak{E}_\epsilon \ , \quad Z = \Sigma \bar{Z}_{\delta\epsilon} \mathfrak{D}_\delta \mathfrak{E}_\epsilon$$

$$(ip + (\lambda + \frac{c^2}{ip})m^2 + \lambda n^2)\bar{Z} = - ip\bar{I} \ ,$$

$$\bar{Z} = - a\bar{I}, \quad a = \frac{ip}{ip + \lambda(m^2+n^2) + \frac{c^2m^2}{ip}}$$

$\bar{I}_\delta$ is the product of the earlier $\bar{I}_\delta$ and $\bar{I}_\epsilon$ (pages 45, 41–2). For a plane case for which $\frac{e}{d} = E$,

$$\frac{n_\epsilon}{m_\delta} = \frac{\epsilon}{\delta E}$$

and resonance is again revealed by an increase in the value of the relevant multiplier. Thus when $p = cm_1, cm_3 \ldots\ldots$,

$$a_{11} = \frac{ic}{\lambda m_1(1 + \frac{1}{E^2})}, \quad a_{31} = \frac{ic}{\lambda m_3(1 + \frac{1}{9E^2})} \ \ldots\ldots$$

Taking $E = 1$, at the first resonance

$$a_{11} : a_{13} : a_{15} \ldots\ldots = \frac{1}{1+1} : \frac{1}{1+9} : \frac{1}{1+25} \ldots\ldots$$

whereas normally since $\frac{p}{\lambda m^2} \gg 1$ for the lower values of m

$$a_{11} : a_{13} : a_{15} \ldots\ldots = 1 : 1 : 1 \ldots\ldots$$

this corresponding to the thickening of the boundary layer at resonance revealed by the earlier representation.

The results of numerical calculations are given in Figures 3.8 – 3.13. In every case the fluid is taken to be inviscid. Figures 3.8 and 3.9 show the effect of side walls on the field at the centre line $X = 0$ for plane systems of different width for which $\wedge = .01$ and $.1$. In either case the rapid fall off of performance as the ratio $E = \frac{e}{d}$ falls below 1 is apparent. If $E > 2$ the performance approaches the one-dimensional performance. Figures 3.10 and 3.11 show the extension outwards of the side wall effect to distances of about d and $\frac{d}{3}$ at the fundamental and first harmonic resonances for a plane system of square section for which $\wedge = .01$. To obtain a flat profile at the fundamental resonance the width would have to be several times the depth. Figures 3.12 and 3.13 show the effect of the torus radius ratio on the field at the centre line $X = 0$ at first resonance for systems of square section for which $\wedge = .01$ and $.1$. The field at the inner boundary is taken as the same for each case, and the displacement inwards of the point of maximum field disturbance as $\frac{r_2}{r_1}$ increases is apparent. However, the ratio of the field at the section centre point to the field at the same point in an air gap hardly declines from about

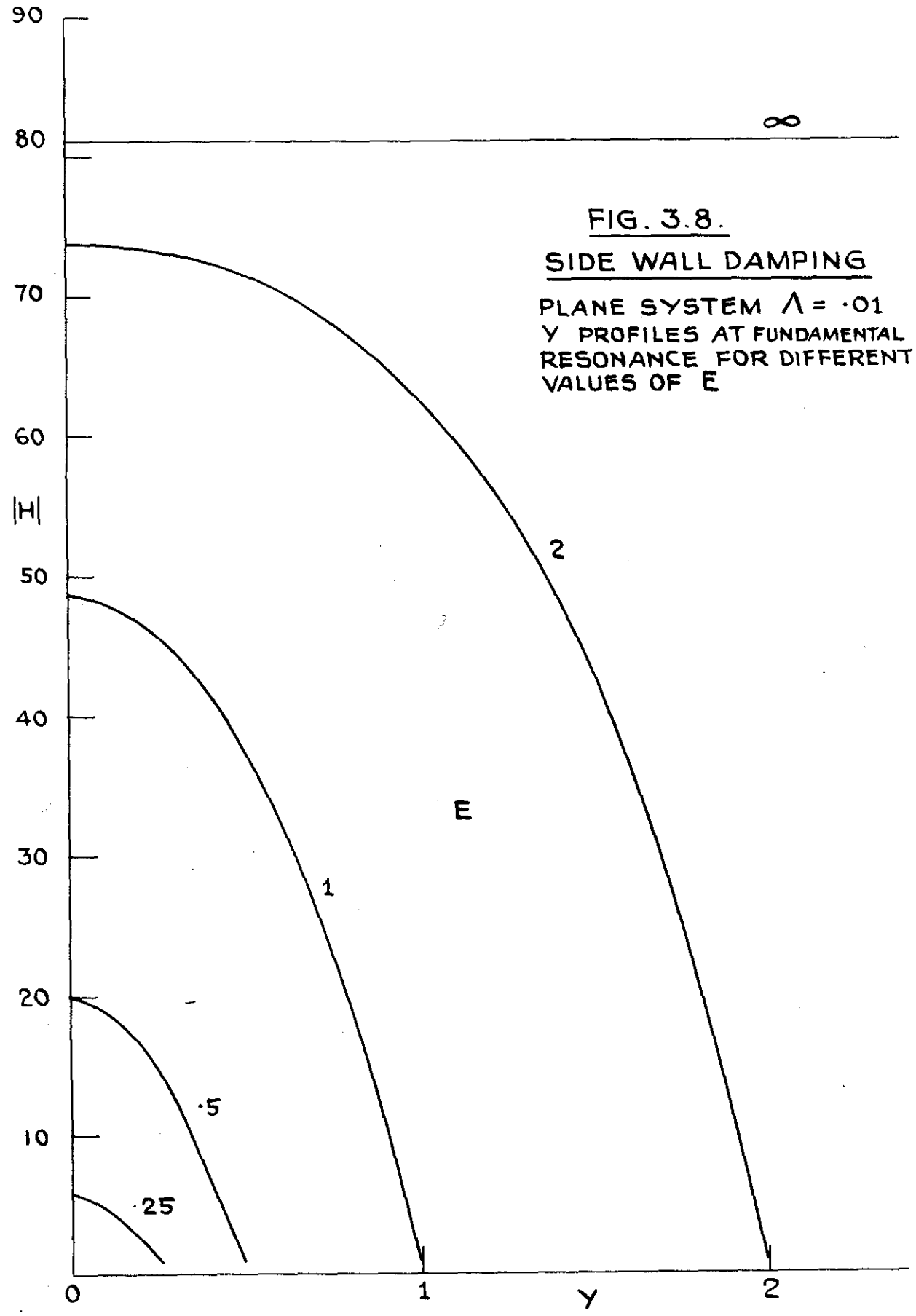

FIG. 3.8.

SIDE WALL DAMPING

PLANE SYSTEM $\Lambda = \cdot 01$
Y PROFILES AT FUNDAMENTAL RESONANCE FOR DIFFERENT VALUES OF E

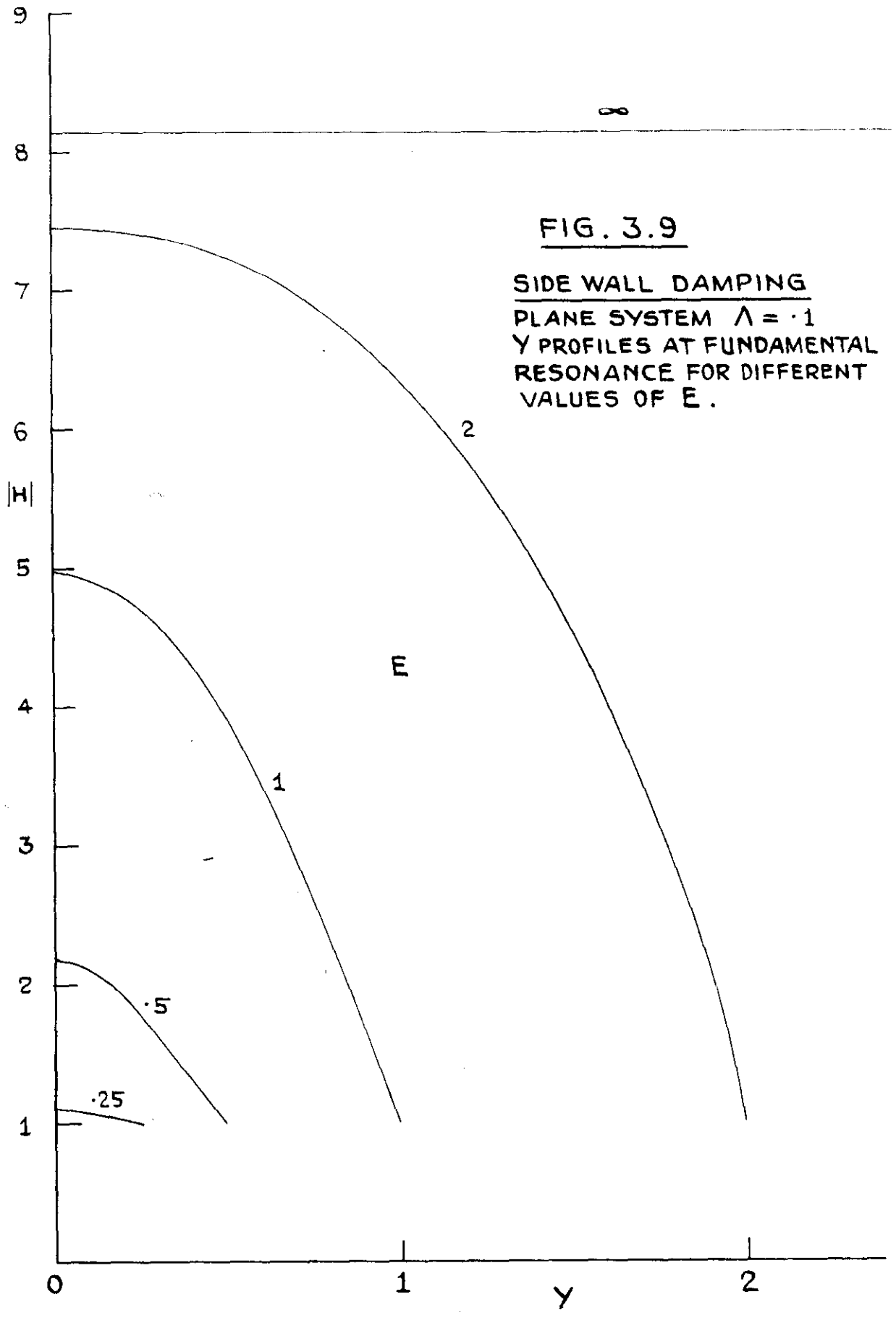

FIG. 3.9

SIDE WALL DAMPING

PLANE SYSTEM $\Lambda = \cdot 1$

Y PROFILES AT FUNDAMENTAL RESONANCE FOR DIFFERENT VALUES OF E.

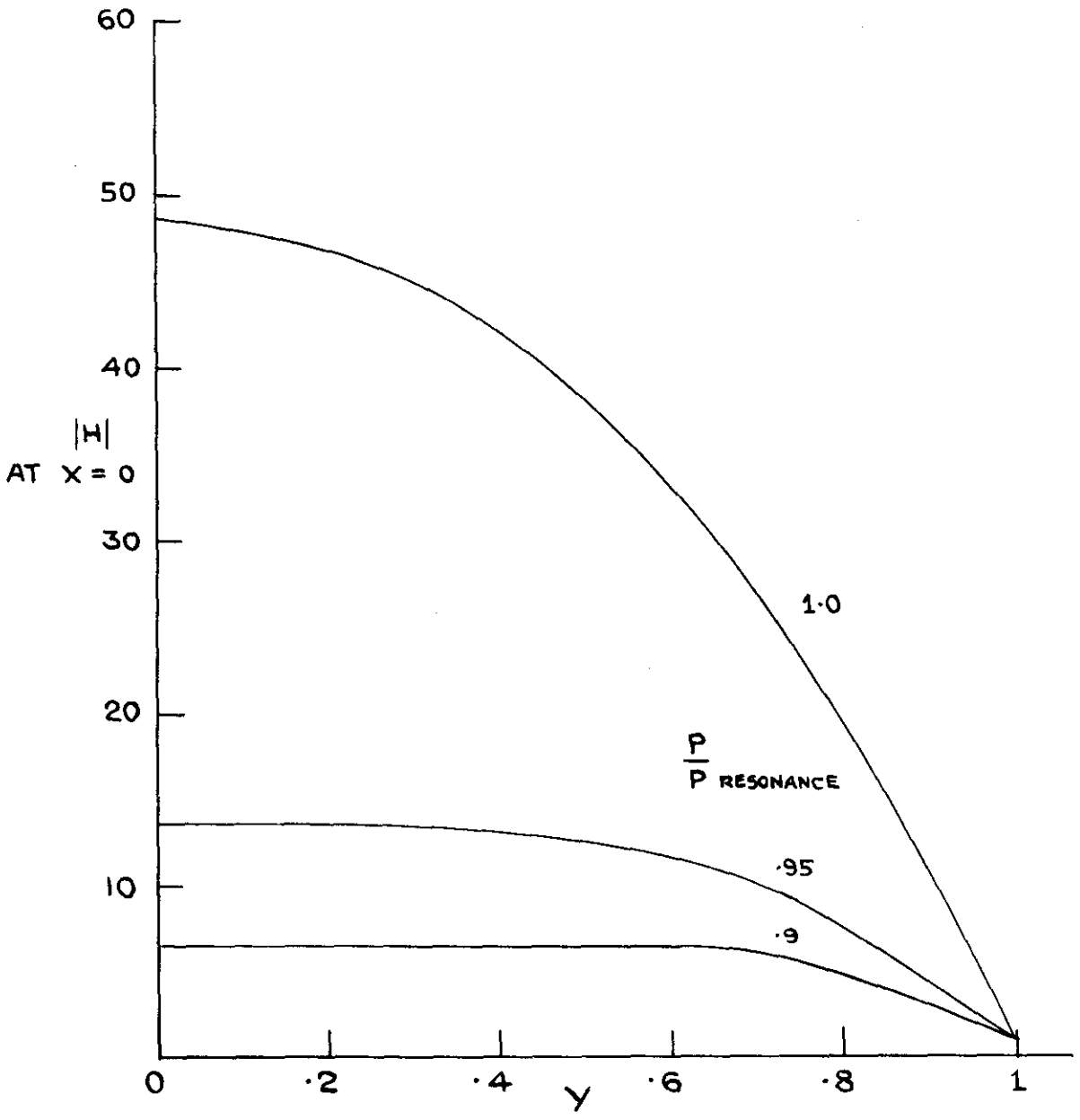

FIG. 3.10

BOUNDARY LAYER THICKENING AT FUNDAMENTAL RESONANCE Y PROFILES AT X = 0 FOR FREQUENCIES APPROACHING RESONANT FREQUENCY

PLANE SYSTEM $\Lambda = \cdot 01$ $N = 0$ $E = 1$

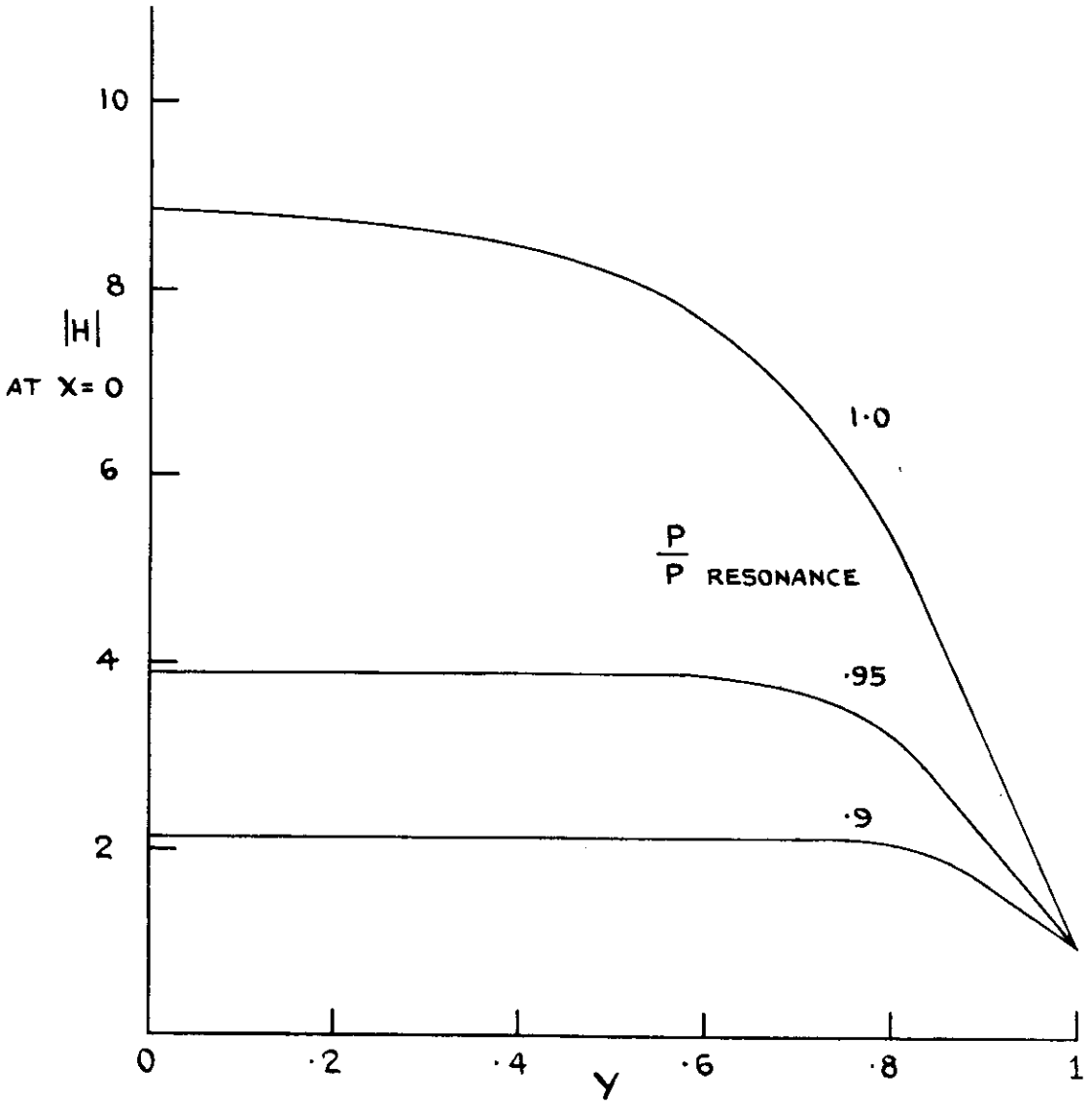

FIG. 3.11

BOUNDARY LAYER THICKENING AT FIRST HARMONIC RESONANCE Y PROFILES AT X = 0 FOR FREQUENCIES APPROACHING RESONANT FREQUENCY.

PLANE SYSTEM $\Lambda = \cdot 01$ $N = 0$ $E = 1$

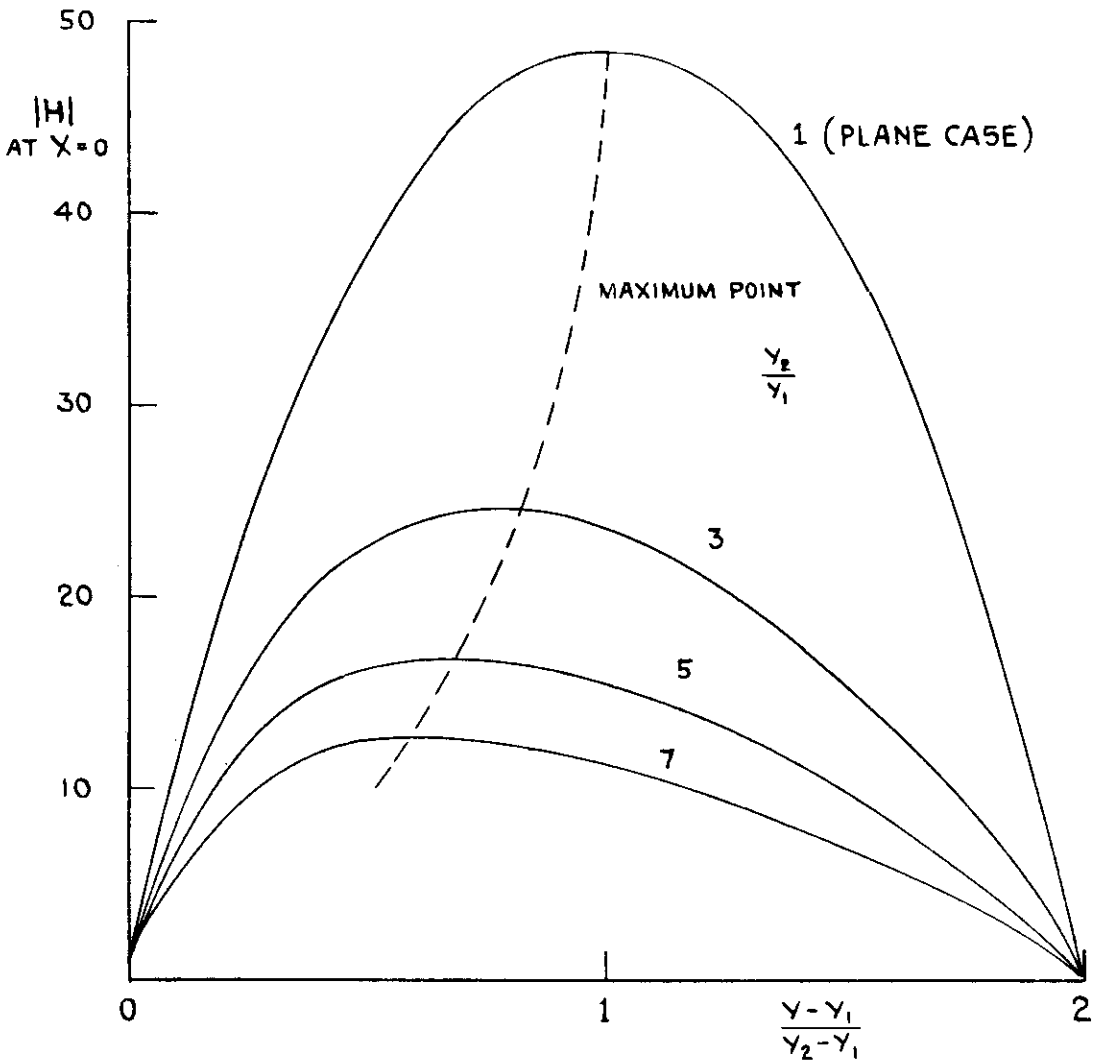

FIG. 3.12. EFFECT OF TORUS RADIUS RATIO ON AXIAL SYSTEMS Y PROFILES AT X = 0 FOR DIFFERENT RADIUS RATIOS AT FUNDAMENTAL RESONANCE.

$P = \frac{\pi}{2}$ $\Lambda = \cdot 01$ $N = 0$ $E = 1$

INNER BOUNDARY VALUE $H = 1$

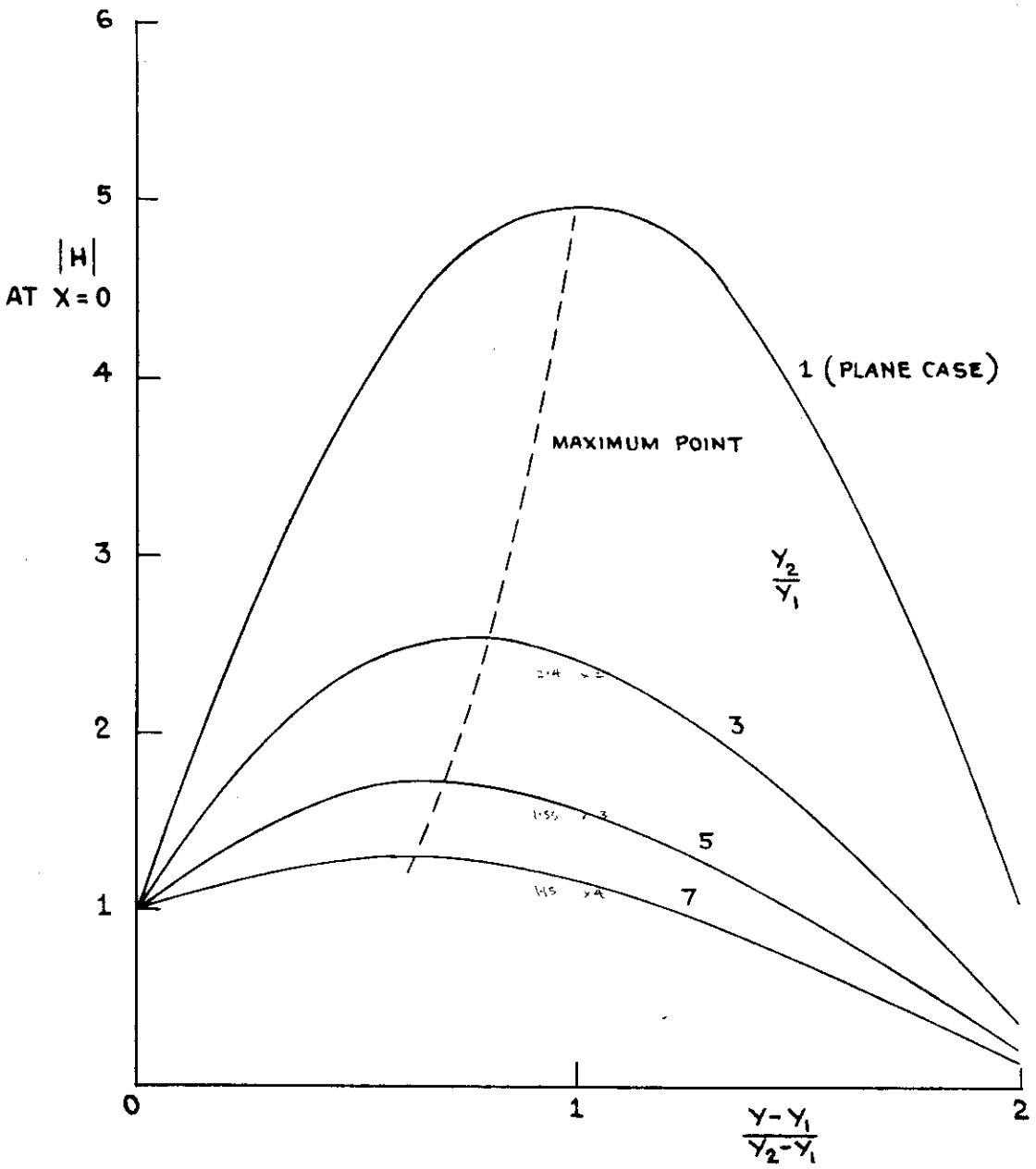

FIG. 3.13. EFFECT OF TORUS RADIUS RATIO ON AXIAL SYSTEMS Y PROFILES AT X = 0 FOR DIFFERENT RADIUS RATIOS AT FUNDAMENTAL RESONANCE.

$P = \frac{\pi}{2}$ $\Lambda = \cdot 1$ $N = 0$ $E = 1$

INNER BOUNDARY VALUE $H = 1$

48 as $\frac{Y_2}{Y_1}$ increases from 1 when $\Lambda = .01$, and declines only slightly from about 4.9 when $\Lambda = .1$, so the true effect of torus radius ratio is not great in this range.

In Lehnert's experiment E was .27, so that side wall damping dominated the experiment.

3.8 The effect of conducting material at a boundary.

The presence of conducting material at a boundary will alter the performance of the system. The effect on a magnetically excited system can be illustrated by the case $\nu = 0$.

Consider first a one-dimensional system with conducting slabs inserted between the existing current sheet and the fluid.

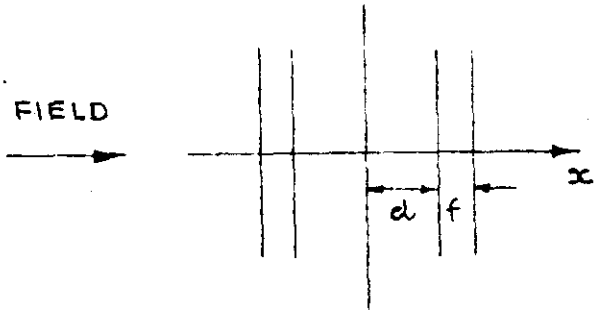

ONE - DIMENSIONAL SYSTEM

Fig.3.14

Denoting the fluid by a suffix a, the walls by a suffix b,

$$(ip - \lambda_a \frac{\partial^2}{\partial x^2}) H_a = c \frac{\partial U_a}{\partial x} ,$$

$$ip\, U_a = c \frac{\partial H_a}{\partial x} ,$$

$$(ip - (\lambda_a + \frac{c^2}{ip}) \frac{\partial^2}{\partial x^2}) H_a = 0 ,$$

$$(ip - \lambda_b \frac{\partial^2}{\partial x^2}) H_b = 0 ,$$

$H_b = 1$ at the outer surface,

$$H_a = H_b,\ \lambda_a \frac{\partial H_a}{\partial x} + c\, U_a = (\lambda_a + \frac{c^2}{ip}) \frac{\partial H_a}{\partial x} = \lambda_b \frac{\partial H_b}{\partial x}$$

at the joining surface.

The last condition derives from continuity of the tangential component of $\underline{E}$ (2.2).

The differential equations give

$$H_a = A \cos kx ,$$

$$k^2 = \frac{p^2}{c^2 + i \lambda_a p} ,$$

$$H_b = B_1 e^{jx'} + B_2 e^{-jx'} ,$$

$$x' = d + f - x, \quad x + ve, \quad j^2 = \frac{ip}{\lambda_b} .$$

To satisfy the boundary conditions

$$B_1 + B_2 = 1$$

$$B_1 e^{jf} + B_2 e^{-jf} = A \cos kd,$$

$$B_1 e^{jf} - B_2 e^{-jf} = s A \sin kd,$$

$$s = \frac{\sigma^2 + i\lambda_a p}{i\lambda_b p} \frac{k}{j} = \frac{-ip}{\lambda_b jk} \quad \left(\frac{\partial}{\partial x'} = -\frac{\partial}{\partial x}\right),$$

$$2B_1 = A (\cos kd + s \sin kd) e^{-jf},$$

$$2B_2 = A (\cos kd - s \sin kd) e^{jf},$$

$$B_1 + B_2 = A (\cosh jf \cos kd - s \sinh jf \sin kd) = 1,$$

$$H_a = \frac{\cos kx}{\cosh jf \cos kd - s \sinh jf \sin kd}$$

The solution, denoted by a suffix o, for a simple system without the slabs is

$$H_o = \frac{\cos kx}{\cos kd}$$

The phasor for the corresponding flux acting on one wall is $(\mu\rho)^{\frac{1}{2}} \int_o^d H \, dx$, and the exciting current is $\left(\frac{\rho}{\mu}\right)^{\frac{1}{2}}$, so the flux phasor for unit exciting current is

$$\Phi_o = \mu \int_o^d H \, dx = \frac{\mu \tan kd}{k}$$

In terms of this therefore

$$s \tanh kd = \frac{sk\Phi_o}{2} = -\frac{ip\Phi_o}{2\lambda_b j}$$

Hence, representing the wall resistance/unit length by

$$R = \frac{\tau_b}{f} = \frac{2\lambda_b}{f} ,$$

$$\frac{H}{H_o} = \frac{1}{\cosh jf + \frac{ip\Phi_o}{R}\frac{\sinh jf}{jf}} \rightarrow \frac{1}{1 + \frac{ip\Phi_o}{R}} \quad \text{as} \quad jf \rightarrow 0.$$

H is reduced by the currents which are induced in the slabs by the alternating flux, the reduction being greater at resonance, when Φ_o is large.

When the slabs are thin enough for skin effect not to be important, so that the current flow can be assumed uniform in them, the approximate result can be obtained directly. Suppose the system is excited by a current I_1, and a current I_2 flows in the slabs. Then with Φ defined as the flux phasor for unit exciting current

$$I_2 R = ip\, I_2 \Phi ,$$

$$\frac{H}{H_o} = \frac{\Phi}{\Phi_o} = \frac{I_1 - I_2}{I_1} = 1 - \frac{ip\Phi}{R} ,$$

$$\Phi + \frac{ip}{R}\Phi\Phi_o = \Phi_o ,$$

$$\frac{H}{H_o} = \frac{1}{1 + \frac{ip\Phi_o}{R}}$$

In a plane or axial system slabs may be placed either at the end or at the side boundaries

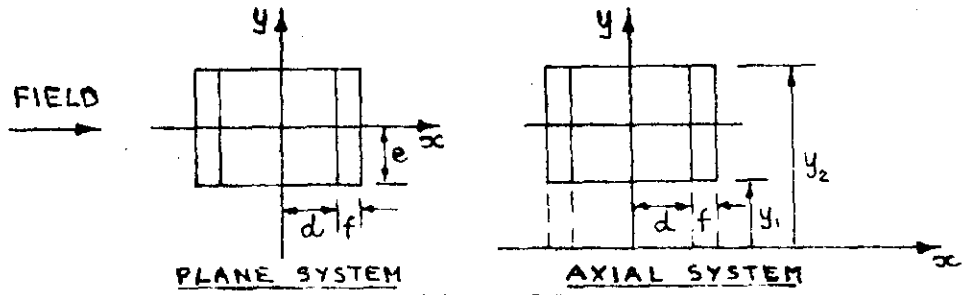

Fig.3.15

With end slabs the equations for a plane system are

$$(ip - (\lambda_a + \frac{c^2}{ip}) \frac{\partial^2}{\partial x^2} - \lambda_a \frac{\partial^2}{\partial y^2}) H_a = 0$$

$$(ip - \lambda_b \frac{\partial^2}{\partial x^2} - \lambda_b \frac{\partial^2}{\partial y^2}) H_b = 0$$

$H_b = 1$ at the outer surface, $H_a = 1$ at the sides,

$$H_a = H_b, \quad \lambda_a \frac{\partial H_a}{\partial x} + cU_a = (\lambda_a + \frac{c^2}{ip}) \frac{\partial H_a}{\partial x} = \lambda_b \frac{\partial H_b}{\partial x}$$

at the joining surface.

For an axial system $\frac{\partial^2}{\partial y^2}$ is replaced by $\frac{\partial^2}{\partial y^2} + \frac{1}{y} \frac{\partial}{\partial y} - \frac{1}{y^2}$ and the outer boundary value is $\frac{y_1}{y}$ instead of 1.

We can now proceed as in 3.7, using the same representation for both regions to eliminate y.

Writing I for 1 or $\frac{y_1}{y}$, we put

$$H = I + Z, \quad I = \Sigma \bar{I}_a \epsilon_a, \quad Z = \Sigma \bar{Z}_a \epsilon_a$$

where the eigenfunctions $\epsilon(y)$ satisfy

$$\epsilon'' = -n^2 \epsilon \quad \text{or} \quad \epsilon'' + \frac{\epsilon'}{y} - \frac{\epsilon}{y^2} = -n^2 \epsilon,$$

n having a value such that

$$\epsilon(y_1) = \epsilon(y_2) = 0,$$

and $\bar{I}$ takes the same value as before. (pages 41–42)

The solution is now similar to the one-dimensional solution.

The differential equations are satisfied if

$$(ip + \lambda_a n^2 - (\lambda_a + \frac{e^2}{ip}) \frac{\partial^2}{\partial x^2}) \; Z_a = -ip \bar{I}$$

$$(ip + \lambda_b n^2 - \lambda_b \frac{\partial^2}{\partial x^2}) \; Z_b = -ip \bar{I}$$

$$Z_a = A \cos kx - a\bar{I}$$

$$Z_a = \frac{ip}{ip + \lambda_a n^2}, \quad k^2 = \frac{p^2 - i\lambda_a n^2 p}{c^2 + i\lambda_a p}$$

$$Z_b = B_1 e^{jx'} + B_2 e^{-jx'} - b\bar{I},$$

$$x' = d + f - x, \; x + ve, \quad b = \frac{ip}{ip + \lambda_b n^2}, \quad j^2 = \frac{ip}{\lambda_b} + n^2$$

The boundary conditions are satisfied if

$$B_1 + B_2 = b\bar{I}$$

$$B_1 e^{jf} + B_2 e^{-jf} = A \cos kd + (b-a)\bar{I}$$

$$B_1 e^{jf} - B_2 e^{-jf} = s A \sin kd$$

$$s = \frac{\lambda_a + \frac{c^2}{ip}}{\lambda_b} \frac{k}{j} = - \frac{ip}{\lambda_b a j k} ,$$

$$\bar{I} (a \cosh jf + b(1-\cosh jf)) = A(\cosh jf \cos kd - s \sinh jf \sin kd)$$

$$\bar{Z}_a = a\bar{I} \left(\frac{1 + \frac{b}{a}(\operatorname{sech} jf - 1)}{1 - s \tanh jf \tan kd} \frac{\cos kx}{\cos kd} - 1\right)$$

The effect of the slabs is exhibited in the factor

$$\gamma = \frac{1 + \frac{b}{a}(\operatorname{sech} jf - 1)}{1 - s \tanh jf \tan kd}$$

which acts on the principal term $\frac{\cos kx}{\cos kd}$ of the solution for $\bar{Z}_a$. As $\lambda_b \to \infty$, $b \to 0$, $s \to 0$, $\gamma \to 1$, giving the solution for a system without the slabs (3.7, page 45). As $\lambda_b \to 0$, $b \to 1$, $s \to \infty$, $\gamma \to 0$; the solution for H_a is then the solution of the equations with the x variation terms deleted, just the solution for a simple side skin effect. The slabs thus detract from the performance, as in the one-dimensional case. Now $\frac{\tan kd}{k}$ corresponds to the alternating flux of the particular term of the expansion, and

the reduction in performance will again be greater at resonance.

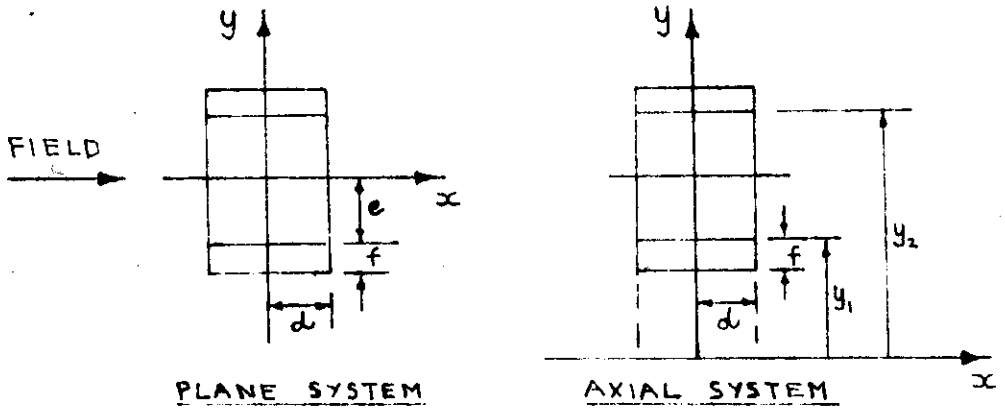

Fig.3.16

With side slabs the equations of a plane system are

$$(ip - (\lambda_a + \frac{c^2}{ip})\frac{\partial^2}{\partial x^2} - \lambda_a \frac{\partial^2}{\partial y^2})H_a = 0$$

$$(ip - \lambda_b \frac{\partial^2}{\partial x^2} - \lambda_b \frac{\partial^2}{\partial y^2})H_b = 0$$

$H_b = 1$ at the outer surface, $H_a = 1$ at the ends.

$H_a = H_b$, $\lambda_a \frac{\partial H_a}{\partial x} = \lambda_b \frac{\partial H_b}{\partial x}$ at the joining surface,

these differing from the earlier equations in that there is no $\underline{u} \times \underline{B}$ term in the condition for $\underline{E}$.

Again the equations of an axial system are obtained by replacing $\frac{\partial^2}{\partial y^2}$ by $\frac{\partial^2}{\partial y^2} + \frac{1}{y}\frac{\partial}{\partial y} - \frac{1}{y^2}$, and the outer boundary value 1 by $\frac{y_1}{y}$.

The appropriate representation is now in eigenfunctions

of x. For the plane case we put

$$H = 1 + Z, \quad 1 = \Sigma \bar{I}_\delta \Phi_\delta, \quad Z = \Sigma \bar{Z}_\delta \Phi_\delta,$$

where the eigenfunctions are

$$\Phi(x) = \cos mx \quad \text{or} \quad \sin mx$$

satisfying

$$\Phi'' = -m^2 \Phi.$$

For these

$$\bar{I}_1 = \frac{4}{\pi}, \quad \bar{I}_2 = 0, \quad \bar{I}_3 = -\frac{4}{3\pi}, \ \ldots\ldots$$

the sine terms dropping out by symmetry.

The differential equations are now satisfied if

$$(ip + (\lambda_a + \frac{c^2}{ip})m^2 - \lambda_a \frac{\partial^2}{\partial y^2})\bar{Z}_a = -ip\bar{I}$$

$$(ip + \lambda_b m^2 - \lambda_b \frac{\partial^2}{\partial y^2})\bar{Z}_b = -ip\bar{I}$$

$$\bar{Z}_a = A \cosh ky - a\bar{I}$$

$$a = \frac{ip}{ip + \lambda_a m^2 + \frac{c^2 m^2}{ip}}, \quad k^2 = \frac{ip}{\lambda_a} + m^2 + \frac{c^2 m^2}{i\lambda_a p},$$

$$\bar{Z}_b = B_1 e^{jy'} + B_2 e^{-jy'} - b\bar{I}$$

$$y' = e + f - y, \quad y + ve, \quad b = \frac{ip}{ip + \lambda_b m^2}, \quad j^2 = \frac{ip}{\lambda_b} + m^2$$

The boundary conditions are satisfied if

$$B_1 + B_2 = b\bar{I}$$

$$B_1 e^{jf} + B_2 e^{-jf} = A \cos ke + (b-a)\bar{I}$$

$$B_1 e^{jf} - B_2 e^{-jf} = - s A \sinh ke$$

$$s = \frac{\lambda_a k}{\lambda_b j} = \frac{ip}{\lambda_b ajk}$$

$$\bar{I}\,(a\cosh jf + b(1-\cosh jf)) = A(\cosh jf\cosh ke + s\sinh jf\sinh ke)$$

$$\bar{Z}_a = - a\bar{I}\left(1 - \frac{1 + \frac{b}{a}(\operatorname{sech} jf - 1)}{1 + s\tanh jf \tanh ke}\,\frac{\cosh ky}{\cosh ke}\right)$$

In this case the effect of the slabs is again represented by a factor

$$\gamma = \frac{1 + \frac{b}{a}(\operatorname{sech} jf - 1)}{1 + s\tanh jf \tanh ke}$$

but the term $\frac{\cosh ky}{\cosh ke}$ on which it acts is no longer the principal term, but the side wall damping term, resonant effects being exhibited by changes in a (3.7, page 46). As $\lambda_b \to \infty$, $b \to 0$, $s \to 0$, $\gamma \to 1$, giving the solution for a system without the slabs (3.7, page 46). As $\lambda_b \to 0$, $b \to 1$, $s \to \infty$, $\gamma \to 0$, this now resulting in the same solution for H_a as would be obtained with the y instead of the x variation terms deleted, just the one-dimensional solution. Side slabs thus

suppress the side wall damping and improve the performance. This is because there is no component of $\underline{u} \times \underline{B}$ along the slabs, so that the continuity of the tangential component of $\underline{E}$ at the boundary implies a current flow in the slabs in the same sense as in the fluid, helping the build up of the field towards the centre: with end slabs on the other hand, the $\underline{u} \times \underline{B}$ term causes a quite different current flow in the fluid to that in the walls.

The conclusions for an axial system would be the same, the y terms now being expressed with Bessel functions instead of elementary functions.

If the system is completely surrounded by conducting material it is no longer possible to produce a solution with separated variables. However because of the different nature of the current flow in end and side slabs, the one being in a sense to reduce the performance, the other in a sense to increase it, caused by the presence or absence of a component of $\underline{u} \times \underline{B}$ along the boundary, the end and side slabs should act nearly independently, the current in each flowing into the sodium, so that separate estimates can be made of the effect of each.

In the case of end slabs but not in the case of side slabs it is possible to extend the solution to take into account viscosity, it still being possible to satisfy the boundary conditions with an eigenfunction representation. The equations for a plane system are

$$(ip - \lambda_a (\frac{\partial^2}{\partial x^2} + \frac{\partial^2}{\partial y^2}))H_a = c \frac{\partial U_a}{\partial x}$$

$$(ip - \nu_a (\frac{\partial^2}{\partial x^2} + \frac{\partial^2}{\partial y^2}))U_a = c \frac{\partial H_a}{\partial x}$$

$$(ip - \lambda_b (\frac{\partial^2}{\partial x^2} + \frac{\partial^2}{\partial y^2}))H_b = 0$$

$H_b = 1$ at the outer surface, $H_a = 1$ at the sides,

$H_a = H_b$, $\lambda_a \frac{\partial H_a}{\partial x} = \lambda_b \frac{\partial H_b}{\partial x}$ at the joining surface,

$U_a = 0$ at the sides and joining surface.

For an axial system $\frac{\partial^2}{\partial y^2}$ is replaced by $\frac{\partial^2}{\partial y^2} + \frac{1}{y}\frac{\partial}{\partial y} - \frac{1}{y^2}$

outer boundary value of 1 by $\frac{y_1}{y}$ as before.

The procedure is unchanged.

Writing I for 1 or $\frac{y_1}{y}$ we put

$$H = \bar{I} + Z, \quad I = \sum \bar{I}_\epsilon \mathcal{E}_\epsilon , \quad Z = \sum \bar{Z}_\epsilon \mathcal{E}_\epsilon , \quad U = \sum \bar{U}_\epsilon \mathcal{E}_\epsilon$$

Then the differential equations are satisfied if

$$(ip + \lambda_a n^2 - \lambda_a \frac{\partial^2}{\partial x^2})\bar{Z}_a = c \frac{\partial \bar{U}_a}{\partial x} - ip\bar{I}$$

$$(ip + \nu_a n^2 - \nu_a \frac{\partial^2}{\partial x^2})\bar{U}_a = c \frac{\partial \bar{Z}_a}{\partial x}$$

$$(ip + \lambda_b n^2 - \lambda_b \frac{\partial^2}{\partial x^2})\bar{Z}_b = - ip\bar{I}$$

$$\bar{Z}_a = r_1 A_1 \cosh k_1 x + r_2 A_2 \cosh k_2 x - a\bar{I}$$

$$\bar{U}_a = A_1 \sinh k_1 x + A_2 \sinh k_2 x$$

$$c = \frac{ip}{ip + \lambda_a n^2}$$

$$k^2 = - \alpha \pm (\alpha^2 + \beta)^{\frac{1}{2}}$$

$$2\alpha = \frac{c^2 + i(\lambda_a + \nu_a)p + 2\lambda_a \nu_a n^2}{\lambda_a \nu_a}, \quad \beta = \frac{p^2 - i(\lambda_a + \nu_a)pn^2 - \lambda_a \nu_a n^4}{\lambda_a \nu_a}$$

$$r^2 = \frac{ip + \nu_a n^2 + \nu_a k^2}{ip + \lambda_a n^2 + \lambda_a k^2}$$

$$\bar{Z}_b = B_1 e^{jx'} + B_2 e^{-jx'} - b\bar{I}$$

$$x' = d + f - x, \quad x + ve,$$

$$b = \frac{ip}{ip + \lambda_b n^2}, \quad j^2 = \frac{ip}{\lambda_b} + n^2$$

The boundary conditions are satisfied if

$$B_1 + B_2 = b\bar{I},$$

$$B_1 e^{jf} + B_2 e^{-jf} = r_1 A_1 \cos k_1 d + r_2 A_2 \cos k_2 d + (b-a)\bar{I},$$

$$B_1 e^{jf} - B_2 e^{-jf} = s_1 r_1 A_1 \sin k_1 d + s_2 r_2 A_2 \sin k_2 d,$$

$$0 = A_1 \sin k_1 d + A_2 \sin k_2 d,$$

$$s_1 = \frac{\lambda_a}{\lambda_b}\frac{k_1}{j}, \qquad s_2 = \frac{\lambda_a}{\lambda_b}\frac{k_2}{j},$$

whence

$$\bar{Z}_a = a\bar{I}\left(\frac{(1 + \frac{b}{a}(\operatorname{sech} jf - 1))(\frac{r_1 \cos k_1 x}{\sin k_1 d} - \frac{r_2 \cos k_2 x}{\sin k_2 d})}{r_1(\cot k_1 d - s_1 \tanh jf) - r_2(\cot k_2 d - s_2 \tanh j_2 f)} - 1\right),$$

where in a plane case (page 41)

$$\bar{I}_1 = \frac{4}{\pi}, \quad \bar{I}_2 = 0, \quad \bar{I}_3 = -\frac{4}{3\pi} \ldots\ldots$$

in an axial case (page 42)

$$\bar{I} = \pi \frac{\frac{L}{C} - 1}{L^2 - 1}, \quad C = \frac{y_2}{y_1}, \quad L = \frac{J_1(ny_1)}{J_1(ny_2)} = \frac{Y_1(ny_1)}{Y_1(ny_2)}$$

When $\nu_a \to 0$ $r_2 \to 0$, giving the inviscid solution.

CHAPTER 4.

TRANSIENT THEORY.

4.1 Ideal case.

A representative exciting disturbance for the analysis of transient behaviour is a unit step at the boundary in either the magnetic field or the velocity. Here magnetic excitation will be considered.

For an undamped case the equations

$$\frac{\partial h}{\partial t} = c\frac{\partial u}{\partial x}, \quad \frac{\partial u}{\partial t} = c\frac{\partial h}{\partial x}$$

give for h the general solution

$$h = f(x - ct) + g(x + ct).$$

The unit step boundary condition can then be satisfied by taking h as the sum of the two square waves travelling to the left and right respectively, figure 4.1.

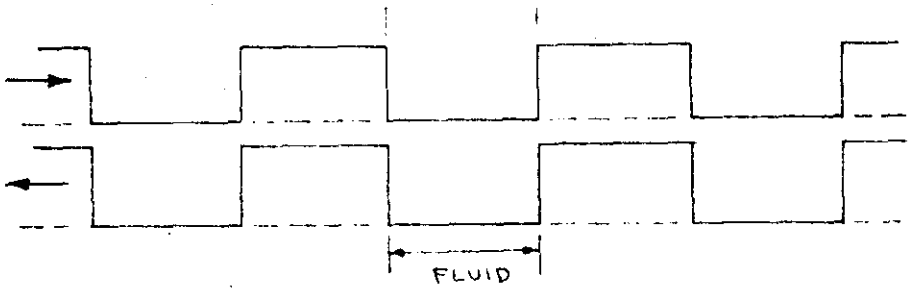

TRAVELLING SQUARE WAVES

Fig. 4.1

The field changes in steps first to the boundary value, then to twice the boundary value, then back to

the boundary value, then to zero, and so on. At the wave fronts there are current sheets, these giving impulses to the fluid by the $\underline{j} \times \underline{B}$ forces in opposite directions, so that when the fronts meet the velocity cancels.

If $\lambda > 0$ such current sheets are impossible, and if $\nu > 0$ velocity steps are impossible; so in either case the wave fronts must disperse.

4.2 General case of a one-dimensional system.

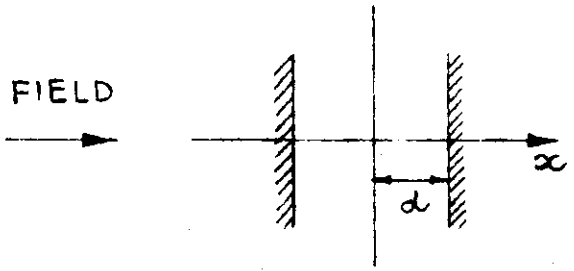

ONE - DIMENSIONAL SYSTEM

Fig.4.2

The general case of a one-dimensional system for which

$$\left(\frac{\partial}{\partial t} - \lambda \frac{\partial^2}{\partial x^2}\right) h = c \frac{\partial u}{\partial x}$$

$$\left(\frac{\partial}{\partial t} - \nu \frac{\partial^2}{\partial x^2}\right) u = c \frac{\partial h}{\partial x}$$

$h = 1$ when $x = \pm d$,

$h = u = 0$ elsewhere when $t = 0$

can be tackled by the use of the Laplace transformation[9] to separate t.

We put

$$\bar{h} = \int_0^\infty h\, e^{-pt}\, dt, \quad \bar{u} = \int_0^\infty u\, e^{-pt}\, dt.$$

Then h and u can be expressed as

$$h = \frac{1}{2\pi i} \int_P \bar{h}\, e^{pt}\, dp, \quad u = \frac{1}{2\pi i} \int_P \bar{u}\, e^{pt}\, dp,$$

where P is a path from $-i\infty$ to $i\infty$ lying to the right of any poles of $\bar{h}$, $\bar{u}$.

Then h and u satisfy the original equations if

$$(p - \lambda \frac{\partial^2}{\partial x^2})\, \bar{h} = c \frac{\partial \bar{u}}{\partial x}$$

$$(p - \nu \frac{\partial^2}{\partial x^2})\, \bar{u} = c \frac{\partial \bar{h}}{\partial x}$$

$$\bar{h} = \frac{1}{p}, \quad \bar{u} = 0 \text{ when } x = \pm d.$$

These are the same as the one-dimensional steady state equations with p replacing ip and give

$$\bar{h} = \frac{1}{p} \frac{\frac{r_1 \cos k_1 x}{\sin k_1 d} - \frac{r_2 \cos k_2 x}{\sin k_2 d}}{r_1 \cot k_1 d - r_2 \cot k_2 d}, \quad \bar{u} = \frac{1}{p} \frac{\frac{\sin k_1 x}{\sin k_1 d} - \frac{\sin k_2 x}{\sin k_2 d}}{r_1 \cot k_1 d - r_2 \cot k_2 d}$$

$$k^2 = -\alpha \pm (\alpha^2 - \beta)^{\frac{1}{2}}$$

$$2\alpha = \frac{c^2 + (\lambda + \nu)\, p}{\lambda \nu}, \quad \beta = \frac{p^2}{\lambda \nu}$$

$$r^2 = -\frac{p + \nu k^2}{p + \lambda k^2}$$

The expressions for $\bar{h}$ and $\bar{u}$ have no branch points because taking the alternative roots for k_1, k_2 changes the numerator and denominator equally.

They have poles when

$$r_1 \cot k_1 d = r_2 \cot k_2 d .$$

Because of the factor $\frac{1}{p}$ the integrals $\int \bar{h}\, e^{pt}\, dp$, $\int \bar{u}\, e^{pt}\, dp$ round a semi-circle to the left closing the path P in the p plane $\to 0$ as the radius of the semi-circle $\to \infty$, so that P can be replaced by the closed loop of P with the semi-circle[9], figure 4.3.

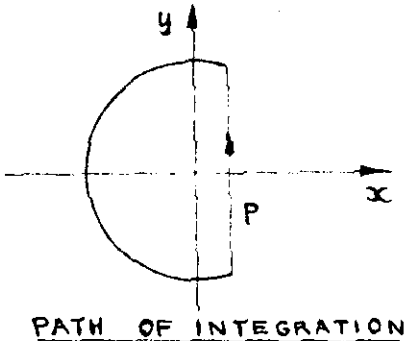

PATH OF INTEGRATION

Fig.4.3

The integrals for h and u can therefore be evaluated as the sums of the residues of the poles of $\bar{h}$ and $\bar{u}$, all of which lie within this loop by the definition of P. Since the poles have to be found by solving transcendental equations the evaluation is difficult.

When $\nu = 0$ the situation is much simpler. The solution for $\bar{h}$ now reduces to

$$\bar{h} = \frac{\cos kx}{p \cos kd}, \qquad k^2 = -\frac{p^2}{c^2 + \lambda p}$$

There are poles when $p = 0$ and when

$$k = \pm m, \quad m = \frac{\pi}{2d}, \frac{2\pi}{2d} \ldots\ldots,$$

that is, when

$$p^2 + \lambda m^2 p + c^2 m^2 = 0,$$

$$p = -a \pm ib$$

$$a = \frac{\lambda m^2}{2}, \quad a^2 + b^2 = c^2 m^2.$$

The residue when $p = 0$ is 1.

Also

$$2k \frac{\partial k}{\partial p} = -\frac{\partial p}{c^2 + \lambda p} + \frac{\lambda p^2}{(c^2 + \lambda p)^2},$$

$$\frac{\partial k}{\partial p} = \frac{k}{p}\left(1 + \frac{\lambda k^2}{2p}\right)$$

Thus when $p = -a + ib$, $k = m$,

$$p \frac{\partial}{\partial p} \cos kd = -pd \frac{\partial k}{\partial p} \sin kd = -md\left(1 + \frac{\lambda m^2}{2p}\right) \sin md$$

$$= \frac{ibmd \sin md}{a - ib}$$

and the residue when $p = -a + ib$ is therefore

$$-\frac{(1-\frac{a}{ib})}{md\sin md}e^{(-a+ib)t}\cos mx$$

We then obtain, after adding the pairs of terms corresponding to $p = -a \pm ib$,

$$h = 1 - \Sigma \frac{\cos mx}{md\sin md} e^{-at}(\cos bt - \frac{a}{b}\sin bt),$$

the sum taken over successive values $\frac{\pi}{2d}, \frac{3\pi}{2d}, \ldots$ of m.

Putting

$$\frac{\lambda m}{2c} = \sin\theta, \quad a = cm\sin\theta, \quad b = cm\cos\theta$$

this can be written

$$h = 1 - \Sigma \frac{e^{-cm\sin\theta t}}{md\sin md}\left(\begin{array}{l}\cos m(x+c\cos\theta t) + \cos m(x-c\cos\theta t)\\ -\tan\theta(\sin m(x+c\cos\theta t) - \sin m(x-c\cos\theta t))\end{array}\right)$$

In terms of dimensionless variables

$$X = \frac{x}{d}, \quad T = \frac{tc}{d}, \quad \Lambda = \frac{\lambda}{cd}, \quad M = md$$

these last formulae become

$$\sin\theta = \frac{\Lambda M}{2},$$

$$h = 1 - \Sigma \frac{e^{-M\sin\theta T}}{M\sin M}\left(\begin{array}{l}\cos M(X+\cos\theta T) + \cos M(X-\cos\theta T)\\ -\tan\theta(\sin M(X+\cos\theta T) - \sin M(X-\cos\theta T))\end{array}\right)$$

The situation is entirely determined by Λ.

When $\Lambda = 0$ the solution reduces to the Fourier

representation of the two travelling square waves which then comprise the solution (4.1). When $\Lambda > 0$, because of the factor M in θ, the decay of the higher harmonics is faster than that of the lower harmonics. This represents the dispersion of the wave fronts which results from the impossibility of current sheets (4.1).

This solution for an inviscid case can also be obtained directly as a representation in eigenfunctions of x, since with no condition on u when $t > 0$ such functions are now adequate for the boundary conditions. To eliminate x from

$$(\frac{\partial}{\partial t} - \lambda\frac{\partial^2}{\partial x^2})h = c\frac{\partial u}{\partial x}$$

$$\frac{\partial u}{\partial t} = c\frac{\partial h}{\partial x}$$

we take functions

$$\mathfrak{P}(x) = \cos mx \qquad \text{or} \qquad \sin mx$$

for which

$$\mathfrak{P}'' = -m^2\mathfrak{P}$$

and put

$$h = 1 + z, \quad z = \Sigma \bar{z}_\delta \mathfrak{P}_\delta, \quad u = \Sigma \bar{u}_\delta \frac{\mathfrak{P}'_\delta}{m_\delta},$$

The equations are then satisfied if

$$(\frac{\partial}{\partial t} + \lambda m^2)\,\bar{z} = -c\,m\bar{u}$$

$$\frac{\partial \bar{u}}{\partial t} = cm\,\bar{z}$$

and the boundary conditions

$$h = 1 \quad \text{when} \quad x = \pm d$$

$$h = u = 0 \quad \text{elsewhere when} \quad t = 0$$

are satisfied if where

$$1 = \Sigma \bar{I}_\delta \mathfrak{P}_\delta ,$$

$$\bar{z} = -\bar{I} , \quad \bar{u} = 0 \quad \text{when} \quad t = 0.$$

We obtain

$$\bar{z} = -\bar{I}\, e^{-at} (\cos bt - \frac{a}{b} \sin bt), \quad \bar{u} = \frac{cm\bar{I}}{b} e^{-at} \sin bt,$$

$$a = \frac{\lambda m^2}{2} , \quad a^2 + b^2 = c^2 m^2 .$$

Also

$$\bar{I}_1 = \frac{4}{\pi} , \quad \bar{I}_2 = 0, \quad \bar{I}_3 = -\frac{4}{3\pi} \quad \ldots\ldots$$

the sine terms dropping out by symmetry,
so this is the same solution as before.

It is impossible to eliminate u completely from the equations because of the initial condition on u.

The method is very easily extended to a case where the variation of the boundary value of h with time is arbitrary. If this value is $h_0(t)$ we put

$$h = h_0 + z, \quad z = \Sigma \bar{z}_\delta \mathfrak{P}_\delta, \quad u = \Sigma \bar{u}_\delta \frac{\mathfrak{P}'_\delta}{m_\delta}$$

Then where

$$1 = \Sigma \bar{I}_\delta \Phi_\delta$$

the equations are satisfied if

$$(\frac{\partial}{\partial t} - \lambda m^2)\ \bar{z} = - cm\bar{u} - h_o'\ \bar{I}$$

$$\frac{\partial \bar{u}}{\partial t} = cm\bar{z}$$

$$\bar{z} = - h_o \bar{I},\ \ \bar{u} = 0 \quad \text{when} \quad t = 0.$$

In this way the inversion of a Laplace transform is avoided.

The situation is again less complex when $\lambda = \nu$. Then in the solution obtained earlier for $\bar{h}$, $\bar{u}$ in the general case (page 65)

$$a = \frac{\sigma^2}{2\lambda^2} + \frac{p}{\lambda},\ \ \beta = - \frac{p^2}{\lambda^2};\ \ (a^2-\beta)^{\frac{1}{2}} = \frac{\sigma}{\lambda}\left((\frac{\sigma}{2\lambda})^2 + \frac{p}{\lambda}\right)^{\frac{1}{2}},$$

$$k^2 = - \frac{\sigma^2}{2\lambda^2} - \frac{p}{\lambda} \pm \frac{\sigma}{\lambda}\left((\frac{\sigma}{2\lambda})^2 + \frac{p}{\lambda}\right)^{\frac{1}{2}} = - \left(\frac{\sigma}{2\lambda} \pm \left((\frac{\sigma}{2\lambda})^2 + \frac{p}{\lambda}\right)^{\frac{1}{2}}\right)^2$$

$$k = i\left(\frac{\sigma}{2\lambda} \pm \left((\frac{\sigma}{2\lambda})^2 + \frac{p}{\lambda}\right)^{\frac{1}{2}}\right),\ \ k_2 - k_1 = 2i\left((\frac{\sigma}{2\lambda})^2 + \frac{p}{\lambda}\right)^{\frac{1}{2}}$$

$$r_1 = r_2 = i$$

$$\bar{h} = \frac{1}{p} \frac{\cos k_1 x \sin k_2 d - \cos k_2 x \sin k_1 d}{\sin(k_2 - k_1)d}$$

This simplification, as in the steady state case, results from the lower order of the governing system of equations (2.5). There are now poles when

$$k_2-k_1 = \pm 2m, \quad m = \frac{\pi}{2d}, \frac{\pi}{d}, \ldots\ldots,$$

that is, when

$$p = -\lambda(m^2 + (\frac{\sigma}{2\lambda})^2), \quad k = i\frac{\sigma}{2\lambda} \pm m$$

There is no pole when $k_1 = k_2$ because then the numerator also vanishes.

The residue when $p = 0$ is 1.

Also when $k_2-k_1 = 2m$

$$\frac{\partial}{\partial p}\sin(k_2-k_1)d = -\frac{2d\cos(k_2-k_1)d}{\lambda(k_2-k_1)} = -\frac{d\cos 2md}{\lambda m}$$

so the residue when $k_2-k_1 = 2m$ is

$$-\frac{\cos(\frac{i\sigma}{2\lambda}+m)x\sin(\frac{i\sigma}{2\lambda}-m)d-\cos(\frac{i\sigma}{2\lambda}-m)x\sin(\frac{i\sigma}{2\lambda}+m)d}{\frac{d}{m}(m^2+(\frac{\sigma}{2\lambda})^2)}e^{-\lambda(m^2+(\frac{\sigma}{2\lambda})^2)t}$$

The numerator can be written

$$(\cosh\tfrac{\sigma x}{2\lambda}\cos mx - i\sinh\tfrac{\sigma x}{2\lambda}\sin mx)(i\sinh\tfrac{\sigma d}{2\lambda}\cos md - \cosh\tfrac{\sigma d}{2\lambda}\sin md)$$

$$-(\cosh\tfrac{\sigma x}{2\lambda}\cos mx + i\sinh\tfrac{\sigma x}{2\lambda}\sin mx)(i\sinh\tfrac{\sigma d}{2\lambda}\cos md + \cosh\tfrac{\sigma d}{2\lambda}\sin md)$$

$$= -2(\cosh\tfrac{\sigma x}{2\lambda}\cos mx\cosh\tfrac{\sigma d}{2\lambda}\sin md - \sinh\tfrac{\sigma x}{2\lambda}\sin mx\sinh\tfrac{\sigma d}{2\lambda}\cos md)$$

Also when $md = \frac{\pi}{2}, \frac{3\pi}{2}\ldots\ldots$, $\cos md = 0$, $\cos 2md = -1$,

and when $md = \pi, 2\pi \ldots\ldots$, $\sin md = 0$, $\cos 2md = 1$.

Thus the solution for h reduces to

$$h = 1 - 2\sum \frac{e^{-\lambda(m^2+(\frac{c}{2\lambda})^2)t}}{\frac{d}{m}(m^2+(\frac{c}{2\lambda})^2)} \left(\begin{matrix} \sin md \cos mx \cosh \frac{cd}{2\lambda} \cosh \frac{cx}{2\lambda} \\ + \cos md \sin mx \sinh \frac{cd}{2\lambda} \sinh \frac{cx}{2\lambda} \end{matrix} \right)$$

The individual terms do not have the form of a travelling wave.

This solution can also be obtained directly as a representation in terms of eigenfunctions of x deriving from the equations (2.5)

$$(\frac{\partial}{\partial t} - c\frac{\partial}{\partial x} - \lambda\frac{\partial^2}{\partial x^2})\, v = 0$$

$$(\frac{\partial}{\partial t} + c\frac{\partial}{\partial x} - \lambda\frac{\partial^2}{\partial x^2})\, w = 0$$

which are obtained by the substitutions

$$h + u = v, \qquad h - u = w.$$

The appropriate eigenfunctions for the two equations have then to satisfy

$$\Phi'' + \frac{c}{\lambda}\Phi' = -m^2\Phi, \quad \Phi'' - \frac{c}{\lambda}\Phi' = -m^2\Phi,$$

These are

$$\Phi(x) = e^{-\frac{cx}{2\lambda}} \cos mx \text{ or } e^{-\frac{cx}{2\lambda}} \sin mx$$

for the one case

$$\Phi(x) = e^{\frac{cx}{2\lambda}} \cos mx \text{ or } e^{\frac{cx}{2\lambda}} \sin mx$$

for the other, m satisfying

$$\cos md \text{ or } \sin md = 0$$

The sum divided by two of the solutions for v and w then gives for h the solution already obtained.

Unfortunately the convergence is bad when λ is small, since then for the earlier terms $(\frac{c}{2\lambda})^2 \gg m^2$, so that the relative size of successive terms is mainly determined by the factor $\frac{d}{m}$ on the underneath, which decreases; the first terms of the series therefore increase. These difficulties of convergence must also apply to the general case for which $\lambda \neq \nu$.

The results of numerical calculations when viscosity is absent are given in figures 4.4 and 4.5. These show the development of the wave pattern when $\Lambda = .01$ and $.1$. In each figure the longitudinal profile of the field is given for values of the dimensionless time $T = \frac{tc}{d}$ of .5, 1.5 and 2.5, these corresponding to instants when the wave fronts in an ideal case would be at the quarter points of the system, before the first collision, after it, and after the first reflection. The increasing dispersion of the wave fronts can be seen. When $\Lambda = .1$ the fronts have already degenerated almost to a sine wave form before the first reflection.

4.3 Plane and cylindrical systems.

In an undamped system with side walls the current sheets at the wave fronts turn along the walls forming a current loop which closes on itself, reverses direction as

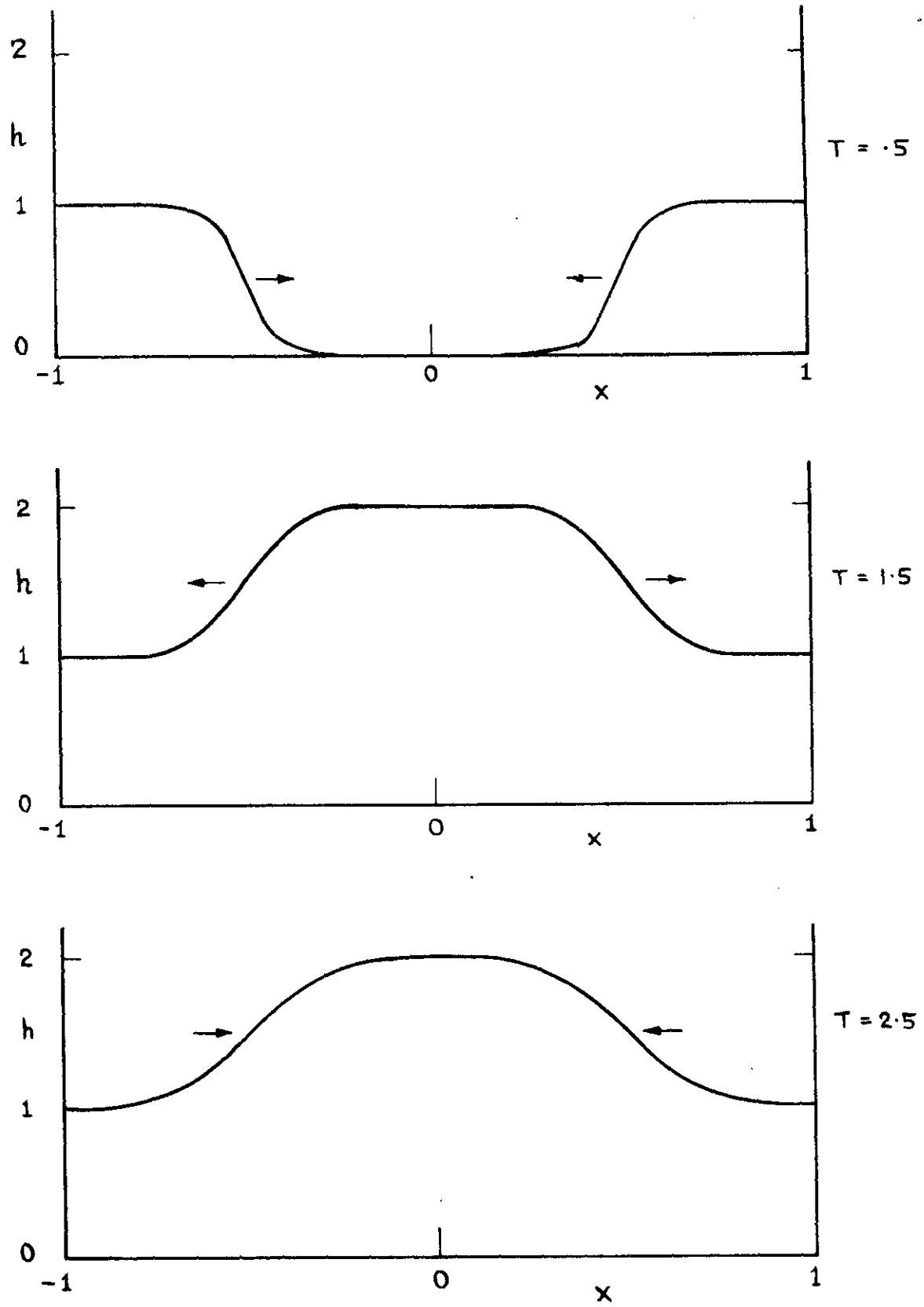

FIG. 4.4 PROFILES OF h AT SUCCESSIVE INSTANTS FOR A ONE DIMENSIONAL SYSTEM $\Lambda = \cdot 01$

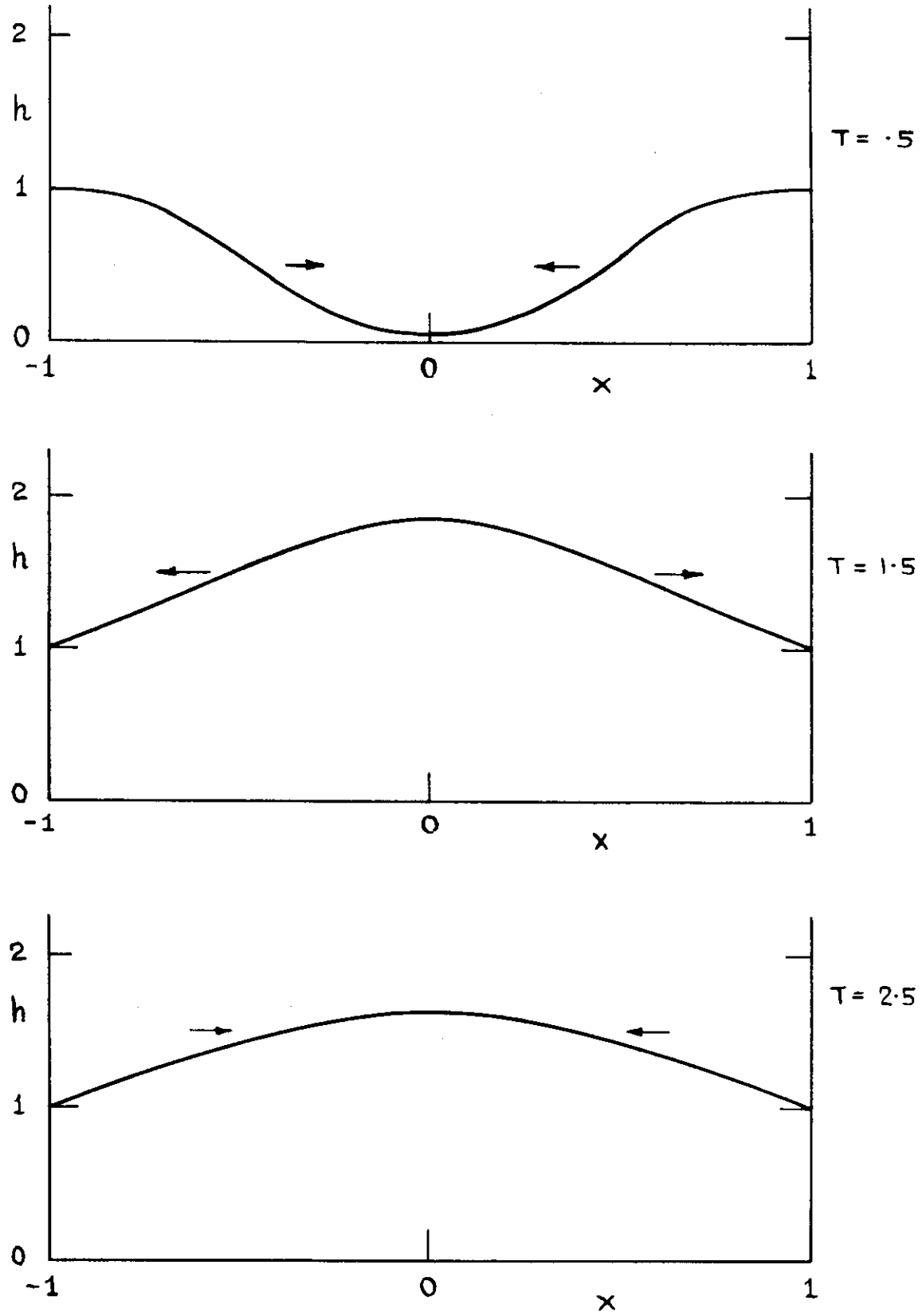

FIG. 4.5 PROFILES OF h AT SUCCESSIVE INSTANTS FOR A ONE DIMENSIONAL SYSTEM $\Lambda = \cdot 1$

the fronts pass each other and opens until the fronts reach the walls and are reflected, when it begins to close again, figure 4.6.

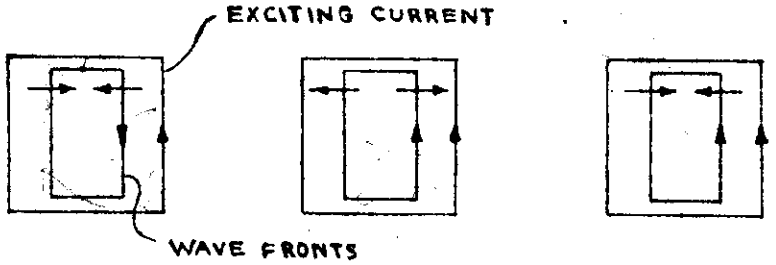

SUCCESSIVE SITUATIONS IN AN IDEAL CASE

Fig.4.6

When λ and $\nu > 0$ the side walls cause additional damping because of the resistance to the path of the current and the viscous drag along the sides. Here only the case $\lambda > 0$ will be considered.

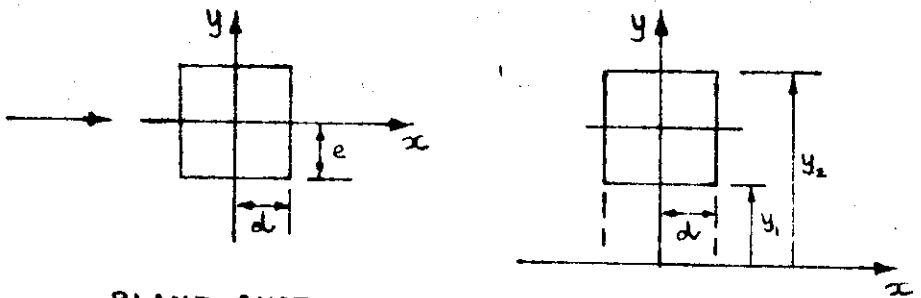

PLANE SYSTEM CYLINDRICAL SYSTEM

Fig.4.7.

For a plane system the equations are then

$$\left(\frac{\partial}{\partial t} - \lambda\left(\frac{\partial^2}{\partial x^2} + \frac{\partial^2}{\partial y^2}\right)\right) h = c\,\frac{\partial u}{\partial x}$$

$$\frac{\partial u}{\partial t} = c\,\frac{\partial h}{\partial x}$$

$h = 1$ at the boundaries,

$h = u = 0$ elsewhere when $t = 0$.

For a cylindrical system they are the same with $\frac{\partial^2}{\partial y^2}$ replaced by $\frac{\partial^2}{\partial y^2} + \frac{1}{y}\frac{\partial}{\partial y} - \frac{1}{y^2}$, and the boundary value 1 by $\frac{y_1}{y}$. A double expansion in eigenfunctions of x and y is the most convenient method. These will be the same as before,

$\mathfrak{D}(x) = \cos mx$ or $\sin mx$,

$\mathfrak{E}(y) = \cos ny$ or $\sin ny$ for a plane system,

$J_1(y)\, Y_1(y_1) - Y_1(y)\, J_1(y_1)$ for an axial system,

satisfying

$$\mathfrak{D}'' = -m^2\mathfrak{D},$$
$$\mathfrak{E}'' = -n^2\mathfrak{E} \quad \text{or} \quad \mathfrak{E}'' + \frac{\mathfrak{E}'}{y} - \frac{\mathfrak{E}}{y^2} = -n^2\mathfrak{E}$$

Then writing I for the boundary value, and

$$h = I+z, \quad I = \sum \bar{I}_{\delta\epsilon}\mathfrak{D}_\delta\mathfrak{E}_\epsilon, \quad z = \sum \bar{z}_{\delta\epsilon}\mathfrak{D}_\delta\mathfrak{E}_\epsilon, \quad u = \sum \bar{u}_{\delta\epsilon}\frac{\mathfrak{D}'_\delta}{m_\delta}\mathfrak{E}_\epsilon$$

the equations are satisfied if

$$\left(\frac{\partial}{\partial t} + \lambda(m^2+n^2)\right)\bar{z} = -cm\bar{u}$$
$$\frac{\partial \bar{u}}{\partial t} = cm\bar{z}$$
$$\bar{z} = \bar{I}, \quad \bar{u} = 0 \quad \text{when} \quad t = 0.$$

These are the same as for the one-dimensional case, with $\lambda(m^2+n^2)$ replacing λm^2. They give

$$\bar{z} = -Ie^{-at}(\cos bt - \frac{a}{b}\sin bt), \quad \bar{u} = \frac{cm\bar{I}}{b}\, e^{-at}\sin bt,$$
$$a = \frac{\lambda(m^2+n^2)}{2}, \quad a^2 + b^2 = c^2m^2.$$

$I_{\delta\epsilon}$ is obtained as the product of the coefficients I_δ and I_ϵ evaluated in 3.7 (pages 45 and 41-42). In a plane case

$$I = \frac{4\sin m\delta \sin n\epsilon}{mn\epsilon}$$

and in a cylindrical case

$$I = \frac{4\pi \sin m\delta}{m\delta} \frac{\left(\frac{L}{C} - 1\right)}{L^2 - 1}, \quad L = \frac{J_1(my_1)}{J_1(my_2)}, \quad C = \frac{y_2}{y_1}$$

The damping is now determined by a factor

$$e^{-\frac{\lambda(m^2+n^2)t}{2}} \quad \text{instead of} \quad e^{-\frac{\lambda m^2}{2}t}$$

or in terms of the dimensionless variables

$$T = \frac{tc}{d}, \quad \Lambda = \frac{\lambda}{cd}, \quad M = md, \quad N = nd$$

$$e^{-\frac{\Lambda(M^2+N^2)}{2}T}$$

The additional damping due to the side walls is represented by the part $\frac{\Lambda N^2}{2}$. Since the negative exponent increases when both M and N increase, not only is there a longitudinal dispersion of the wave fronts, but also there is a transverse degeneration to a profile across the section of sine wave form.

The results of numerical calculations for a square section plane system are given in figures 4.8 and 4.9.

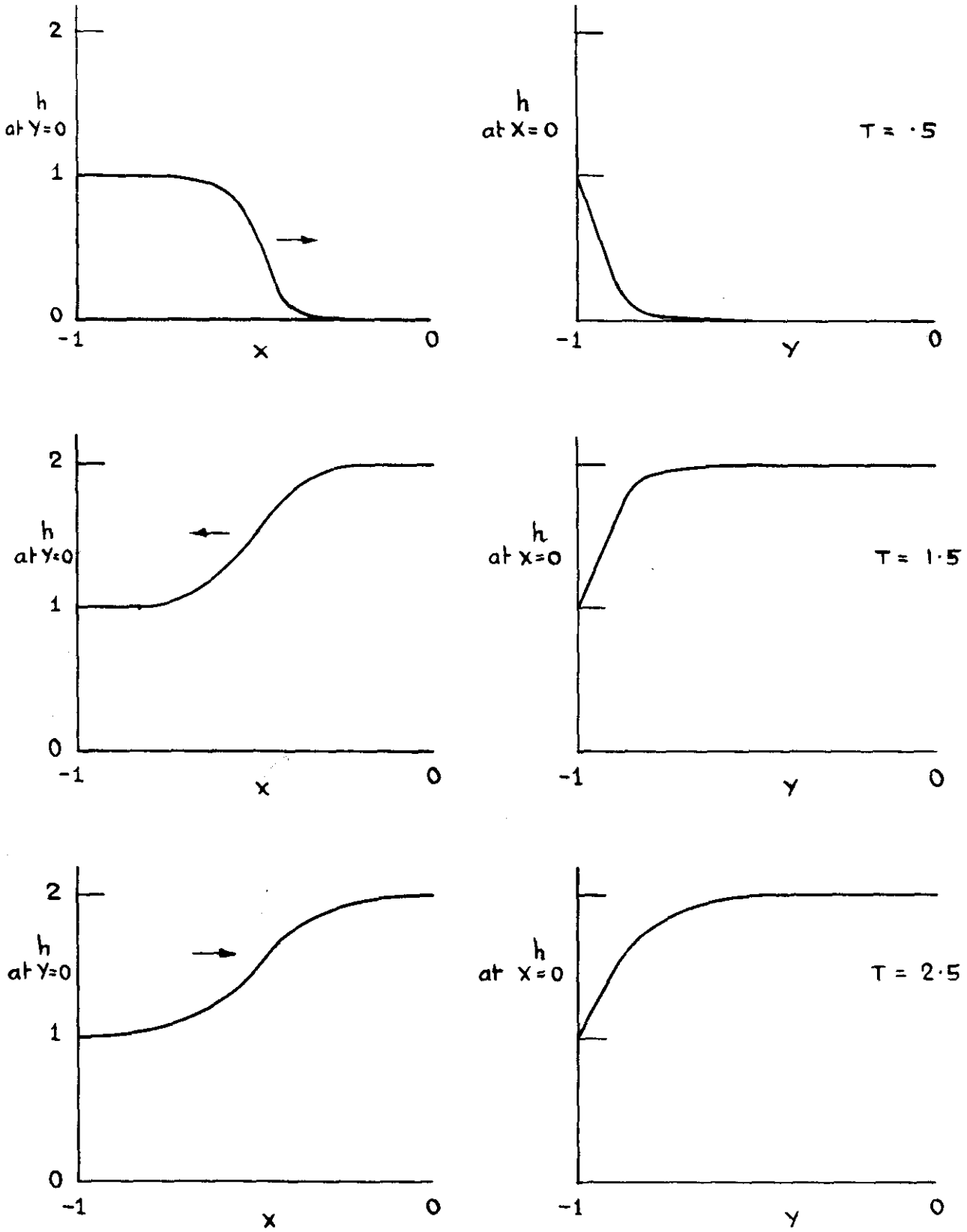

FIG.4.8 X AND Y PROFILES OF h AT SUCCESSIVE INSTANTS FOR A SQUARE SECTION PLANE SYSTEM $\Lambda = \cdot 01$

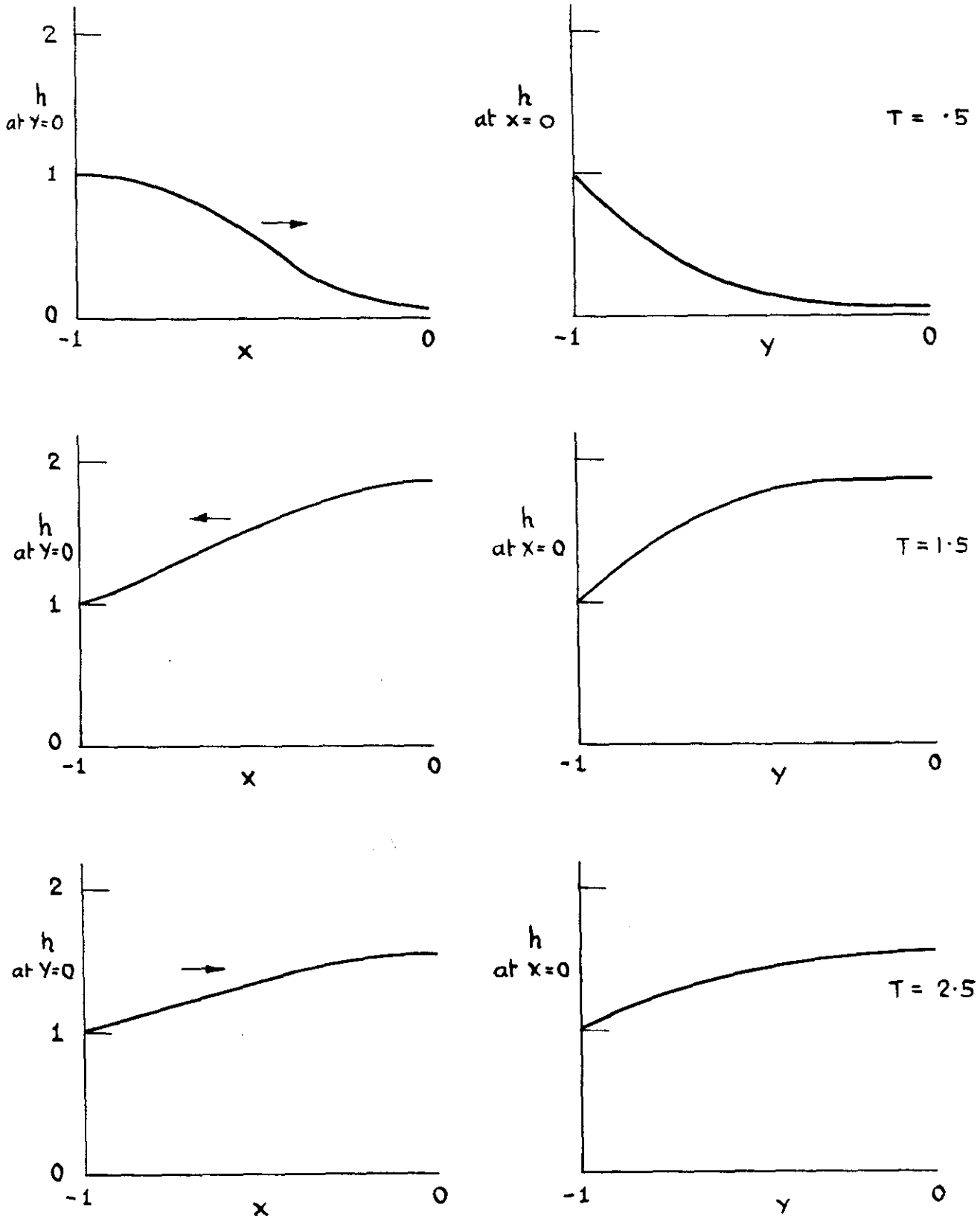

FIG. 4.9 X AND Y PROFILES OF h AT SUCCESSIVE INSTANTS FOR A SQUARE SECTION PLANE SYSTEM $\Lambda = \cdot 1$

These show the additional transverse degeneration caused by the side walls at the same values .01 and .1 of Λ as were taken for the one dimensional calculations (figures 4.4 and 4.5).

CHAPTER 5

EXPERIMENTS

5.1 Overall design of an experiment.

When it became clear from the theoretical work that it should be possible to produce quite well-developed waves in apparatus of laboratory size, contrary to Lehnert's conclusion[3], it was decided to proceed with an experiment.

The available liquid conductors are liquid metals, notably mercury and sodium potassium alloy which are liquid at room temperature, and sodium which liquefies at 97°C. Their main characteristics[10] are given in Table 5.1.

Table 5.1
Properties of liquid metals.

	Density ρ kg/m^3	Viscous diffusivity ν m^2/s	Electric diffusivity $\lambda = \frac{1}{\mu\sigma}$ m^2/s
Mercury at 20°C	13.6 10^3	1.19 10^{-7}	7.55 10^{-1}
56% sodium 44% potassium at 20°C	.87 10^3	8.0 10^{-7}	2.80 10^{-1}
Sodium at 120°C	.93 10^3	6.77 10^{-7}	.82 10^{-1}

Sodium and sodium potassium are both highly corrosive,

and moreover oxidize on exposure to air, so that they are difficult to handle. For all three liquids $\nu \ll \lambda$. The damping of waves will be determined by $\Lambda + N = \frac{\lambda + \nu}{cd}$, where c is the wave speed, d the half depth of a closed system (3.3). Also for a main field B_o the wave speed is $\frac{B_o}{(\rho\mu)^{\frac{1}{2}}}$. Taking $B_o = 1$ weber/m^2, and $\Lambda + N = .05$ for purposes of comparison, so that a harmonic resonance is just possible (3.3), d has to be 196, 18.5 and 5.6 cm for mercury, sodium potassium and sodium respectively, the large depth needed by mercury being partly a result of the lower wave speed associated with its higher density. On the basis of these figures it was decided that sodium would have to be used as the medium for an experiment despite the attendent difficulties. The need for heating apparatus to liquefy it is a nuisance. On the other hand, bearing in mind its corrosiveness, the fact that it is a solid at room temperature is an advantage for the handling of apparatus containing it, since it will not escape in the event of damage. The resistivity of sodium increases with temperature, and a working temperature of $120^{\circ}C$ was selected, a safe margin above the melting point, but not so high as to incur a serious increase in resistivity.

An experiment must use an axial geometry with the main field along the axis, to allow circular disturbances

in the field and free movement of the fluid round the axis. To restrict the size of the apparatus the maximum use must be made of the available space in the magnetic region. A possible way of increasing the utilization of the space in the axial direction is to use a system open at one face. Such a system behaves like a closed system bisected, the depth accommodating a quarter instead of a half wavelength at the fundamental resonance. The length for comparison with other systems becomes therefore the full depth instead of the half depth, with a corresponding gain. Lundquist[2] and Lehnert[3] used systems of this type. However, such systems involve difficulties of excitation. Simple magnetic excitation can no longer be used for lack of a current path, so that some form of wall movement must be used. But with liquid metals simple mechanical excitation is ineffective because $\nu \ll \lambda$ (3.3). It becomes necessary to use a conducting wall carrying induced currents like Lehnert, or a ribbed wall like Lundquist. The first method introduces additional losses, the second an element of uncertainty. The necessary mechanical drive will occupy much of the space which might have been gained. Also the inertial forces will be a source of difficulty, and it becomes impossible to produce a sharp pulse for excitation of transient waves. For these reasons a closed system excited by a sheet of electric current flowing round the

section was chosen.

The overall conception once decided, the design of the apparatus could be divided into three main problems:

1) the design of a magnet to produce a uniform field of the required strength over the required region;

2) the design of the sodium container;

3) the design of equipment to excite and measure steady state and transient waves.

5.2 Optimum shape.

The magnetic region should be chosen to have an optimum shape. In 3.7 it was shown (page 43) that the amplitude at resonance of a particular term of the solution is approximately

$$\frac{1}{(\theta+\zeta)P+\eta}$$

where

$$2\theta = (\Lambda+\mathcal{M})P, \quad 2\zeta = \frac{(\Lambda+\mathcal{M})N^2}{P}, \quad \eta = \left(\frac{\mathcal{M}}{\Lambda}\right)^{\frac{1}{2}}$$

The most important term of the solution is the first for which N has a value between $\frac{\pi d}{2e}$ and $\frac{5\pi d}{8e}$, where d and e are the half depth and width of the section, which depends on the ratio of external to internal radius. At the fundamental resonance $P = \frac{\pi}{2}$. Taking $N = \frac{\pi d}{2e}$ as a sufficient

approximation, and substituting $\Lambda = \frac{\lambda}{cd}$, in a case where γ can be neglected, and ν compared with Λ in θ and β, the amplitude of the first term is then

$$\frac{2cd}{\pi\lambda\left(1 + \left(\frac{d}{e}\right)^2\right)}$$

For a given applied magnetic field the performance with a given fluid is then determined by

$$\frac{d}{1 + \left(\frac{d}{e}\right)^2}$$

For a given ratio of external to internal radius the volume is proportional to de^2. If this is fixed we then find by differentiation that performance is at a maximum when

$$e^2 = 2d^2$$

Thus, on the supposition that the overall cost of the apparatus will be roughly proportional to the volume of the magnetic region, e ought to be about 1.4 d.

5.3 The magnet.

There being no suitable magnet available, it was necessary to build one. To save cost it was decided not to attempt to obtain a field greater than 1 weber/m^2,

a value which can be obtained with mild steel without saturation, so that no more expensive material need be used. For the same reason it was decided to rule out the use of a water cooled coil. Now across the width of the coil there is an unused waste flux. The shell, however, must be large enough to carry this additional flux without any flux concentration, if the full potential performance is to be realized. The required shell size increases rapidly as the current density is reduced, and it was therefore decided to use a coil with a high current density which would heat up while it operated, and to limit the time of operation on any one occasion.

The general problem of the design of a magnet under these conditions is considered in Appendix 3. On the basis of the study outlined there, it was concluded that the best form of construction was simply a coil lying in the slot between two flat steel slabs separated by two spacer pieces providing the flux return path. The arrangement is illustrated in figure 5.1. At an iron face, because of the high permeability of iron, refraction of the lines of force ensures that these leave the iron practically at right angles. Accordingly, with this construction the field is certain to be everywhere vertical, as if the coil were part of a long solenoid, and therefore uniform. The

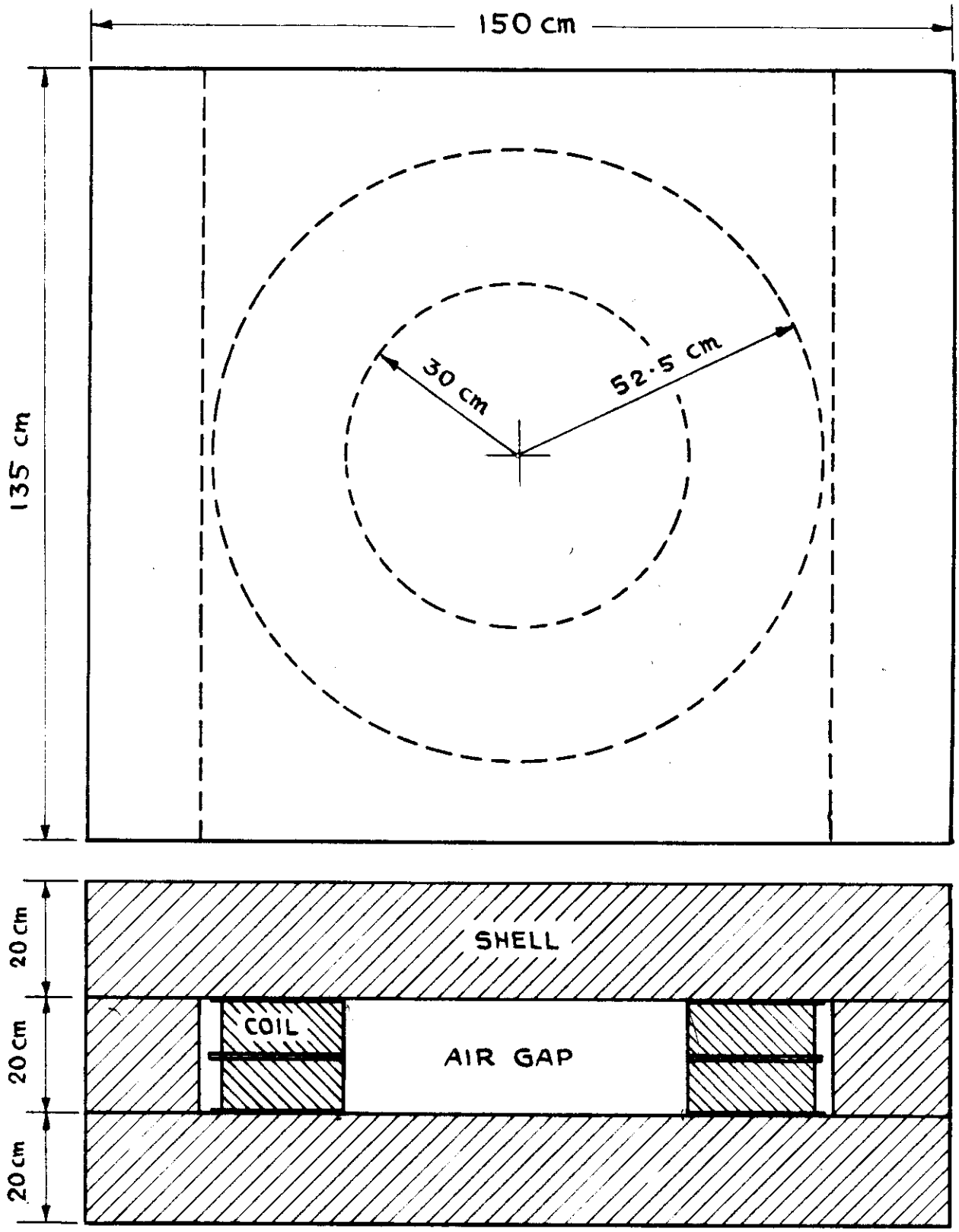

FIG. 5.1 THE MAGNET. SCALE 1:10

arrangement results in a magnetic region for experimental work which is completely enclosed, and access to the region can only be gained by taking the 'lid' off the magnet. In this case the magnet was placed in a laboratory with a travelling crane in the roof, so that this presented no difficulty. Aluminium and copper were possible materials for the coil. Again on the basis of the analysis in Appendix 3, it appeared that the total cost of the magnet would be about the same with either material, and copper was chosen as the more readily available.

To allow for a sodium container of optimum shape (5.2) the magnet was built with a gap 20 cm deep and 60 cm in diameter. With so deep a gap the reluctance of the iron path compared with that of the gap is negligible, provided saturation is not approached. For a field B weber/m^2 and current density j A/m^2 such a gap requires therefore a coil of conducting area

$$A = 159000 \frac{B}{j} m^2 ,$$

Insulators were available which could withstand up to 160°C. Between 20 and 160°C the resistivity of copper rises from 1.73 to 2.70 10^{-8} m. Its heat capacity is 3.40 10^6 Joules/m^3, so in this range the mean heating rate

with a current density j A/m^2 is

$$.65\ 10^{-14}\ j^2\ ^{\circ}C/s.$$

Values

$$\frac{B}{j} = .2\ 10^{-6}\ \text{weber/A}, \qquad A = .03\ m^2$$

were chosen, giving a running time declining to about 14 minutes at a field of 1 weber/m^2, assuming no escape of heat to the surroundings.

The total conducting area once determined by a choice of $\frac{B}{j}$, the number of turns into which this area is divided must be chosen to fit the winding to the voltage supply. Here a 220 V DC supply was available and the coil was designed so that at the maximum temperature the voltage needed to maintain a current sufficient for a field of 1 weber/m^2 would be just less than this. The coil was split horizontally, and the two halves operated in parallel. Each half of the coil had 558 turns of 3.05 mm by 9.14 mm copper strip, rectangular to reduce the wastage of space, in 62 layers of 9 turns each, occupying a total depth of 19.5 cm. The resistance of each half was .92 Ω at 20°C, 1.41 Ω at 160°C.

The strip was insulated with Teramel, a heat resisting enamel, and was wound between cheeks of a heat resistant Tufnel. The turns were bound and glued together with fibre glass strips and Araldite, and once the Araldite had set the two halves of the coil proved rigid enough to

be easily transportable. Each half had one cheek .15 cm thick and one cheek .6 cm thick, and the two halves were placed with the thick cheeks against each other. Matching grooves on their outer faces then provided four tunnels .6 cm deep and 2.5 cm wide for the leads to the sodium container. Also in each half of the coil the lead from the bottom layer was brought out through a groove in the thick cheek. Originally these grooves were placed on the faces against the turns so that these leads would be protected from damage in handling. However, in the course of the experimental programme there was an insulation failure in one half of the coil between the lead coming out and the passing turns. Between turns in successive layers of a coil there is only a very small voltage: between the lead from the bottom and the passing turns, on the other hand, near the outside of the coil the voltage approaches the full voltage on the coil. In this case it appeared on inspection that some fibreglass tape which had been inserted to help resist this greater voltage had been displaced during the winding operation. The half had to be written off, and on the replacement the lead was brought out on the outer face. The cheek of the undamaged half was also sawn into and the lead moved to the outer face.

The complete coil weighed about 700 Kg and the ratio

of conductor to total volume was .77.

The outer radius of the coil was 1.65 times the inner radius: assuming a uniform fall off of the field across the coil width, the total flux with a coil of this radius ratio will be 1.8 times the flux through the pole face. In this case, allowing for half the flux passing each side round the shell, the iron path area necessary to prevent concentration of the field was thus 260 cm^2. The shell was actually built of ordinary mild steel with top and bottom slabs 150 cm long, 135 cm wide, and 20 cm thick, providing an area of 270 cm^2, bridging spacer pieces 20 cm high of the same section. The annular area carrying the pole flux at the inner edge of the coil was 1.33 times the pole face area and this should again have been enough to prevent concentration. The top and bottom slabs each weighed 3 tons, and were split along the centre line to bring the weight of each individual piece within the 2 ton limit of the laboratory crane. The total steel weight was 7.6 tons.

Current was supplied to the magnet from a 220 V, 120 kw 4 pole DC generator driven from the 346 V three phase AC main by a 130 kw 6 pole induction motor. This generating set had been held as a standby supply for the Engineering Laboratory, and to move it to a position beside the magnet it had to be partly dismantled.

The use of the set eliminated switching problems with such an inductive circuit, since all that was necessary was to cut the voltage of the generator by reducing the current to its field windings until the main current was small enough for the circuit to the magnet to be broken. Since there was no starting equipment on the AC machine, it was necessary to start the set with the DC machine acting as a motor, and to switch over when the operating speed of 960 r/m had been reached.

To measure the magnet current, ammeters were inserted in the circuit to each half of the coil. The coil temperature could be estimated by comparing the voltage required with the current, the temperature limit being represented by a resistance of .7Ω.

The general layout of the magnet and its generating set can be seen in the frontispiece.

Tests of the magnet field were made using search coils connected by twisted leads to a moving coil flux meter accurate to ± 2%. To measure the absolute value of the field at the mid depth at points on a particular radius a 10 turn coil of 5.0 cm^2 mean area within ± 1%, giving an end to end deflection of the needle on the flux meter scale for a field change of 2.0 weber/m^2, was simply rotated 180° on a stalk through one of the tunnels between the two halves of the magnet coil. To test the general uniformity of the

field a 100 turn coil of 5.0 cm^2 mean area, giving ten times the sensitivity, was moved around the air gap in the vertical and in any desired horizontal direction with a traversing gear operated by nylon cords through one of these tunnels. The tests showed a variation of the field with the current registered by the ammeters which was linear within ½% in the range up to 1 weber/m^2 at any particular point in the gap, confirming that any non-linear behaviour of the steel was unimportant in this range because of the relatively negligible total reluctance of the steel. On the other hand variations as great as 3% were found between one point and another due apparently to imperfections in manufacture. In particular there was a step in the field across the split along the centre line in the top and bottom slabs, because the pieces on either side of the split did not absolutely match each other. No regular spatial variation of the field was found. Table 5.2 gives the calibration of the magnet at a point at the mid-radius and mid-depth well away from any sharp variation in the field.

Table 5.2

Calibration of magnet.

Current A	Field weber/m^2
100	.325
200	.650
300	.970

The field was about 5% less than might be expected ideally, partly because the gap was in many places deeper than was designed.

As expected, at 300 A the magnet coil took about 15 minutes to reach the temperature limit of 160°C.

5.4 The container.

The sodium container was constructed and filled at the Atomic Energy Establishment, Harwell, under the direction of Mr. D.S. Lacey, an expert in liquid metals. After discussion it was decided that the only readily available materials, with which there would be no danger of fracture, which would withstand a temperature of 120°C, and resist sodium, and which could be easily sealed, were metals, and that the complication of induced wall currents would have to be accepted. An 18% chromium 8% nickel stainless steel was selected for its non-magnetic behaviour and low electric conductivity, and the container was built of 1.2 mm sheet of this material, joined by fusion welding. Walls of this thickness are quite flexible, and when the sodium was liquid the container needed good support if it was to keep its shape.

Figure 5.2 shows a section of the container, as it was finally built. It was a rectangular section torus

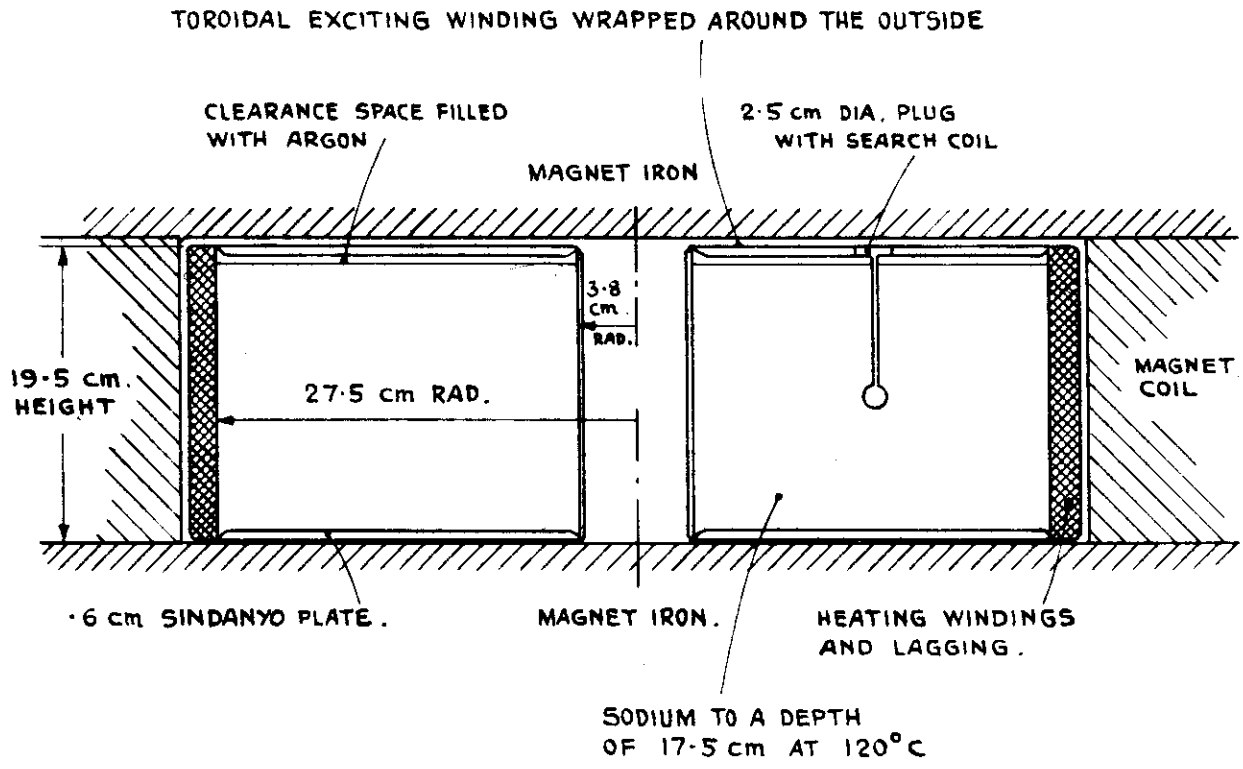

FIG. 5.2 THE CONTAINER. *SCALE 1 : 5*

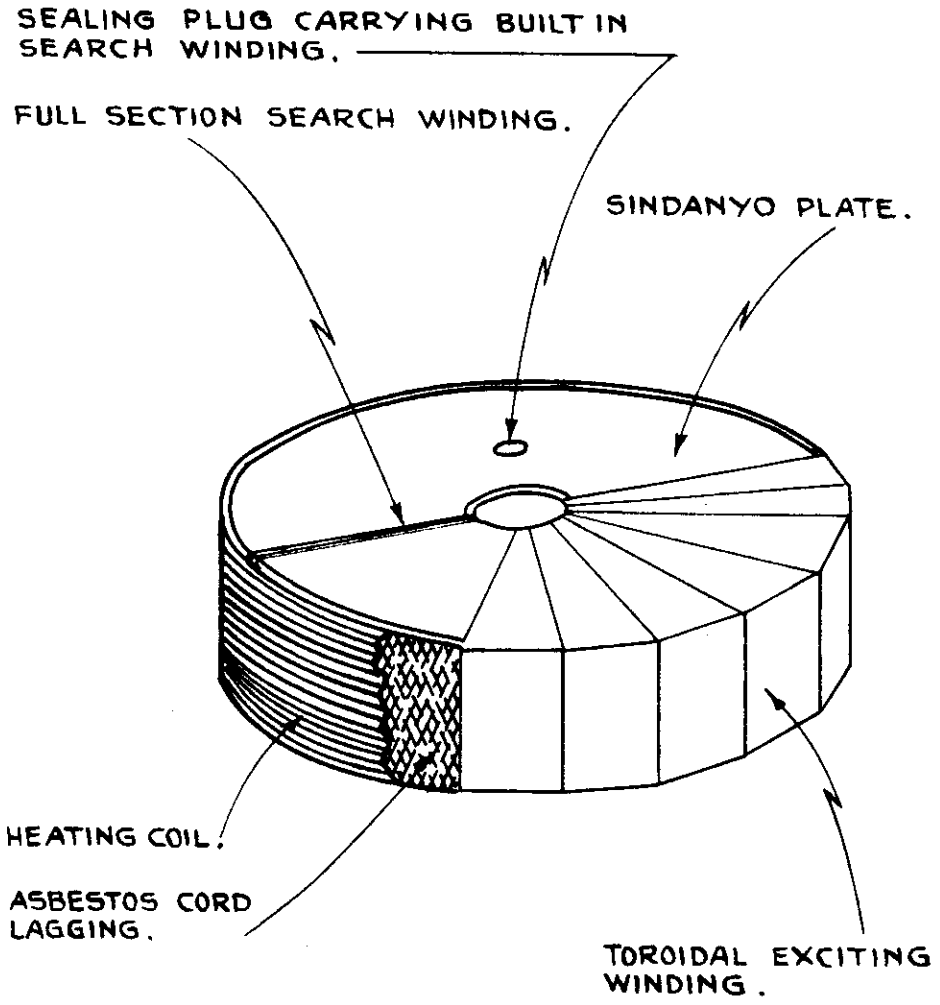

FIG. 5.3 THE CONTAINER WITH ITS WINDINGS PARTLY PEELED OFF.

19.5 cm high overall, and of 55 cm external, 7.5 cm internal diameter, these measurements taken outside the steel. The top and bottom faces were each dished .6 cm inwards for additional strength, and the space within the recesses thus formed was filled with Sindanyo plates top and bottom for heat insulation and extra support. Heating windings were placed round the circumference. The container had a 2.5 cm diameter filling hole positioned at the mid-radius, and attached to the sealing cap there was a small search coil mounted on a stalk. In addition there was a search winding round the full torus section. This passed under the heating coils to escape interference from these, but outside the Sindanyo plates. Finally outside everything there was a toroidal winding of copper segments to excite the waves. The arrangement of the various windings is illustrated in Figure 5.3. The large search winding and the exciting winding were added after the container had been filled.

The container was filled from a large electrically heated sodium tank through a filter of porous stainless steel. The filling line was lagged with asbestos. The container was heated in advance by its own heating winding to the temperature proposed for the later experiments, 120°C, so that the pressure in the container, once sealed,

should be atmospheric, and the section truly rectangular at this temperature. The container and filling line were prefilled with argon supplied from a pressured bottle, to prevent oxidation of the sodium. The sodium was passed into the container through an open funnel -- since argon is denser than air it does not disperse very quickly, and it was therefore considered that argon supplied from the argon line together with the argon displaced from the container by the sodium was sufficient protection. The sodium was pumped from its tank by argon under pressure from its supply bottle. Its flow was controlled by a valve with a bellows seal.

Large quantities of Pyromet extinguishing powder were at hand in case the sodium ignited, and trays of this powder were placed under the apparatus to catch any sodium that might be spilled. There was also a large pressurized Pyromet extinguisher. Everyone working on the container wore protective visors and asbestos coats, gloves and boots.

The density of sodium decreases from .97 g/cm^3 at 20^oC to .93 g/cm^3 at 120^oC, most of the change occurring when it melts. This is more than can safely be accommodated by the flexibility of the walls and a clearance space should be left. To obtain the desired

depth of sodium a probe was placed beside the filling funnel to close an electric circuit through the sodium when the sodium surface reached it, and ring a warning bell. Regrettably this failed, perhaps because of the formation of a film of sodium hydroxide on its surface, with the result that the sodium overflowed and caught fire. The flames were immediately extinguished with the Pyromet powder, and it was then necessary to withdraw some of the sodium with polythene squeeze bottles, which were able to withstand the sodium, temporarily at least. The sodium appeared not to be seriously contaminated. When sufficient sodium had been withdrawn, the sealing cap with its attached search coil was placed in position and fusion welded to the container. The arc was struck from a tungsten rod, surrounded by an argon jet.

The clearance space actually left, which should contain argon, was .6 cm deep at the working temperature of 120°C. The corresponding sodium depth was 17.5 cm. In sodium the wave speed for a field B_o weber/m^2 is 29.2 B_o m/s. At the first resonance the depth contains a half wavelength, so with this depth the resonant frequency is 83.5 B_o c/s. Also the time required for a transient experiment in which the wave fronts travel

several times through this depth and back is about $\frac{.03}{B_o}$ s. Allowing for the wall thickness the width of the sodium section was 23.5 cm., with a ratio of outer to inner radius of 7.0.

With the container once completely sealed the risk of fire was low. The sodium was only heated when in position in the magnet, and in the event of the container developing a leak, perhaps by a failure of one of the welded joins, it would have solidified on the magnet steel. There was no danger of liquid sodium reaching the concrete floor, with which it is liable to explode by extracting and reacting with the water. As a precaution a pressurized Pyromet extinguisher and asbestos clothing were kept at hand.

The appearance of the container with its windings is illustrated in figure 5.4, the leads to the heating and exciting windings can be seen extending to the right at the height at which they would pass through the tunnels in the magnet coil. Figure 5.5, shows the container in position in the magnet. It was a tight fit, and figure 5.6 shows how it was lowered in on a sling of fibreglass tapes. These did not deteriorate when heated and occupied negligible space.

FIG. 5.4
THE SODIUM CONTAINER WITH ITS WINDINGS.

FIG. 5.5
THE CONTAINER IN POSITION.

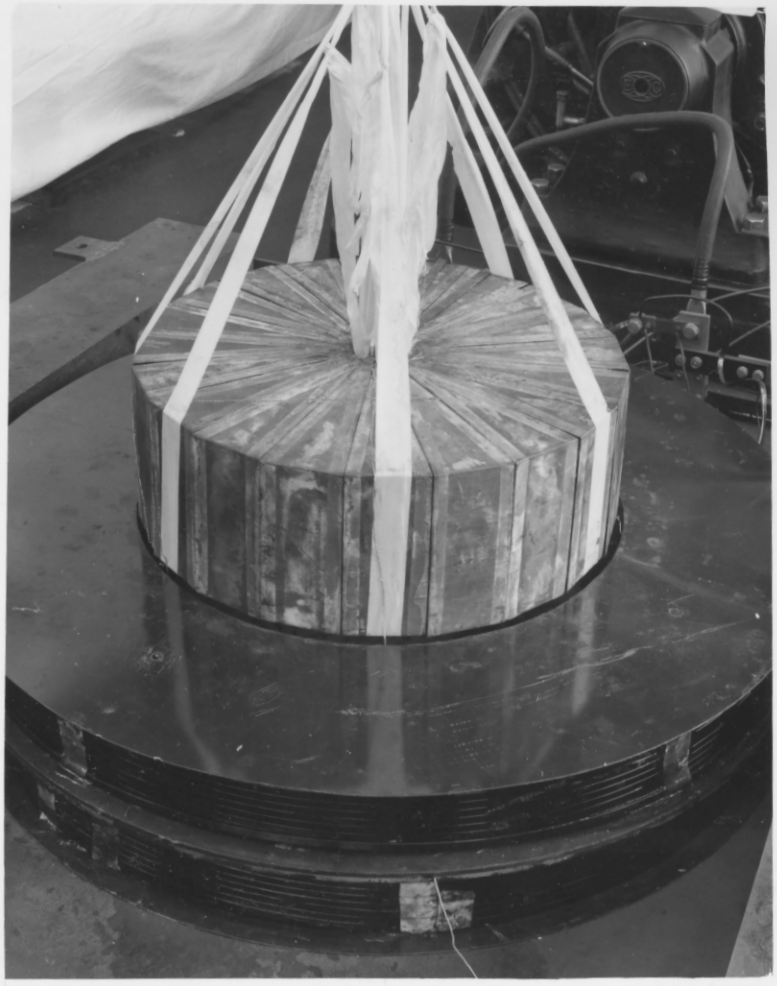

FIG. 5.6

HOW THE CONTAINER WAS MOVED INTO POSITION.

5.5 Heating.

The mass of the sodium was 39.5 kg. The specific heat of sodium is 1.23 Joules/g ^{o}C, and its latent heat of fusion 115 Joules/g, so the total quantity of energy needed to heat this amount of sodium from, say, 20^{o}C to 120^{o}C is 9400 kJoules. Heat was supplied by three windings round the circumference, star connected, and fed from the three phase AC main through three Variac transformers on a single spindle. Such an arrangement has no magnetic effect. The windings were lagged with asbestos cord. Each had 8 turns of Pyrotenac wire, with a resistance of 48 Ω. At 240V, giving 3.6kW, it took 80 minutes to heat the sodium to about 120^{o}C. The temperature could be held near 120^{o}C with the transformers set to 110V, giving .75kW. At 120^{o}C the conductivity of sodium is 84 W/m^{o}C[10]. Allowing for the direct loss of heat outwards from the heating elements, and the heat conducted through the faces, the temperature variation between the inner and outer radii should then have been within 2^{o}C[8]. The temperature was measured at the inner radius, where there could be no hot spots from the heating elements, by a thermocouple connected to a potentiometer. This combination had been calibrated against laboratory thermometers accurate to ± 1^{o}C. The thermocouple was wedged under the exciting winding between some asbestos lagging and the vertical wall. When the sodium was melting the temperature measured was 97^{o}C within ± 2^{o}C, confirming

the accuracy of the method of measurement.

5.6 Detecting apparatus.

To determine the situation in the sodium the e.m.f. induced by changes in the flux through one or other search coil was compared with the current supplied to the exciting winding. In steady state situations the effect of the ~~radius~~ sodium could then be seen as a modification in magnitude and phase of the mutual inductance between the exciting and search windings. In transient situations the time delay before waves travelling from each face reached the search coil at the centre could be observed directly.

The small search coil attached to the sealing cap was positioned at the centre of the torus section. The coil, illustrated in figure 5.7, was encased in a double walled drum .95 cm long and of 1.9 cm mean diameter, of .37 mm stainless steel sheet, mounted on a stainless steel stalk of .6 cm diameter containing the leads. The coil had 10 turns, the maximum number for which there was space, of .37 mm silver copper wire, with a resistance of .2 Ω. The effective area enclosed by the turns, calculated from their diameter at the centre of the wire section, was 2.75 cm^2 within $\pm$ ½%. It was impossible to rewind the coil

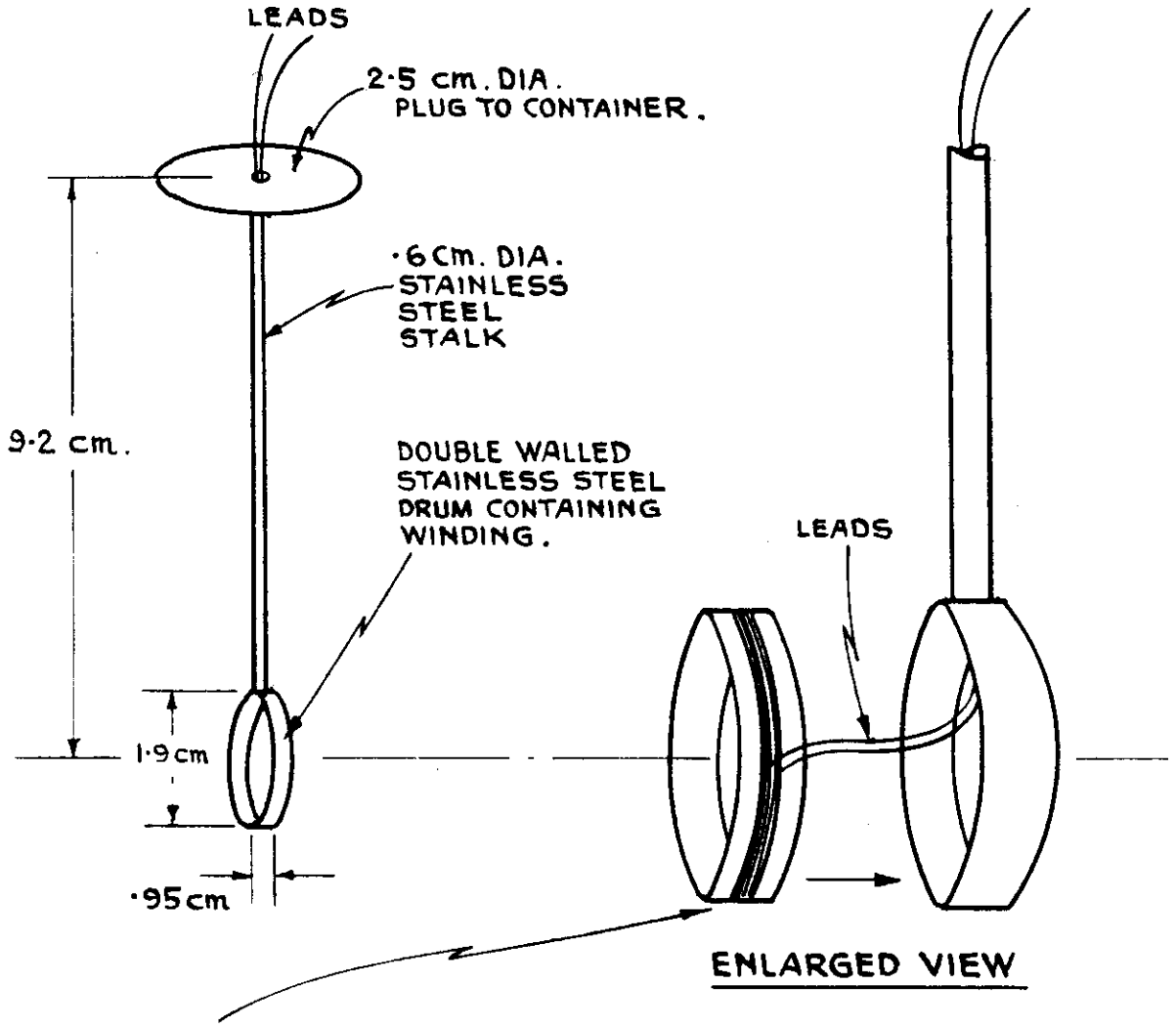

FIG. 5.7 THE CONTAINER SEALING PLUG AND BUILT IN SEARCH COIL

once it was encased, and it was thought unwise to twist the leads for fear of damaging the insulation by abrasion. These therefore might have enclosed an area of about 2 cm^2. The turns were wound on a depression in the inner cylinder of the drum, which was then threaded into the outer cylinder, the leads being passed through a side notch, subsequently plugged. All joins were by fusion welding.

Apart from a small effect due to the separation of the sodium from the top face by the clearance space, the field disturbance should be symmetric about the mid depth of the sodium, so that the currents across the section should be small at this height, and therefore the disturbance caused by the search coil casing should have been small.

The full section search winding consisted simply of 10 turns of .37 mm copper wire with a resistance of 1.0 Ω. Passing outside the Sindanyo plates but inside the heating windings the turns enclosed an area 19.6 cm deep and of 27.5 cm outer, and 3.8 cm inner radius. For protection the turns were glued with Araldite between a pair of fibreglass tapes.

The signals were fed to a Tektronix 551 double beam oscilloscope lent to the magnetohydrodynamics group

by the Atomic Energy Research Establishment. The oscilloscope had a maximum sensitivity of .05 V/cm, and with the small search coil a Telequipment P.S. 2 A.C. preamplifier with a gain of 100 was placed in front of it. The low frequency limit at which the gain was 3 db down was 1 c/s for the Telequipment amplifier, and 2 c/s for the oscilloscope, so this combination was adequate not only for the steady state experiments but also for the transient experiments which required measurements for a time of only about .05 s. The oscilloscope had a square wave calibrator giving signals at 1 kc/s from .2 mV to 100 V accurate to ± 3%, and its time scale was accurate to ± 3%.

5.7 Exciting apparatus.

The exciting apparatus had to produce a power sufficient for measurable signals to be obtained from the small search winding. The field at a radius y in empty space with unit current through an exciting winding of N turns would be

$$\frac{r_o N}{2\pi y}$$

Taking the variation of the field through the small coil to be negligible, the inductance in empty space between

this winding, enclosing with its 10 turns a total area of 27.5 cm^2 at a radius of 15.7 cm, and an exciting winding of N turns would be

$$3.50\ N\ m\mu H$$

At a typical working frequency of 50 c/s the amplitude of the e.m.f. induced in empty space in the small search winding by a current of amplitude I in the exciting winding would thus be

$$1.1\ NI\ \mu V$$

The induced e.m.f. in sodium might be several times this at resonance. To produce, then, a signal $\sim$ 1 mV, the smallest which could be conveniently measured, it was necessary to have a total radial exciting current

$$NI \sim 300\ A$$

Also the flux in empty space through an exciting winding of N turns enclosing a depth h between radii y_1 and y_2 would be

$$\frac{\mu_o Nh}{2\pi} \log \frac{y_2}{y_1}$$

so taking the depth to be 19.6 cm and the radius ratio to be 8 the self inductance in empty space of this winding would be

$$.08\ N^2\ \mu H$$

The load on the supply with an exciting current $\frac{300}{N}$ A would thus be about 2.5 W at 50 c/s in empty space, and in sodium at resonance several times this.

The exciting winding was designed to give an almost continuous current sheet round the fluid section. To obtain a fairly uniform distribution of current in different radial directions, and to reduce the circuit current and consequently the size of the input lead needed to carry the current, without incurring too much complexity of construction, it was divided into 20 segments. The segments were of .9 mm copper sheet soldered together at the inner rim, and insulated with fibreglass cloth glued on by andimpregnated with Araldite. The copper thickness was chosen to give a winding resistance $\sim$ the impedance due to the sodium in the working range, and to give a reasonably low current density with the exciting currents required -- actually 140 A/cm^2 at the inner rim with a total radial current of 300 A.

For steady state experiments current was provided from a Goodmans D 120 oscillator borrowed from the Mechanics Section. This had a frequency range of 10-10 kc/s at an accuracy of $\pm$ 2%, and could produce up to 120 W into 10 Ω. To match the exciting

winding to the oscillator the current was passed through an old welding transformer with a new secondary winding giving a 20 : 1 step down in e.m.f. A eureka resistance of 24.8 mΩ was inserted in series with the exciting winding, and the potential difference across this used to indicate the current. A diagram of the circuit is given in figure 5.8.

For transient experiments a sudden step in current was applied to the exciting winding. To obtain a fast rising current in a circuit to make a sharp step of this type, any inductance there may be must be drowned with a large resistance. To obtain a large current a large voltage must then be used. Here the 230 V D.C. main was simply switched through a resistance of 10.4 Ω in series with the exciting winding to give a step in current of about 21 A. An old two pole magnetically operated switch from the laboratory lift circuit was adapted for the purpose. One pole only was used and this was rebuilt with a curved mating piece for a clean closure. The coil which operated the main switch was energized from the AC main by one pole of a small two pole switch, the other pole of which connected the AC main through a pair of .1 μF condensers to the oscilloscope trigger

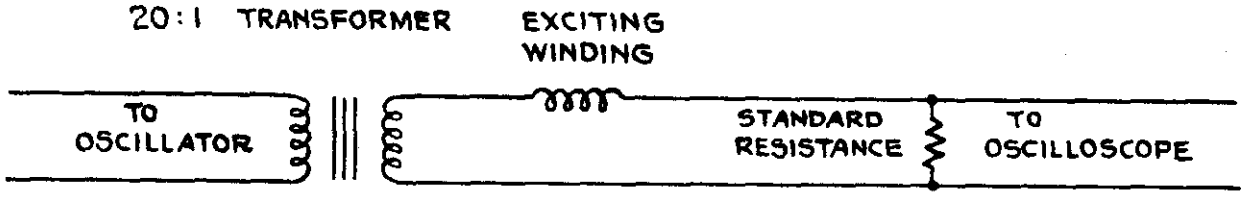

FIG. 5.8 STEADY STATE CIRCUIT.

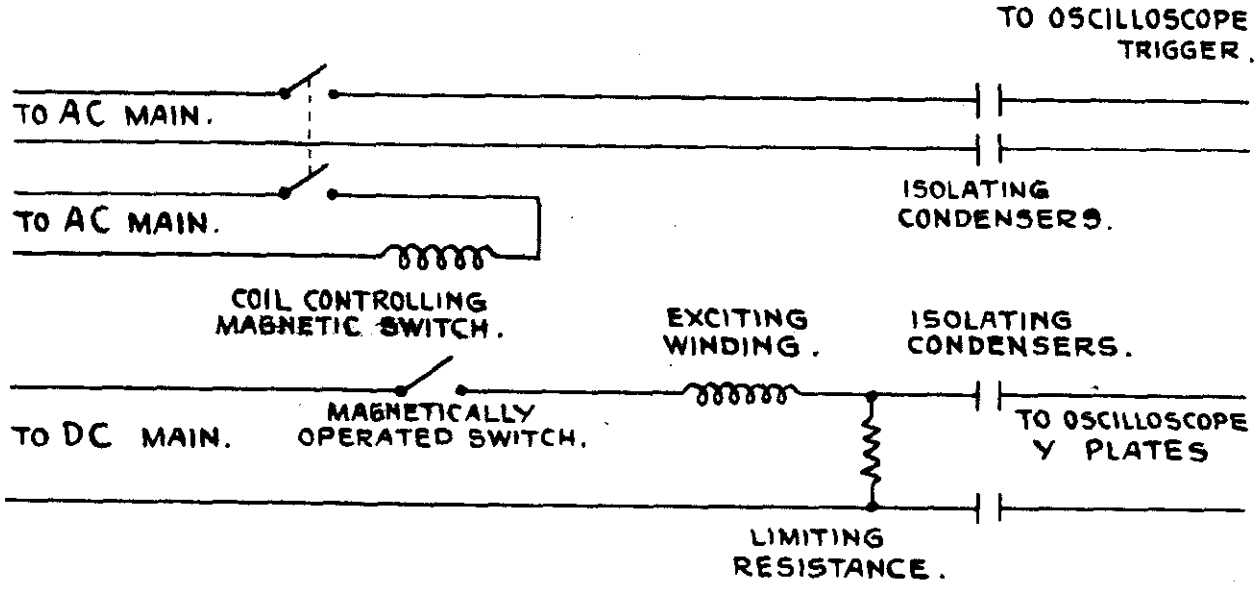

FIG. 5.9 PULSE CIRCUIT.

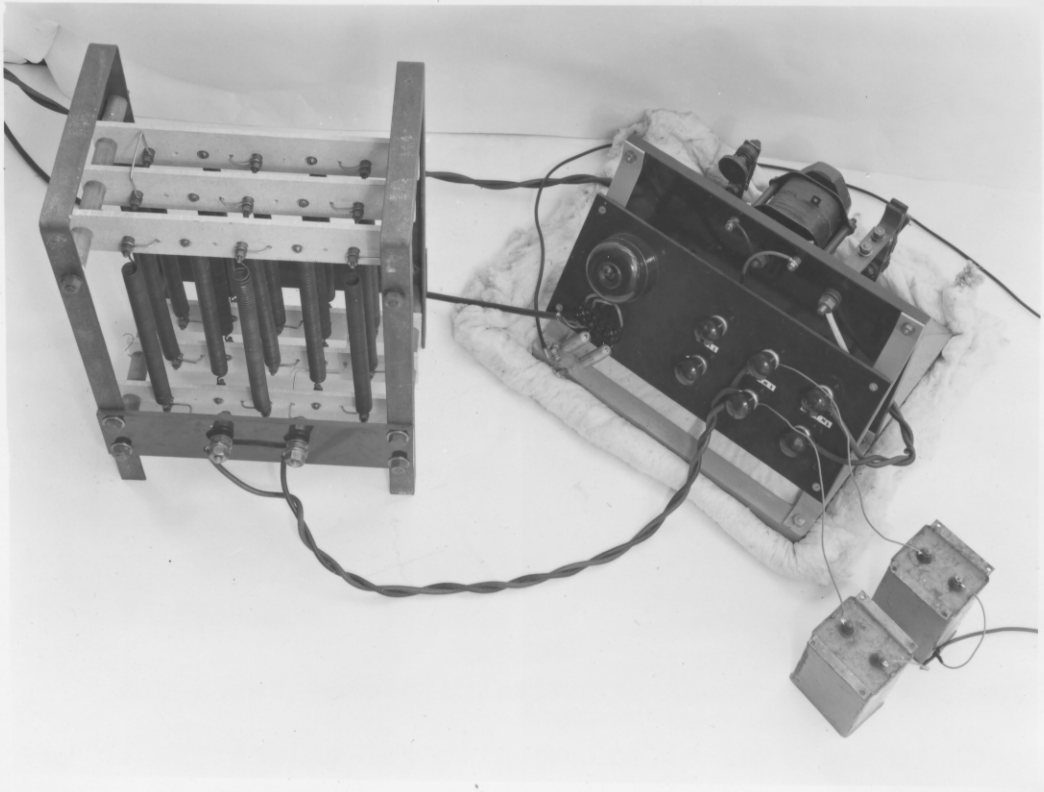

FIG. 5.10

THE SWITCH AND LIMITING RESISTANCE USED TO PRODUCE A SUDDEN CURRENT FOR THE EXCITATION OF TRANSIENT WAVES.

circuit. In this way it was possible to make the oscilloscope beam begin a sweep just before the closure of the main switch, so that the exact instant of closure could be recorded. The potential difference across the limiting resistance was used to indicate the current. A pair of 1 μF condensers was used to isolate the oscilloscope from the DC main. A diagram of the circuit is given in figure 5.9 and the main switch and the limiting resistance are illustrated in figure 5.10.

5.8 Calculation of performance for steady state experiments.

For steady state experiments the most convenient way of expressing the performance is in terms of the inductive coupling between the small or the large search winding and the exciting winding. To estimate this for the small search winding, the coupling which there would have been in empty space was simply multiplied by the ratio of the transverse field in the sodium to the transverse field which there would have been in empty space at the centre of the section, calculated from the solution of the wave equation. The coupling in empty space, with an exciting winding of 20 turns, was estimated by the calculation of 5.7 (pages 99-100) to be

70 m μH. For the large search winding the ratio of the average transverse field in the sodium to the average transverse field in empty space was calculated from the integrated solution of the wave equation, and the coupling in empty space corresponding to the volume occupied by the sodium multiplied by this ratio. The coupling corresponding to the waste space between the sodium and the search winding was then added to give the total coupling. From the formula of 5.7 (page 100) for the flux through a given section, the coupling in empty space between the search winding, its 10 turns enclosing a section 19.6 cm deep with a radius ratio of 7.3, and the exciting winding of 20 turns would have been 15.6 μH, of which the coupling due to the region occupied by the sodium, 17.5 cm deep with a radius ratio of 7.0, would have been 13.6 μH, making a contribution from the waste space of 2.0 μH.

The main problem was to allow for the effect of the conducting walls, which were in contact with the sodium on three sides but separated from it by the clearance space at the top.

In a case where the walls are everywhere in contact with the sodium an estimate can be made from the analysis of 3.8. In such a case it may be expected that the face

and side walls will act more or less independently (3.8, page 60). Neglecting viscosity, the end wall effect is exhibited (3.8, page 55) by a factor

$$\gamma = \frac{1 + \frac{b}{a}(\text{sech}jf - 1)}{1 + sjf\tanh jf \tanh kd}$$

multiplying $\frac{\cosh kx}{\cosh kd}$ in each term of the expansion in eigenfunctions of y, and the side wall effect by a factor (3.8, page 58)

$$\gamma = \frac{1 + \frac{b}{a}(\text{sech}jf - 1)}{1 + sjf\tanh jf \tanh hke}$$

multiplying $\frac{\cosh hky}{\cosh hke}$ in each term of the expansion in eigenfunctions of x.

Taking the resistivity of stainless steel at $120^{\circ}C$ to be $.72\ 10^{-6}$ m [11], values for the experiments were

$d = .0875$ m, $e = .117$ m, $f = .0122$ m

$\lambda_a = .0825$, $\lambda_b = .565$, $c \sim 20$ m/s.

At the fundamental resonance $p = \frac{\pi c}{2d}$. Thus at frequencies in the range near this

$$|jf| \sim \left(\frac{\pi c}{2d\ \lambda_b}\right)^{\frac{1}{2}} \sim .03,$$

$\text{sech}jf \doteq 1$, $\tanh jf \doteq jf$,

showing that the skin effect in steel of this thickness is negligible in the conditions of the experiments. Then for the end wall effect

$$Y = \frac{1}{1 + sjf\tanh hd}$$

and for the side wall effect

$$Y = \frac{1}{1 + sjf\tanh hke}$$

In the case of the side wall effect

$$k^2 = \frac{ip}{\lambda_a} + m^2 + \frac{\sigma^2 m^2}{i\lambda_a p}$$

At the fundamental resonance

$$p = \sigma m_1 , \quad k_1 = m_1$$

At frequencies in the range near this

$$\frac{\sigma^2}{\lambda_a p} \gg 1, \quad |k| \sim \frac{\sigma m}{(\lambda_a p)^{\frac{1}{2}}}$$

and

$$|s| = \frac{\lambda_a}{\lambda_b} \left|\frac{k}{j}\right| \sim \frac{\sigma m}{p} \left(\frac{\lambda_a}{\lambda_b}\right)^{\frac{1}{2}} \sim \frac{m}{m_1} \left(\frac{\lambda_a}{\lambda_b}\right)^{\frac{1}{2}}$$

Also

$$Re(k) \not< 1, \quad \tanh hke \sim 1, \quad \cosh ke \sim 3$$

Thus for the earlier terms the group on the right of the denominator of Y has a magnitude $\sim .05$, and

also $\frac{\cosh ky}{\cosh e}$ is itself only of secondary importance (3.8, page 58), having a magnitude near the centre $\sim \frac{1}{3}$ or less. The side wall effect is thus very small in conditions similar to those of the experiments. The end wall effect on the other hand may be important because $\frac{\cosh x}{\cosh d}$ is the principal part of each term (3.8, page 55) and may become large at resonance, and also s is larger, because in s λ_a is now replaced by $\lambda_a + \frac{c^2}{ip}$. If the side wall effect is neglected, it becomes possible to use the exact solution for a system with end slabs only, and furthermore to take into account viscosity (3.8, page 60).

In a case where the walls are insulated from the fluid it is also fairly easy to estimate the effect of the walls, provided, as has been shown to be the case for the conditions of these experiments, the walls are thin enough for the skin effect in them to be negligible. The method is similar to the approximate method for a one-dimensional system with conducting slabs (3.8, page 52). Let R be the total wall resistance round the section, p the angular frequency, and let I_1 and I_2 be the phasors of the exciting current and the induced wall current, and Φ and H the phasors of the flux and field

for unit exciting current. Then, where a suffix o denotes the values for a system without conducting walls,

$$I_2 R = ip\, I_1 \Phi$$

$$\frac{H}{H_o} = \frac{\Phi}{\Phi_o} = \frac{I_1 - I_2}{I_1} = 1 - \frac{ip\Phi}{R}$$

$$\Phi + \frac{ip}{R}\Phi\ \Phi_o = \Phi_o$$

$$\frac{H}{H_o} = \frac{1}{1 + \frac{ip\Phi_o}{R}}$$

Where τ_b is the resistivity of the walls, f their thickness, h their height, and y_1 and y_2 the inner and outer radii

$$R = \frac{\tau b}{2\pi f}\left(2 \log \frac{y_2}{y_1} + \frac{h}{y_1} + \frac{h}{y_2}\right)$$

With the apparatus used neither method of calculation could be exact. The effects of different assumptions in the calculation of performance are illustrated in figures 5.11 and 5.12. These show for the small and large search coils the envelopes of the peak values of inductive coupling at the fundamental resonance against the resonant frequency in a range from 0 to 100 c/s corresponding to fields from 0 to 1.2 weber/m^2. For the sodium the calculations assumed[10]

$$\lambda = .825\ 10^{-1}\ m^2/s, \qquad \nu = .677\ 10^{-6}\ m^2/s$$

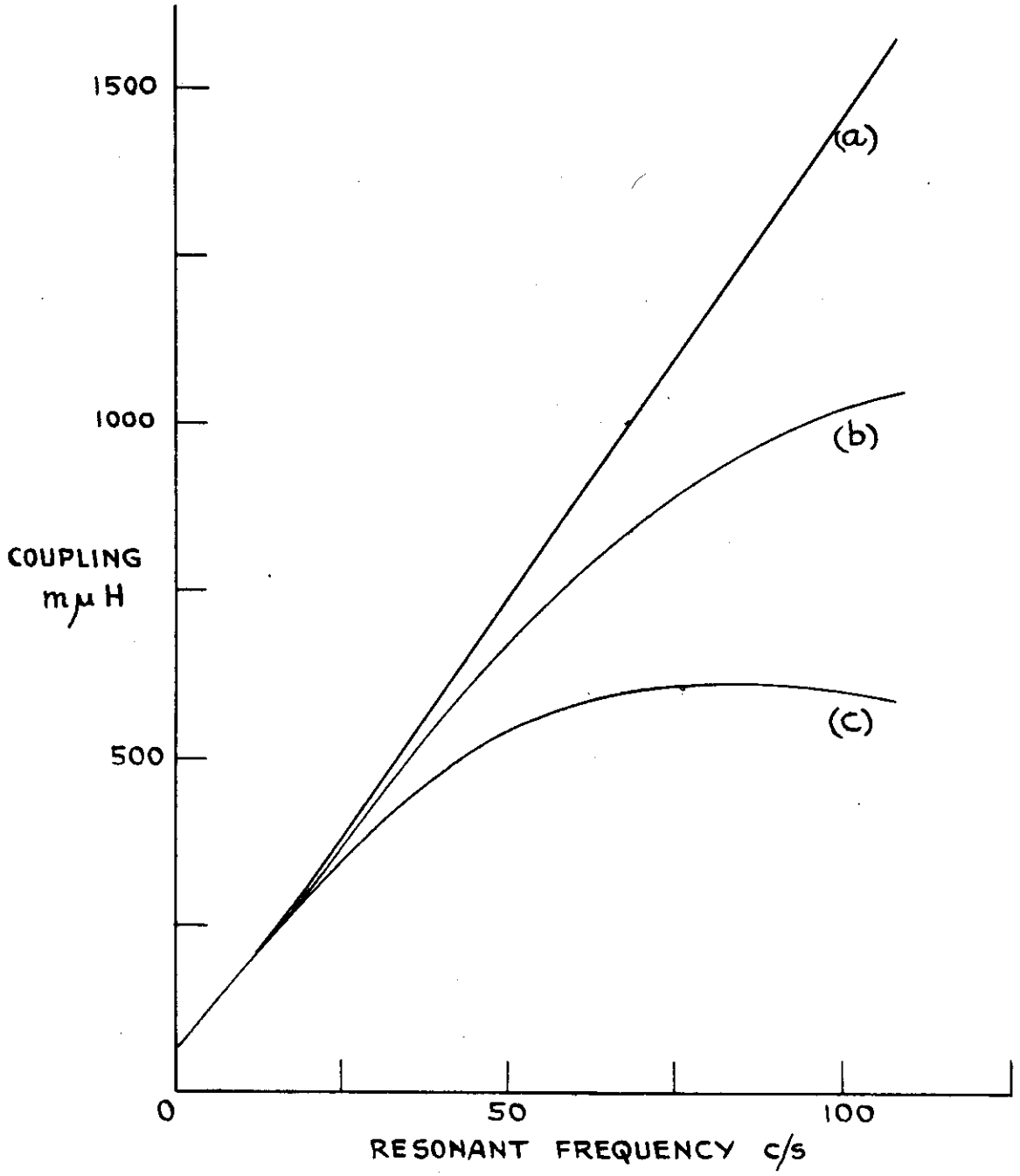

FIG. 5.11

COUPLING AT FUNDAMENTAL RESONANCE BETWEEN THE EXCITING WINDING AND THE SMALL SEARCH WINDING

CALCULATED

(a) WITH NO WALL CORRECTION.

(b) WITH A CORRECTION ASSUMING WALLS INSULATED FROM THE FLUID.

(c) WITH A CORRECTION ASSUMING FREE FLOW OF CURRENT BETWEEN THE WALLS AND THE FLUID.

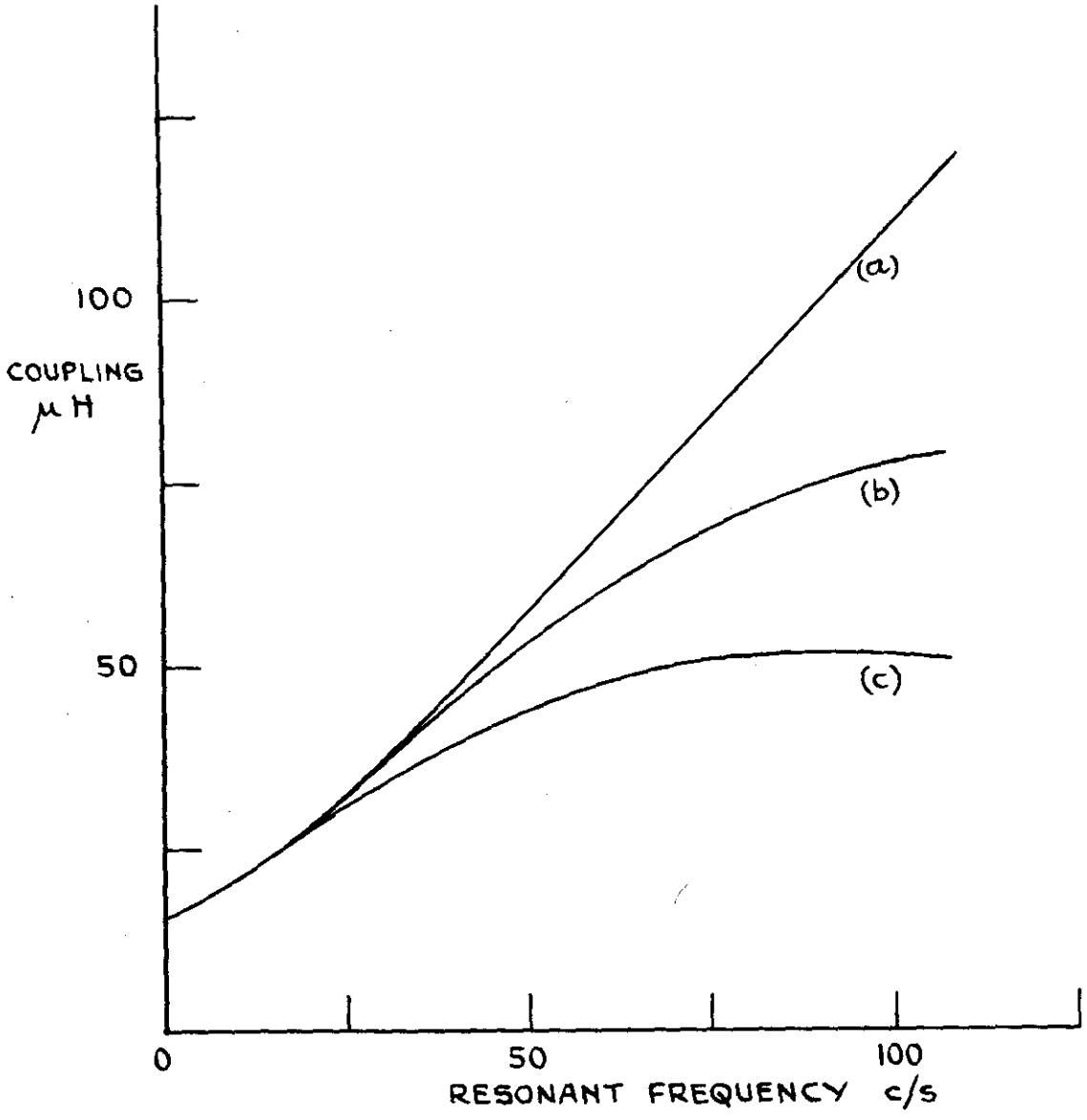

FIG. 5.12

COUPLING AT FUNDAMENTAL RESONANCE BETWEEN THE EXCITING WINDING AND THE LARGE SEARCH WINDING

CALCULATED

(a) WITH NO WALL CORRECTION.
(b) WITH A CORRECTION ASSUMING WALLS INSULATED FROM THE FLUID.
(c) WITH A CORRECTION ASSUMING FREE FLOW OF CURRENT BETWEEN THE WALLS AND THE FLUID.

and for steel they assumed[11]

$$\lambda = .565 \ m^2/s$$

In every case the solution of the wave equations for the field in the sodium was evaluated using the computing machine at the Mathematical Laboratory (Appendix 1).

The upper curves were calculated with no wall correction from the formula obtained in 3.7 (pages 40-42) for an axial system with a resistive and viscous fluid, summed to 20 terms. The viscosity of sodium actually causes a reduction in the performance of about 3% at resonance at a frequency of 50 c/s.

The middle curves were calculated from the same formula, but the field in the sodium was corrected to allow for the effect of the walls by the formula obtained above for a case in which current is everywhere prevented from flowing between the sodium and the walls. The flux through the clearance space between the sodium and the walls was taken into account in determining the correction. For the large search coil the coupling due to the total waste space was taken to be 2.0 μH, as in empty space; any error in this would have a very small effect on the overall result.

The lower curves were calculated assuming a free flow

of current between the sodium and the walls. The side walls were neglected, and the curves were calculated from the formula obtained in 3.8 (pages 60-62) for a system with a resistive and viscous fluid in contact with conducting end slabs, summed to 20 terms. For the large search winding the coupling due to the waste space was again taken to be 2.0 μH. The correction is greater by this method, because the additional currents caused by the presence of the walls flow partly through the sodium which presents less resistance than the walls.

The curves obtained by either method of correction show the increasing importance at resonance of the induced wall currents as the resonant frequency is raised. Finally the currents become so large that the performance starts to decline. Away from resonance the corrections become unimportant because the flux inducing the currents becomes so much smaller, and also beyond the fundamental resonance the flux partly cancels itself, being in opposite directions at different depths. Resonant frequencies in the experiments were below 55 c/s. In this range the correction at the fundamental resonance by the method assuming a free flow of current between the sodium and the walls reaches 30% for the small search winding, 25% for the large search winding, but at frequencies more than 20% different from the frequency of the

fundamental resonance, the maximum difference between the three methods was found to be 9% for the small search winding, 7% for the large search winding, this difference occurring at the first harmonic resonance.

Although the sodium was separated from the top face of the container, the current from this face could flow into the sodium round the corners of the section through the top of the side walls. The method of calculation assuming a free flow of current between the sodium and the walls is therefore probably the most accurate and this method was used for further calculations to predict the performance in the actual experimental conditions. Since however the method assumes contact with the top face, it should underestimate because in the actual apparatus not only could no current flow into the surface of the sodium, but also there was no viscous retarding force at the surface.

5.9 Steady state experiments.

All steady state experiments were conducted with the sodium temperature at $120^{\circ}C$.

Each test was conducted at a constant magnetic field, giving a constant value of the damping factor $\Lambda + \nu$, and measurements were taken at different

frequencies. Three values of magnet current were used, 100, 150 and 200 A, giving fields of .325, .487 and .650 weber/m^2 respectively. The corresponding values of $\Lambda+N$ are .090, .066 and .0495. In this range of current it was found possible to keep the current constant within $\pm$ 1%, despite the rising temperature in the magnet coil, while recording measurements from the oscilloscope. At higher values of current, the rate at which the current decreased was found to be too great to allow accurate reading of the oscilloscope.

Exciting currents of up to about 15A were used. With a current of 15A the horizontal field at the inner wall would have been about .0015 weber/m^2, so that the ratio at the inner wall of the horizontal to the vertical field would have been about .005 in the case of the tests at the lowest field strength. Any non-linear effects (2.1, page 7) should therefore have been negligible.

The magnitude of the coupling was measured by applying the e.m.f. from whichever search winding was being used to one beam of the oscilloscope, and the current signal given by the potential difference across the standard resistance in the exciting circuit (5.7, page 102) to the other beam. The gain of each beam was calibrated

with the square wave calibrator, applied in front of the preamplifier where this was used. The signals could be read to about ± 5%.

In tests using the large search winding the phase difference was measured by applying the current signal to the X amplifier of the oscilloscope so as to produce an ellipse. The amounts of X and Y gain were then adjusted to make the ellipse touch all four sidesof a square on a specially marked dial and the phase difference was read from a scale along one of the diagonals of the square. In this way it was possible to read the phase difference to an accuracy of about ± 2°. In tests using the small search coil not enough Y gain was available to make this possible, and so the signals were applied to the separate beams and the X gain adjusted to make just one wavelength fit across the dial. It was possible only to read to about ± 4°.

Figure 5.13 shows the curves calculated for the small search winding for the three field strengths used. Figures 5.14, 5.15 and 5.16 show comparisons for each field strength between these curves and the results of tests using the small search winding. It can be seen that magnitude displacements within ± 8% or phase displacements within ± 8°, combined with frequency

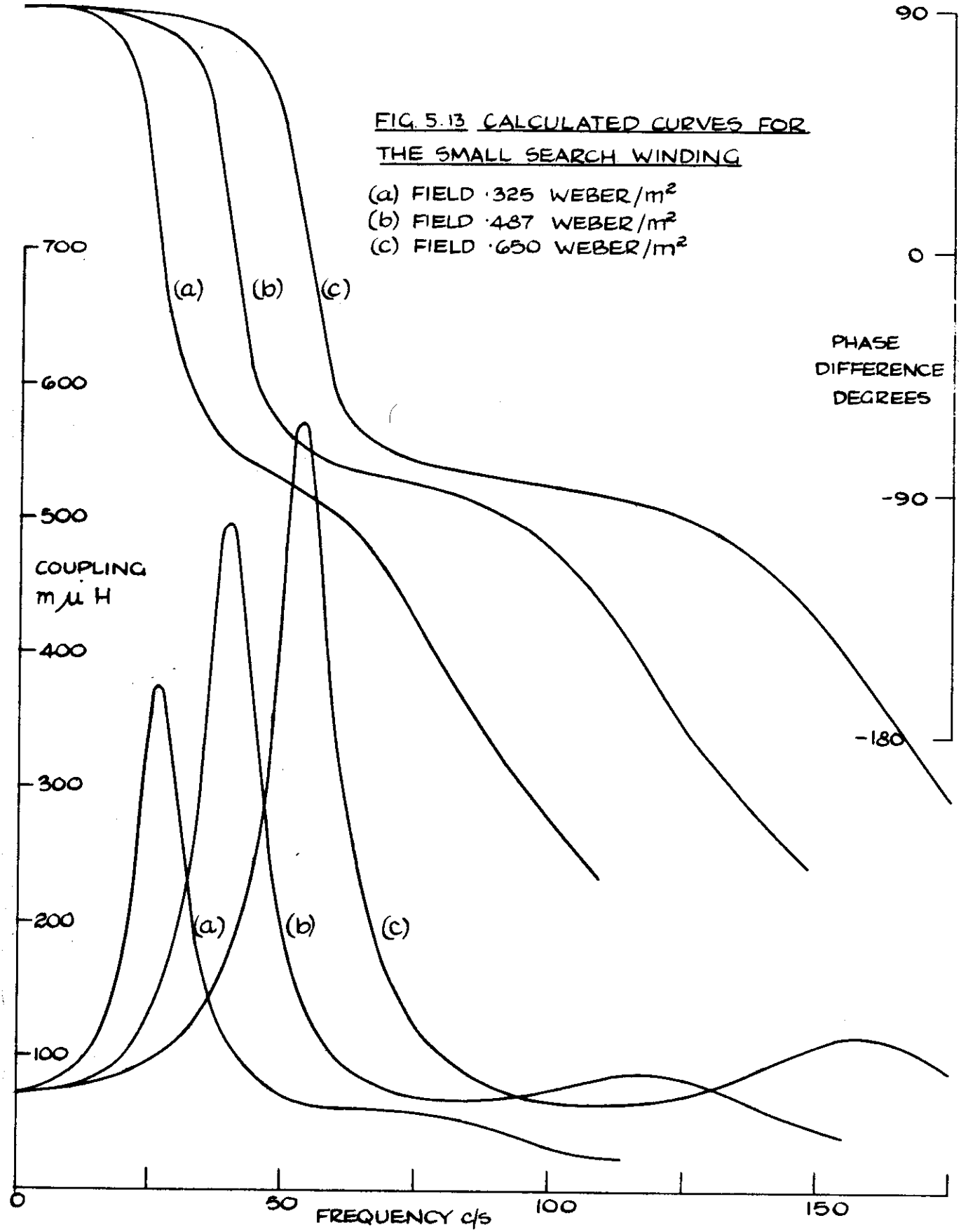
FIG. 5.13 CALCULATED CURVES FOR THE SMALL SEARCH WINDING
(a) FIELD ·325 WEBER/m²
(b) FIELD ·487 WEBER/m²
(c) FIELD ·650 WEBER/m²
90
0
-90
-180
PHASE DIFFERENCE DEGREES
700
600
500
400
300
200
100
COUPLING mμH
(a)
(b)
(c)
(a)
(b)
(c)
0
50
100
150
FREQUENCY c/s

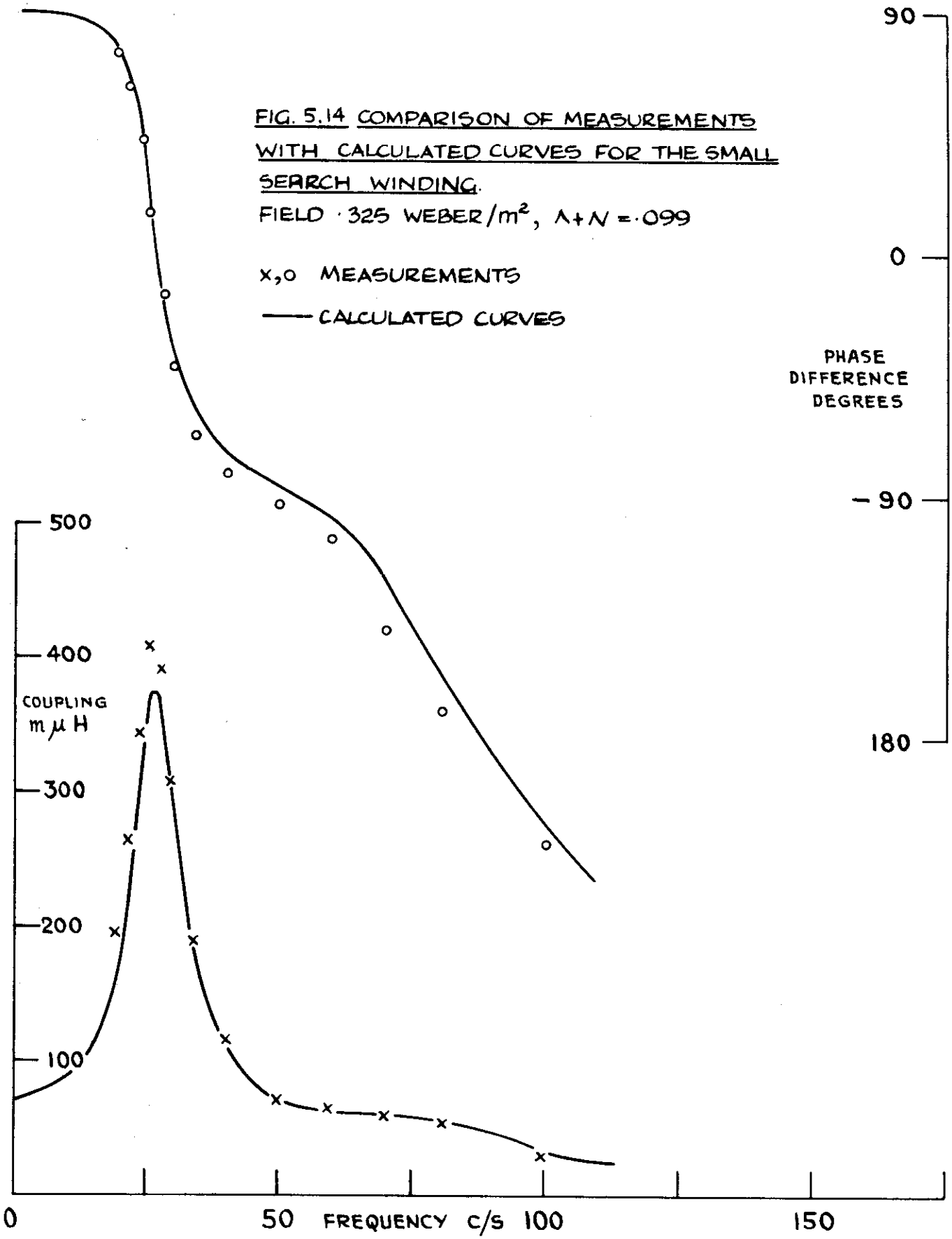

FIG. 5.14 COMPARISON OF MEASUREMENTS WITH CALCULATED CURVES FOR THE SMALL SEARCH WINDING.
FIELD · 325 WEBER/m^2, $\Lambda+N = .099$

x,o MEASUREMENTS

—— CALCULATED CURVES

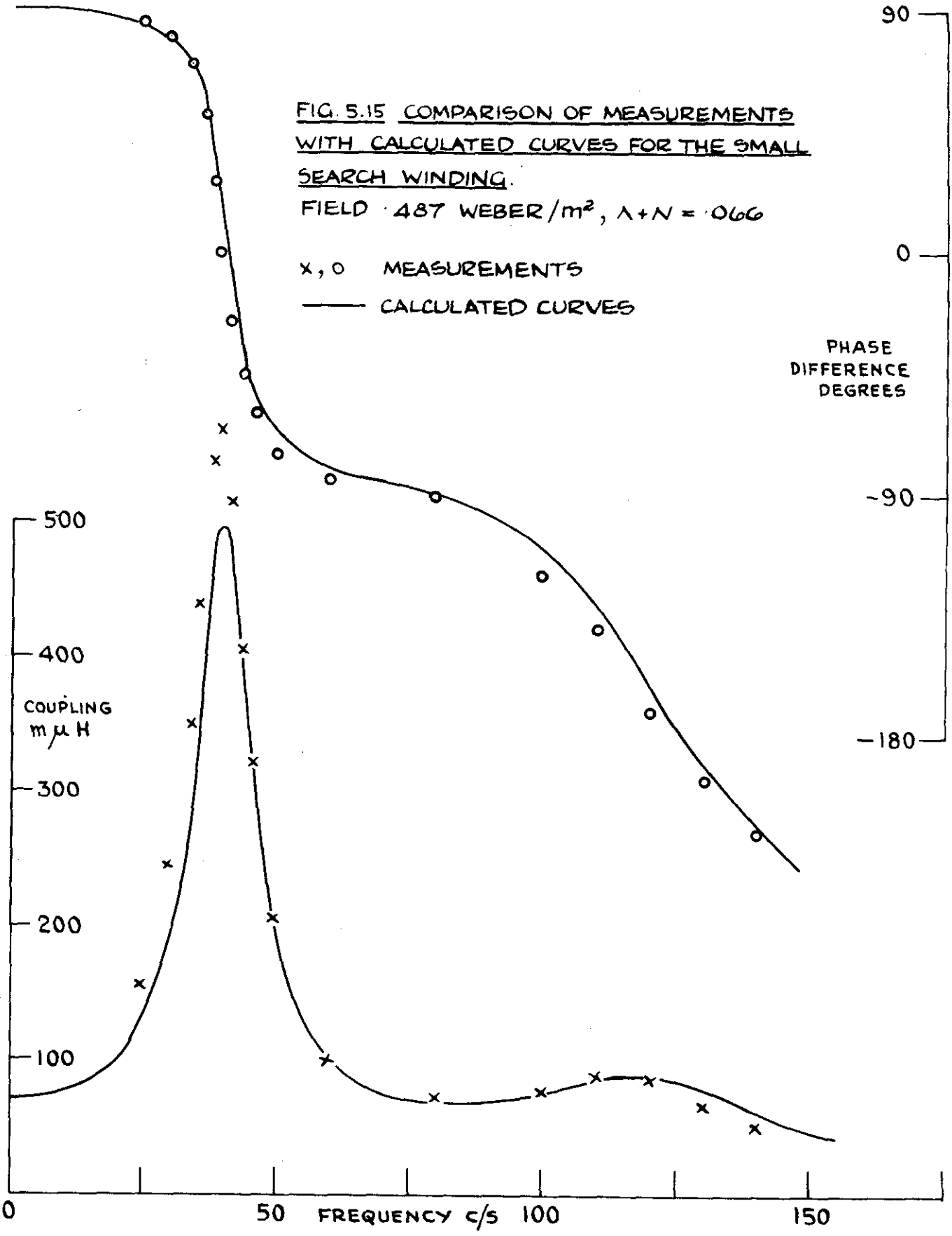

FIG. 5.15 COMPARISON OF MEASUREMENTS WITH CALCULATED CURVES FOR THE SMALL SEARCH WINDING.
FIELD ·487 WEBER/m², Λ+N = ·066

x, o MEASUREMENTS

—— CALCULATED CURVES

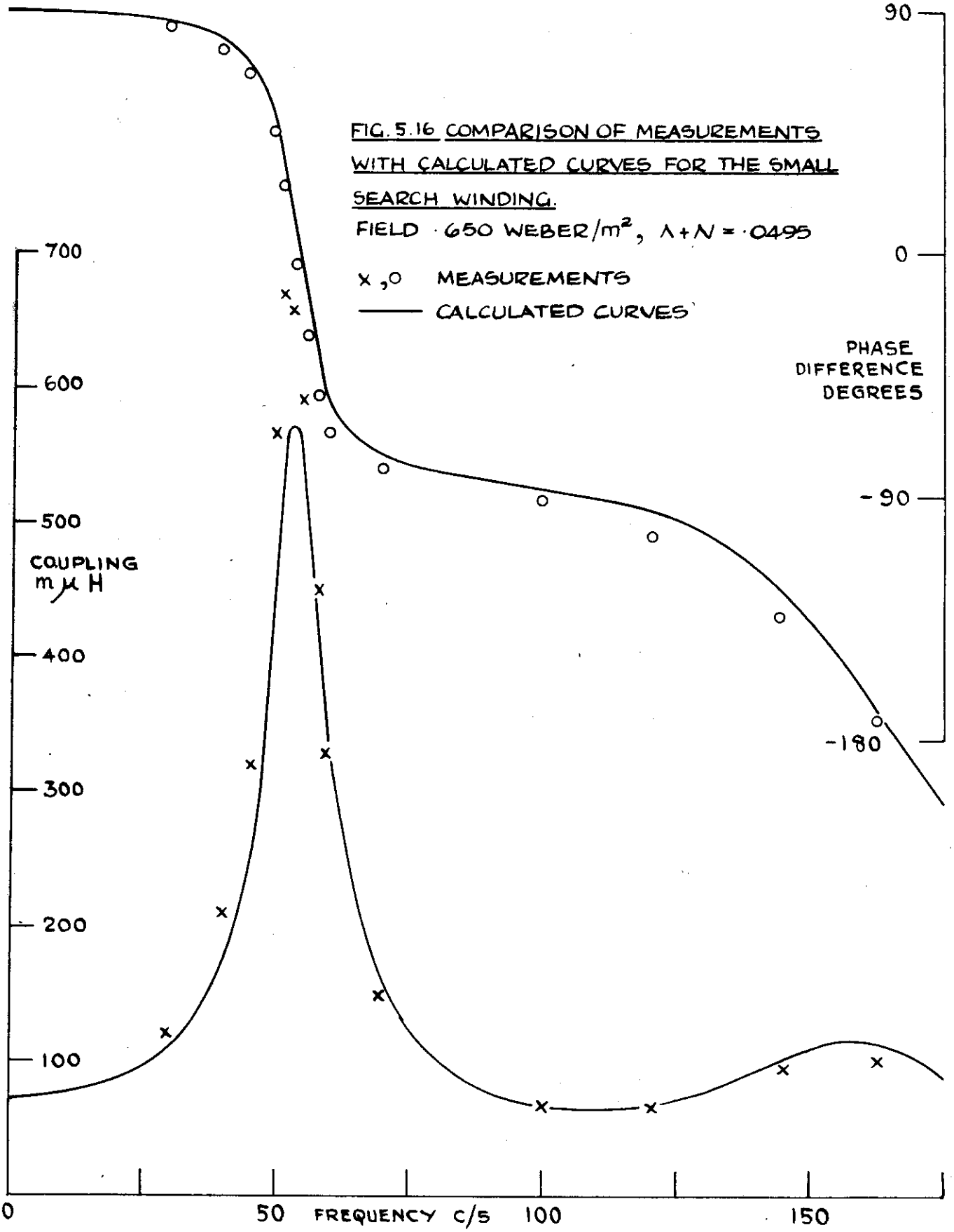
FIG. 5.16 COMPARISON OF MEASUREMENTS WITH CALCULATED CURVES FOR THE SMALL SEARCH WINDING.
FIELD ·650 WEBER/m², Λ+N = ·0495
x ,o MEASUREMENTS
—— CALCULATED CURVES
90
0
-90
-180
PHASE DIFFERENCE DEGREES
700
600
500
400
300
200
100
COUPLING mμH
0
50
FREQUENCY c/s
100
150

displacements within ± 5% would generally be sufficient to bring the measurements into agreement with the calculations except at the fundamental resonance, at which the calculations gave an underestimate of 15% when the field was .650 weber/m^2.

Figure 5.17 shows the curves calculated for the large search winding. The curves collapse beyond the fundamental resonance because then the flux partly cancels itself. Figures 5.18, 5.19 and 5.20 show comparisons between the curves and the results of tests using the large search winding. In this case magnitude displacements within ± 5% or phase displacements within ± 3°, combined with frequency displacements within ± 5% would generally be sufficient to bring the measurements into agreement with the calculations, and at the fundamental resonance the maximum discrepancy is only about 5%.

The results of both tests using the small search winding and the tests using the large search winding are tabulated in Appendix 2.

Since the amplitude calibrator was accurate to ± 3% (5.6, page 99) the magnitude measurements should have been accurate within the margin of error of observation, to about ± 5%. Also with either method of phase measurement the exact amounts of X and Y gain of the oscilloscope were unimportant, so again the measurements

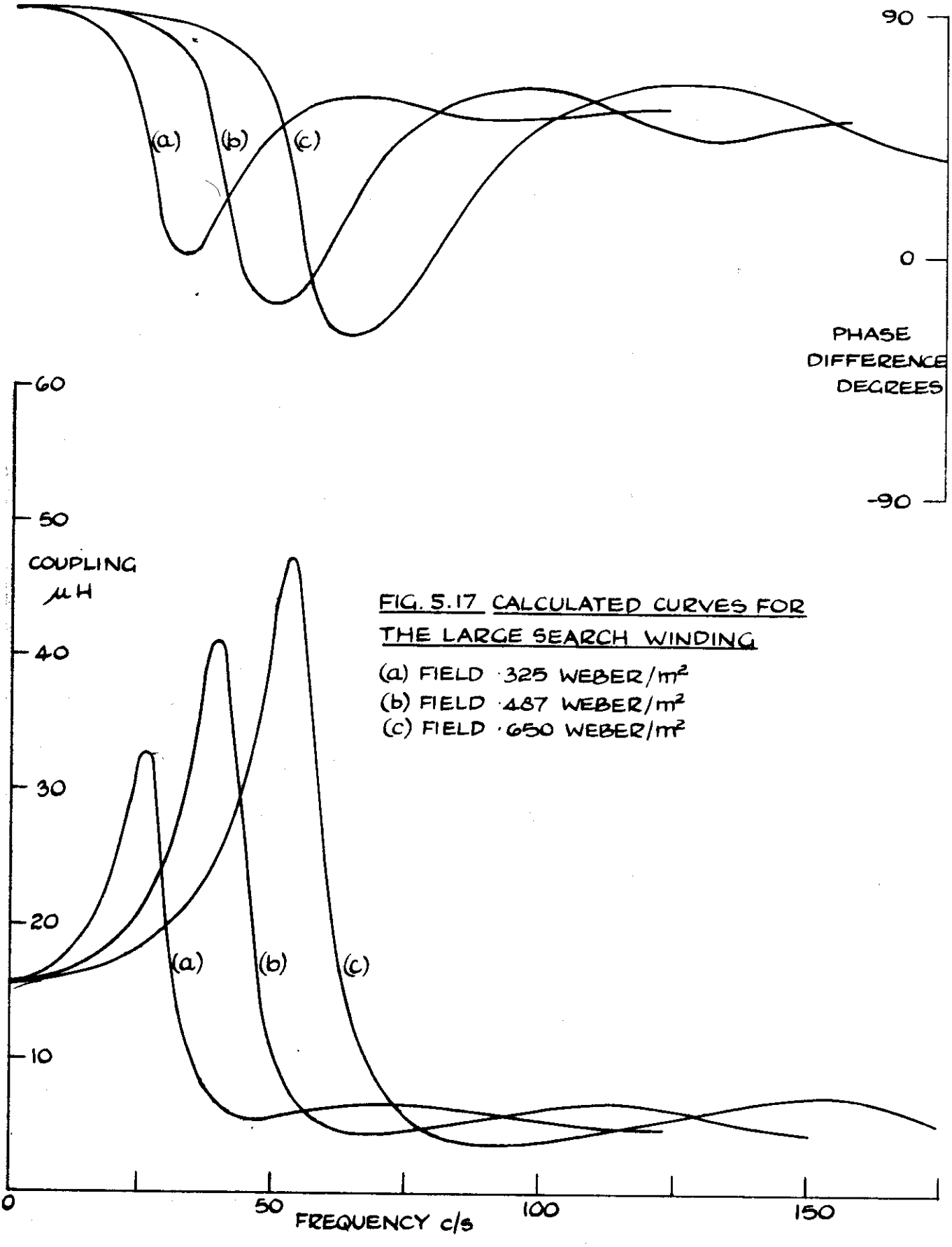

FIG. 5.17 CALCULATED CURVES FOR THE LARGE SEARCH WINDING

(a) FIELD ·325 WEBER/m²
(b) FIELD ·487 WEBER/m²
(c) FIELD ·650 WEBER/m²

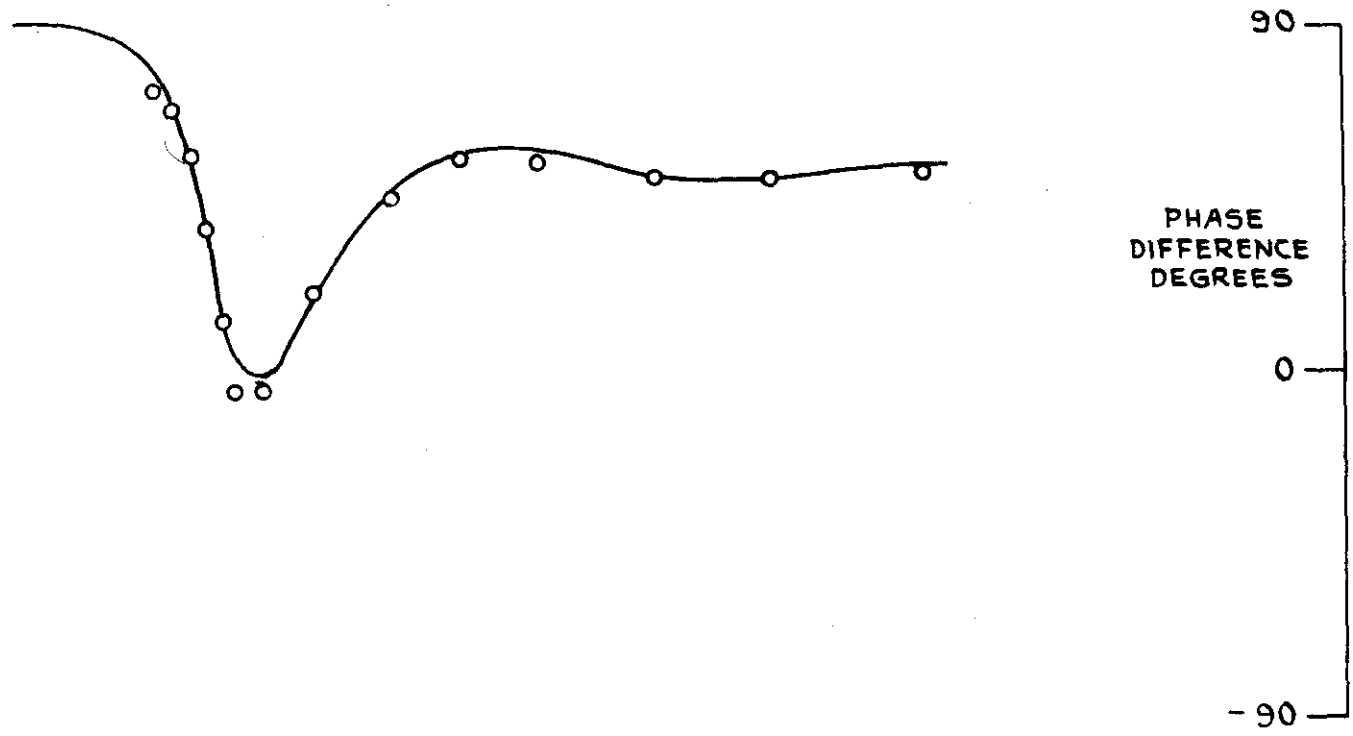

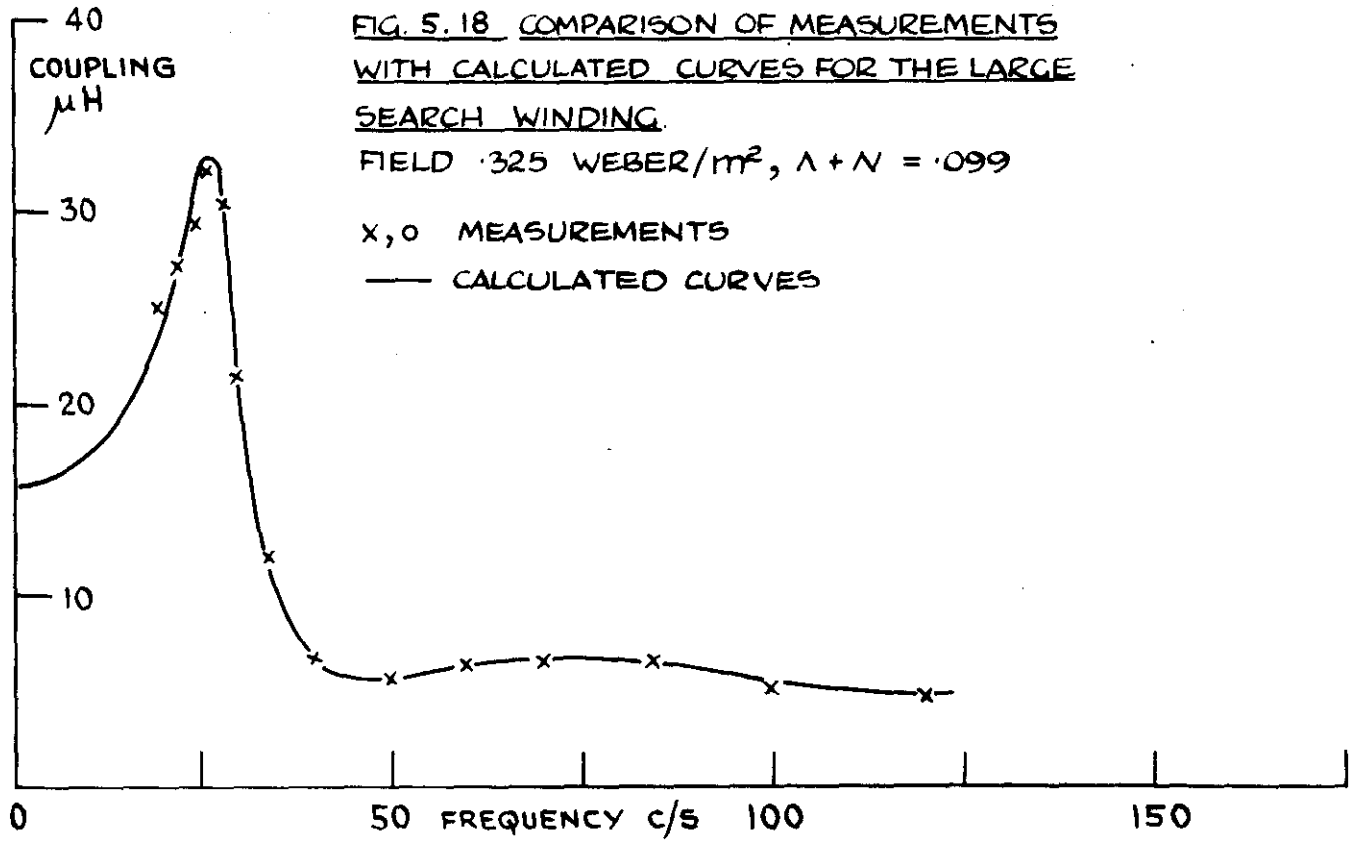

FIG. 5.18 COMPARISON OF MEASUREMENTS WITH CALCULATED CURVES FOR THE LARGE SEARCH WINDING.

FIELD ·325 WEBER/m², Λ + N = ·099

x, o MEASUREMENTS

—— CALCULATED CURVES

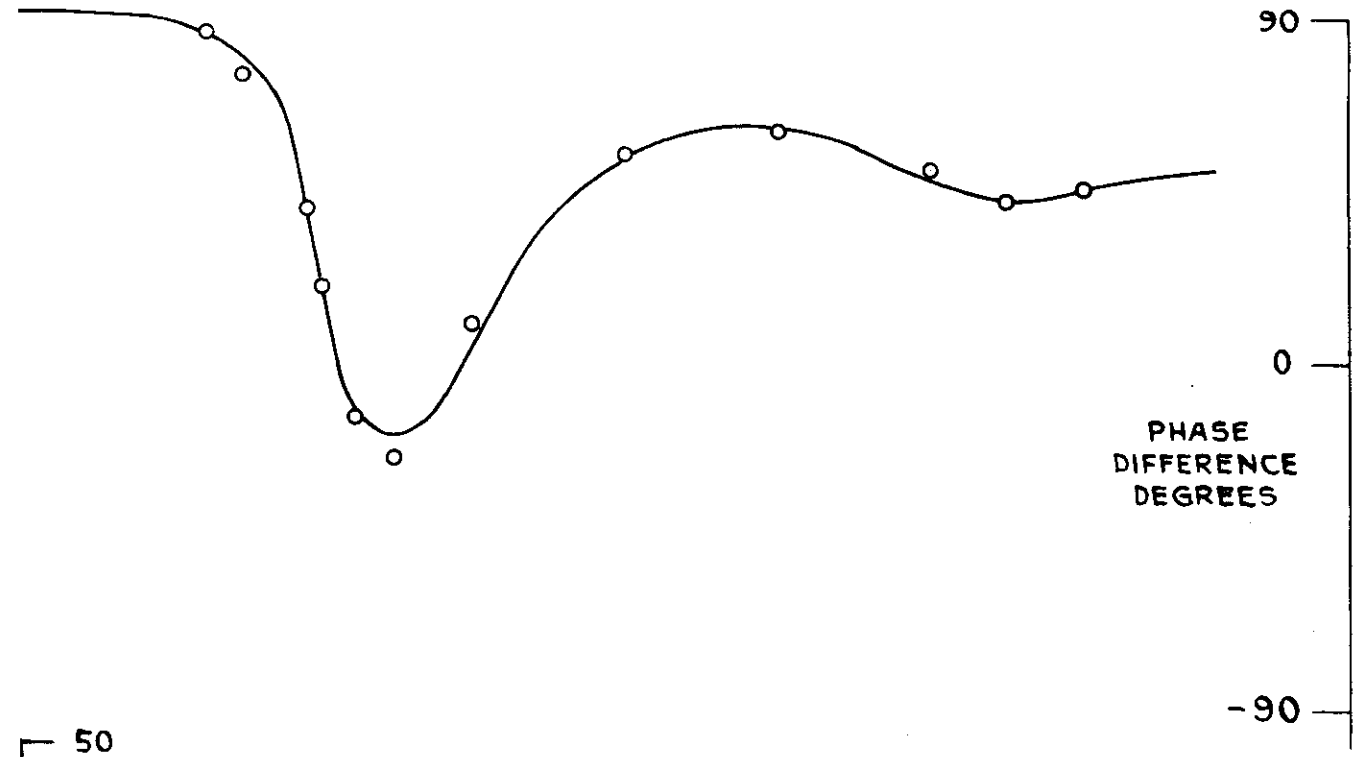

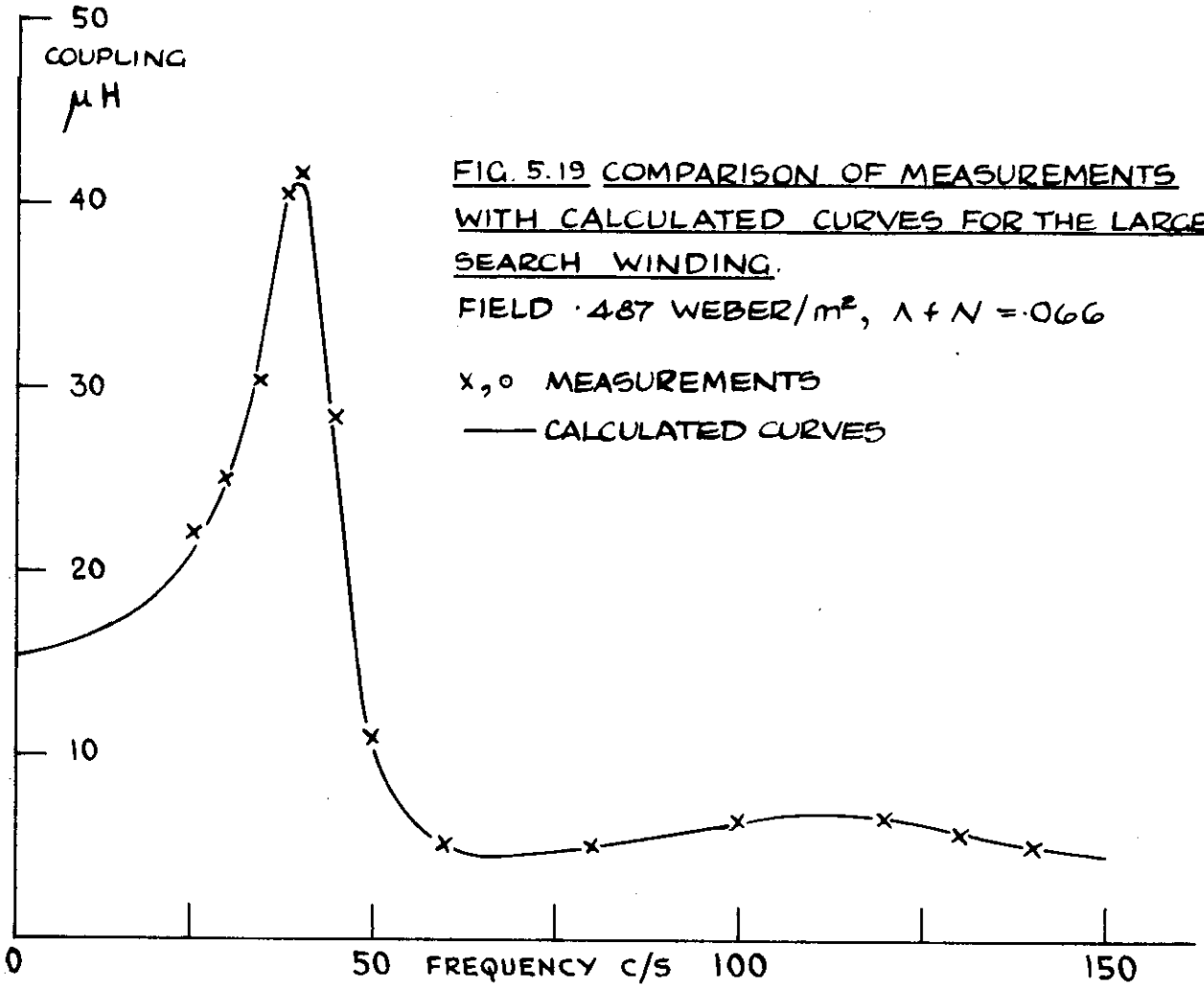

FIG. 5.19 COMPARISON OF MEASUREMENTS WITH CALCULATED CURVES FOR THE LARGE SEARCH WINDING.

FIELD ·487 WEBER/m², $\Lambda \div N = \cdot 066$

x, o MEASUREMENTS

—— CALCULATED CURVES

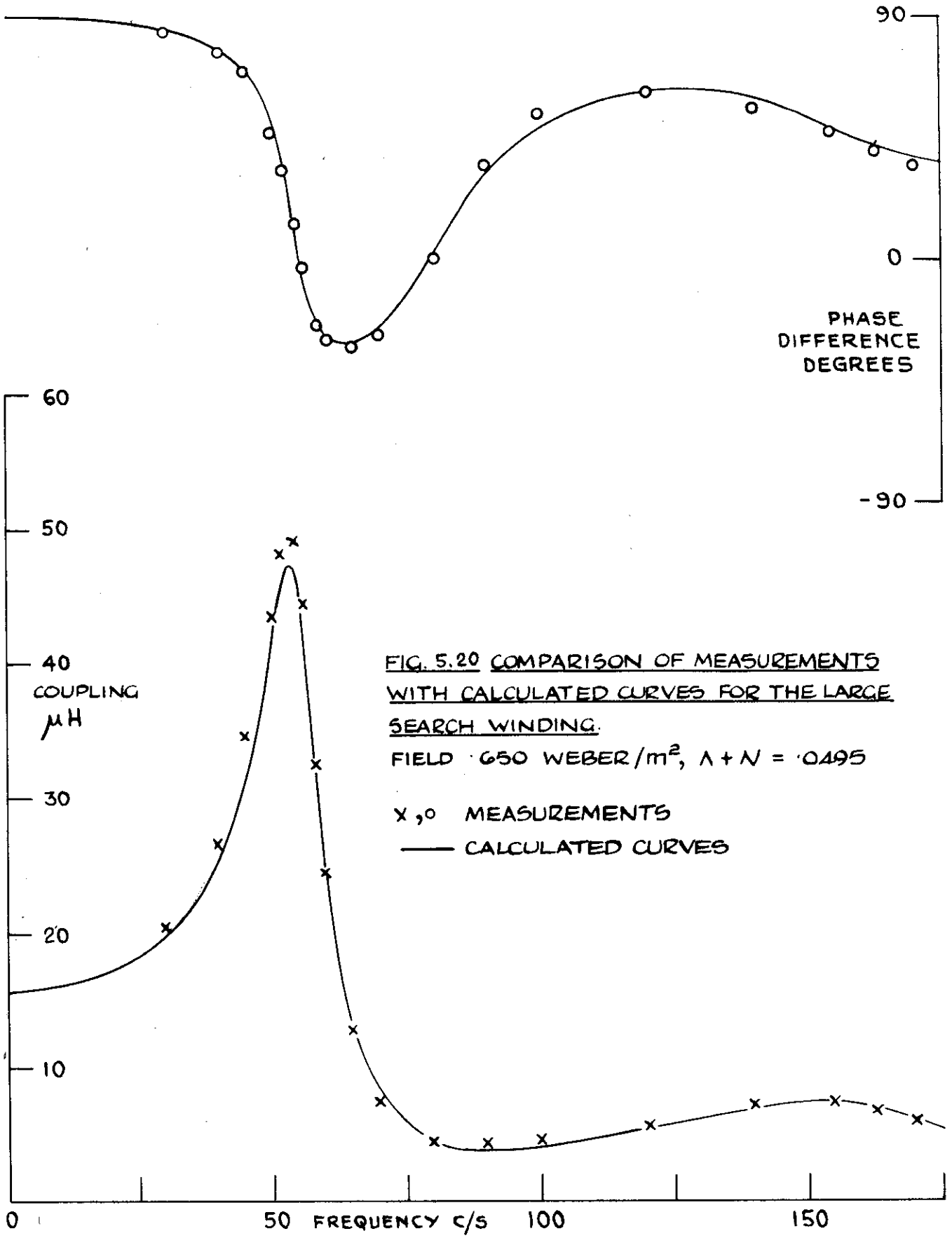

FIG. 5.20 COMPARISON OF MEASUREMENTS WITH CALCULATED CURVES FOR THE LARGE SEARCH WINDING.

FIELD ·650 WEBER/m², Λ + N = ·0495

X, o MEASUREMENTS

—— CALCULATED CURVES

should have been accurate within the margin of error of observation, to about $\pm 4^{\circ}$ in tests using the small search winding, $\pm 2^{\circ}$ in tests using the large search winding. With the oscillator used the frequency should have been accurate within $\pm 2\%$ (5.7, page 101).

To calculate the situation in the sodium at a given field strength it was necessary to know the dimensions of the sodium region, the properties of the sodium, the dimensions of the steel walls, and the properties of the steel. The dimensions of the sodium region were known within about $\pm \frac{1}{2}\%$. There might have been errors of up to about $\pm 3^{\circ}C$ in the temperature (5.5, page 96); a variation of this amount in the temperature would not cause changes of more than about $\pm 2\%$ in the resistivity and viscosity of the sodium[10]. Impurities in the sodium would have tended to have risen to the surface where they would have had little effect. Errors in the properties assumed for the sodium were therefore probably not serious compared with the other errors. The thickness of the walls might have varied slightly. The properties of the steel might also have varied from one place to another; they would hardly have been affected by temperature changes of a few degrees. However an error of even 10% in either the thickness or the resistivity of the steel would have caused an error of at most 3% at resonance, and

generally less, because these factors affected only the wall correction, itself small, particularly away from resonance (5.8).

There was an uncertainty of about ± 3% in the field which should be assumed for a given magnet current, allowing for the possible error in the area of the search coil used in measuring the field, for the flux meter error, and for the non-uniformity of the field (5.3, pages 89-90). In addition there might have been variations in the current as great as ± 1%. These sources could have caused an error of up to about ± 4% in the calculated resonant frequency. At resonance they could have caused a similar error in the calculated magnitude; away from resonance they would have had hardly any effect on the magnitude. The approximations in the method of calculation should have introduced errors generally not more than about ± 5% except at resonance (5.9). Since the calculations assumed contact of the sodium with the walls at both faces the underestimate they gave at the fundamental resonance was to be expected.

The casing of the small search winding must have created some local disturbance, which would have affected its signals, though probably not greatly (5.6, page 98). Also although the area enclosed by the winding itself was

known within $\pm \frac{1}{2}\%$, the area enclosed by its leads was not exactly known, but might have been as great as about 7% of the total area enclosed by all the turns of the winding (5.6, page 98). An error due to the flux through the leads would be consistent with the high values of coupling measured at the fundamental resonance and the low values measured at the first harmonic resonance compared with the calculated values, because this flux would be in opposite directions in these two cases. The area enclosed by the large search winding was known within about $\pm \frac{1}{2}\%$. Any error in the estimate of the contribution from the space outside the sodium to its signal should have caused a negligible overall error (5.8, page 109).

Taking all these sources of error into account, the agreement between the measurements and the calculations was satisfactory. A closer agreement could be expected in the case of the tests using the large search coil, and was obtained.

5.10 Calculation of performance for transient experiments.

With a perfectly conducting inviscid fluid the e.m.f. in the small search winding in a transient experiment using a sudden step in current to excite waves would be zero except at instants when the wave fronts were passing the coil when there would be a sharp pulse of e.m.f.

determined by the wave speed and the coil width; the e.m.f. in the large search winding would rise instantly to a value determined by the wave speed and the section width and would be reversed at each wave reflection. With damping the wave fronts would be dispersed so that the pulses in the small search coil would be spread over a longer time, and the reversals of the e.m.f. in the large search coil would not be sudden.

In the calculation of the e.m.f. to be expected in the experiments any damping and dispersion due to viscosity was ignored. Since the effect of viscosity is only about 3% at resonance and less at other times in steady state situations with similar amounts of resistive and viscous damping the error introduced was probably small. The effect of the conducting walls was also ignored. Again since in steady state situations typical of the conditions of the experiments the effect of the walls is only important when there is magnification of the flux at resonance, it may be supposed that the error introduced was small.

In the experiments Λ was in the range .05 to .1. In this range the wave fronts are dispersed well beyond the width of the small search winding even before the first time that they reach the centre (figures 4.3 and

4.9) so that it is possible to assume a constant rate of change of the field through the area of the coil without serious error. The e.m.f. to be expected in the small search winding was therefore calculated simply by multiplying the area enclosed by the winding by the rate of change of the transverse field at the centre point of the section given by the solution obtained in 4.3 (pages 75-77) summed as far as the 20^{th} term of each component of the double expansion. The e.m.f. to be expected in the large search winding was calculated by multiplying the area of the sodium section by the average rate of change of the transverse field given by the integrated solution. The waste space between the sodium and the winding was ignored, since the field should build up immediately in this space, causing only a temporary pulse in the e.m.f.

The computer at the Mathematical Laboratory was used for the calculations (Appendix 1). There were difficulties of convergence caused by differentiating the series which made the evaluation of the rate of change of the field unreliable near $t = 0$. In conditions typical of the experiments the e.m.f. in the small search winding builds up slowly because of the delay before the wave fronts reach it, and the error due to slow

convergence only becomes important at values of t for which the e.m.f. is still small, so that a good estimate could be made of the shape to be expected of the curve of e.m.f. against time; the e.m.f. in the large search winding on the other hand builds up fast so that it is already large in a range of values of t in which the error is large, and consequently an estimate of the shape could not be made near $t = 0$.

5.11 Transient experiments.

Transient experiments were conducted in the same conditions as the steady state experiments, with the sodium at a temperature of $120^{\circ}C$ and with field strengths of .325, .487 and .650 weber/m^2. Check tests were also made with no field. In all the tests the current signal given by the potential difference across the limiting resistance (5.7, page 103) was applied to the upper beam of the oscilloscope, and the e.m.f. in whichever search winding was being used to the lower beam. The gain of each beam was calibrated with the square wave calibrator.

Figure 5.21 shows the curves of e.m.f. against time calculated for the small search winding. Figure 5.22 shows photographs of typical traces obtained in tests using the small search winding. There was a 300 c/s ripple in the potential of the DC main and consequently

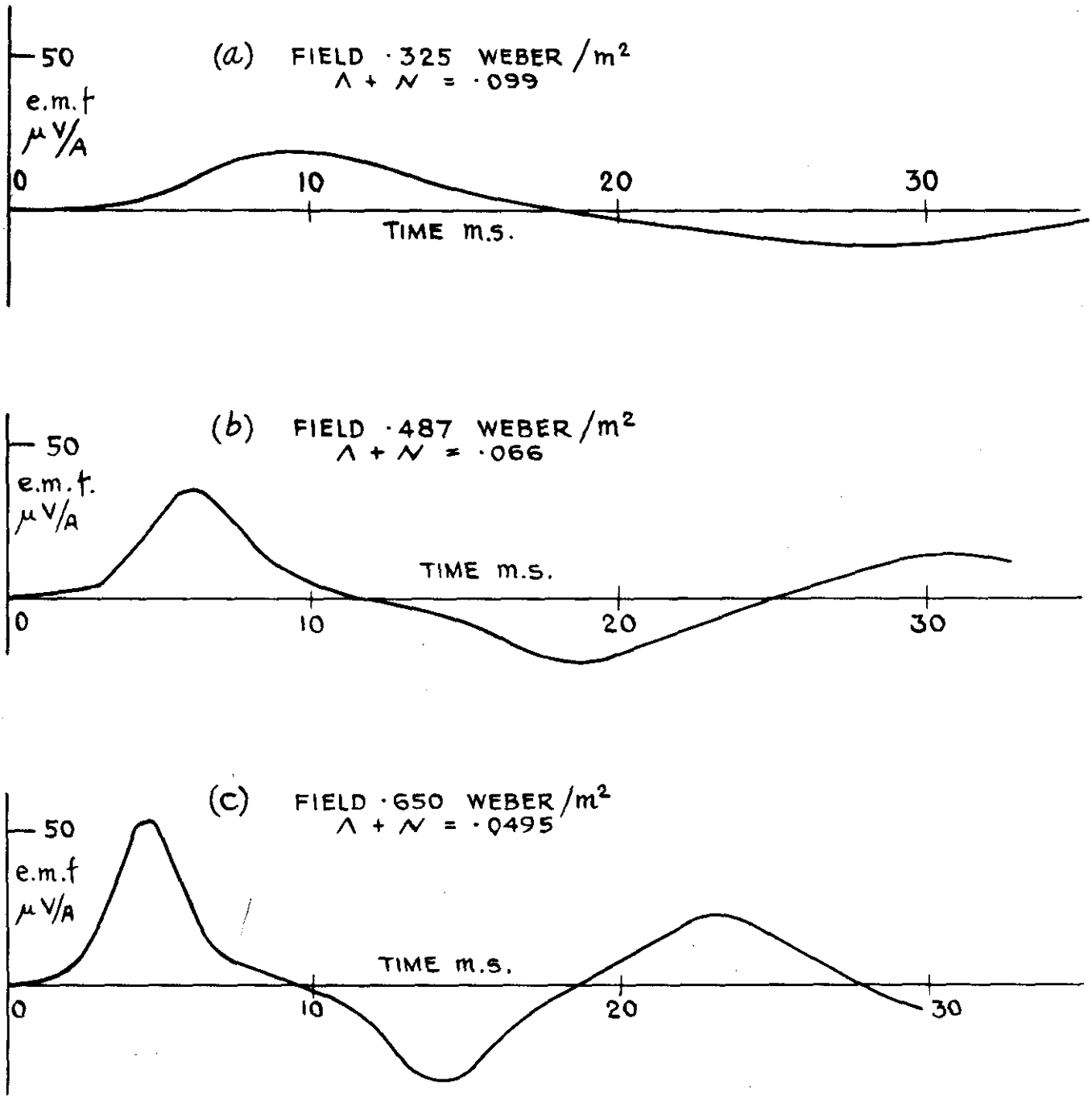

FIG. 5.21 INDUCED e.m.f/UNIT EXCITING CURRENT CALCULATED FOR THE SMALL SEARCH WINDING.

FIG. 5.22

TRANSIENT BEHAVIOUR RECORDED BY THE SMALL SEARCH WINDING.

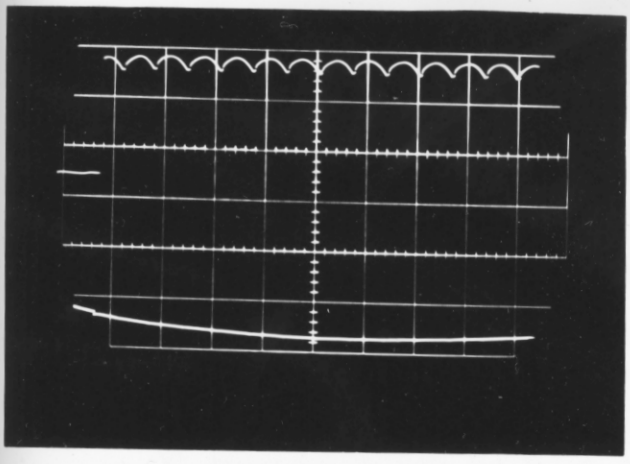

(a) NO FIELD

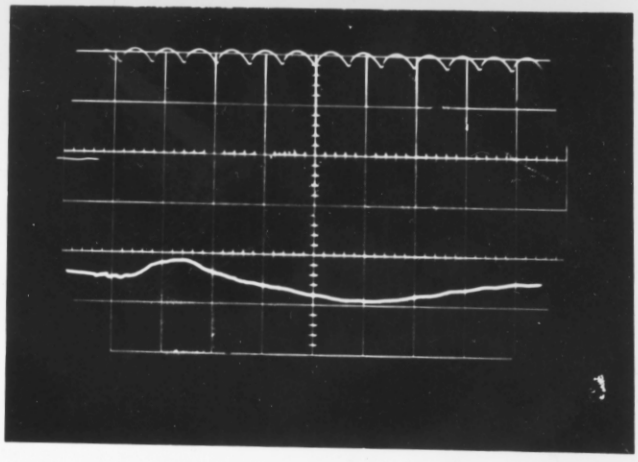

(b) FIELD ·325 WEBER / m^2
$\Lambda + N = \cdot 099$

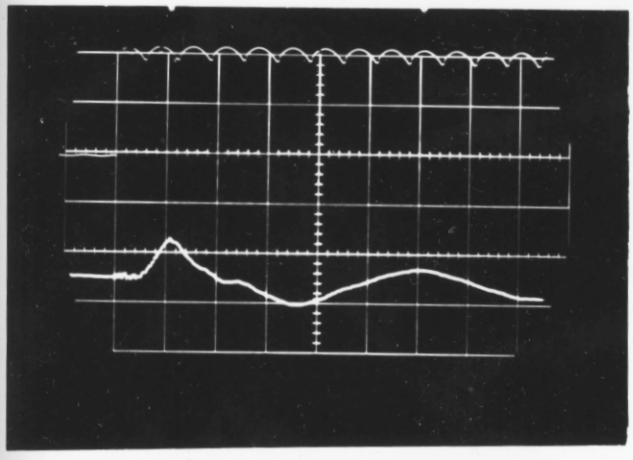

(c) FIELD ·487 WEBER / m^2
$\Lambda + N = \cdot 066$

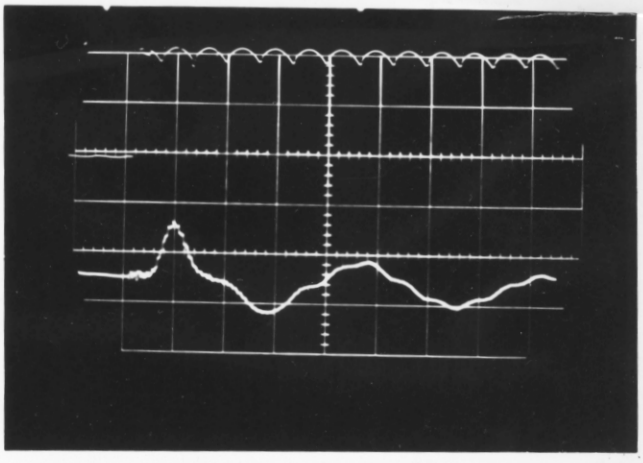

(d) FIELD ·650 WEBER / m^2
$\Lambda + N = \cdot 0495$

UPPER TRACE: CURRENT APPLIED TO THE EXCITING WINDING — SCALE: 10·4A / DIVISION] 10·4A

LOWER TRACE: e.m.f. INDUCED IN THE SEARCH WINDING — SCALE: 1mV DIVISION] 1mV

TIME SCALE: 5ms / DIVISION 5ms

in the exciting current, which caused no perceptible e.m.f. in the search winding, this frequency being sufficiently great for the field not to penetrate to the centre of the sodium. Even using screened leads to the oscilloscope of the shortest possible length, and well separated from the input leads, there was a small e.m.f. in the circuit containing the search winding. Possible sources of this pick-up were the magnetically operated switch and the DC main. It can be seen that the shapes of the traces are in good agreement with the shapes of the calculated curves. Because of the pick-up the traces could only be measured within a margin of error of about ± 10%.

Table 5.3

Comparison of measurements with calculations for the small search winding.

(a) field .325 weber/m^2.

Time ms	Calculated signal μV/A	Measured signal μV/A
9.2	19.1	17
27.6	-10.5	-11

(b) field .487 weber/m^2.

Time ms	Calculated signal μV/A	Measured signal μV/A
6.1	35.0	36
18.4	-20.3	-22
30.7	14.9	14

(c) field .650 weber/m^2.

Time ms	Calculated signal μV/A	Measured signal μV/A
4.6	54.3	51
13.8	-31.6	-30
23.0	23.8	19

Table 5.3 shows a comparison between typical measured values of e.m.f./unit exciting current and the calculated values at the instants approximately of peak e.m.f. It can be seen that the values agree within ± 10%.

Figure 5.23 shows the curves of e.m.f. against time calculated for the large search winding. In this case the curves are not continued to $t = 0$ because of the uncertainty introduced by the convergence difficulties. Figure 5.24 shows photographs of typical oscilloscope traces obtained in tests using the large search winding. The ripple in the exciting current caused, as can be seen, an appreciable ripple in the e.m.f. of the large search winding. The signals being large, any pick-up which there may have been was not important. Apart from the ripple the shapes of the traces are in good agreement with the shapes of the calculated curves. In this case because of the ripple the traces could again only be measured within a margin of error of about ± 10%. Table 5.4 shows a comparison between typical measured values and the calculated values. Again the values agree within ± 10%.

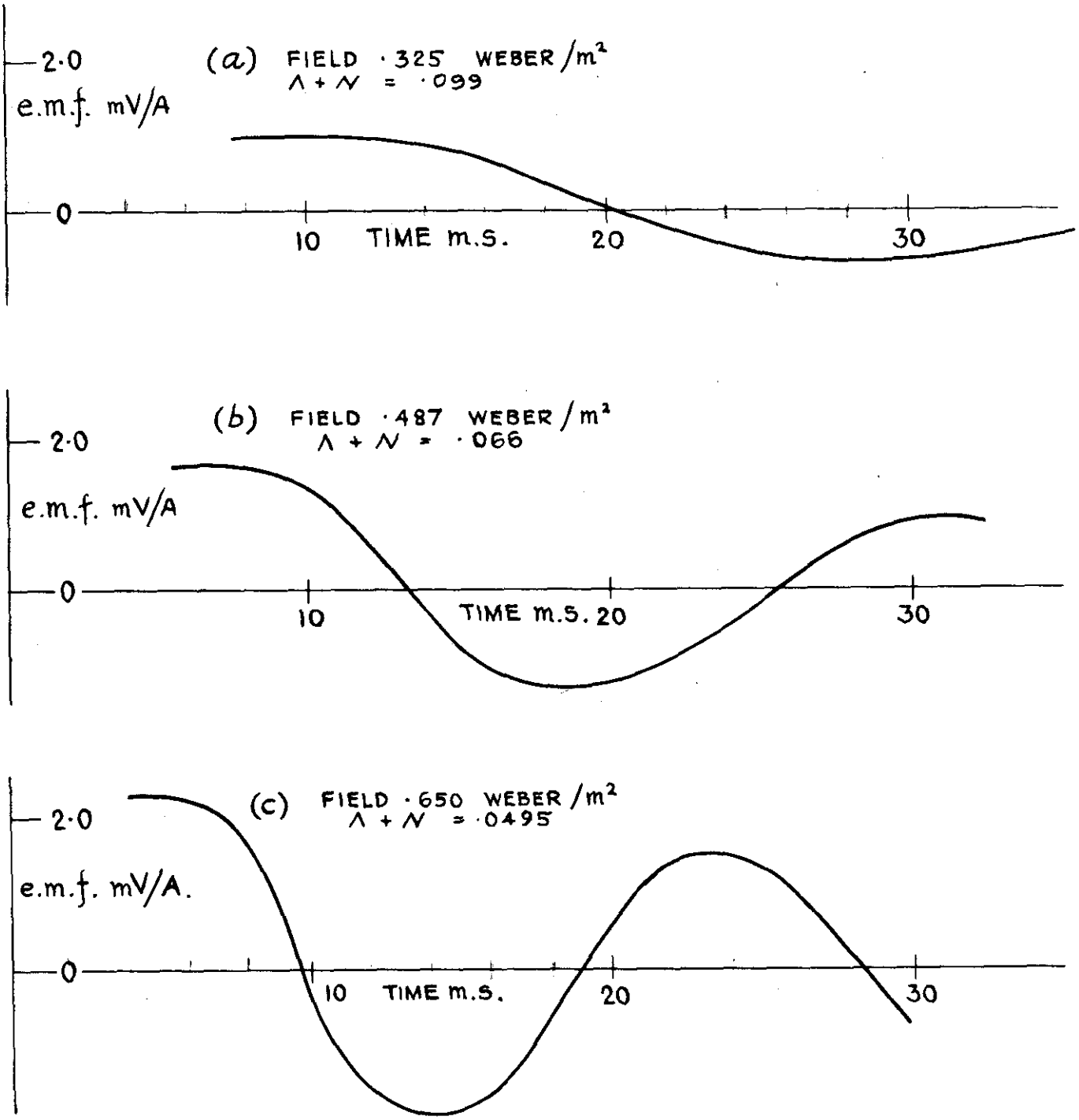

FIG. 5.23 INDUCED e.m.f/UNIT EXCITING CURRENT CALCULATED FOR THE LARGE SEARCH WINDING.

FIG. 5.24

TRANSIENT BEHAVIOUR RECORDED BY THE LARGE SEARCH WINDING

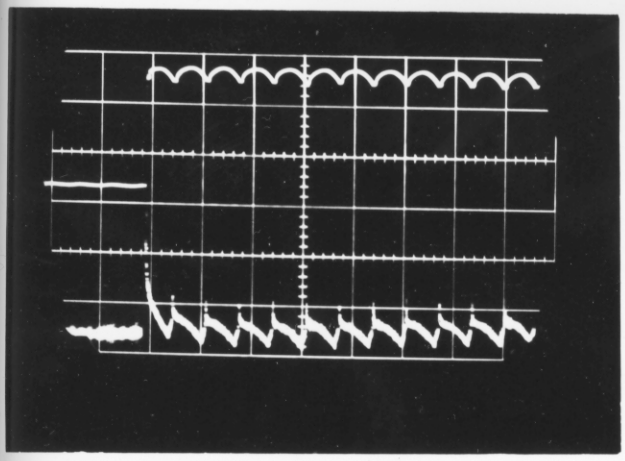

(a) NO FIELD

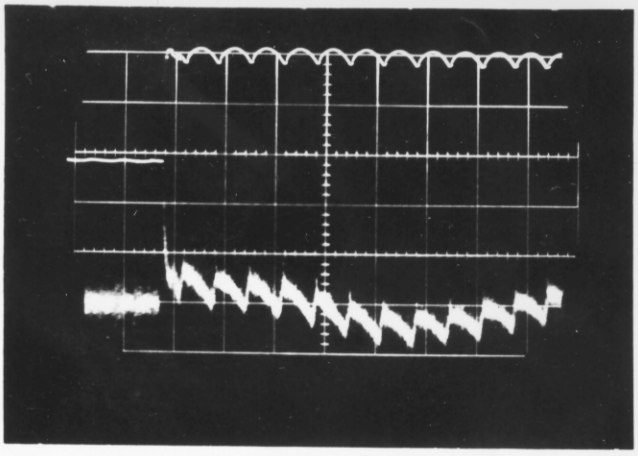

(b) FIELD ·325 WEBER / m^2
$\Lambda + N = \cdot 099$

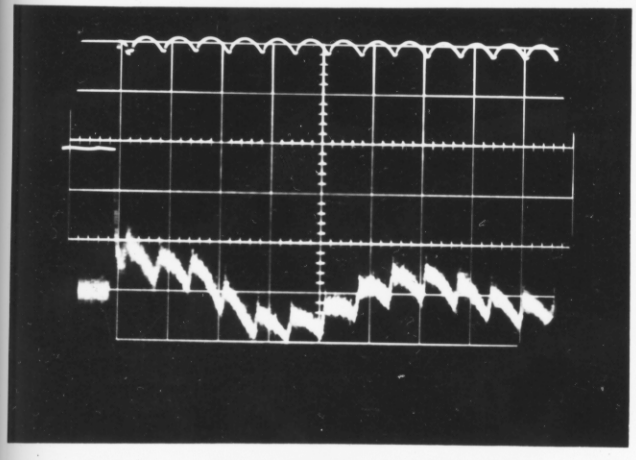

(c) FIELD ·487 WEBER / m^2
$\Lambda + N = \cdot 066$

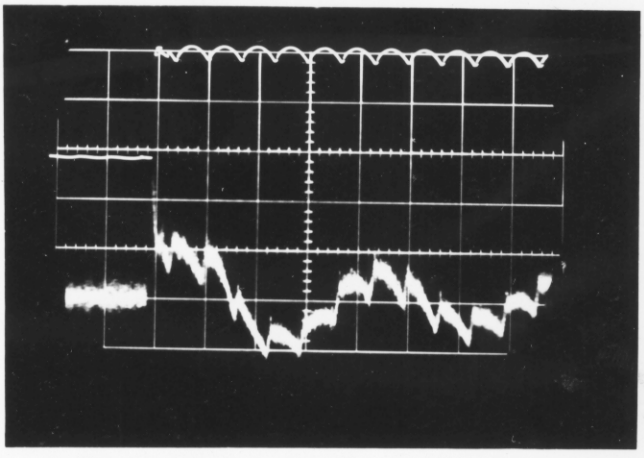

(d) FIELD ·650
$\Lambda + N = \cdot 0495$

UPPER TRACE: CURRENT APPLIED TO EXCITING WINDING —
SCALE: 10·4 A/DIVISION] 10·4A

LOWER TRACE: e.m.f. INDUCED IN SEARCH WINDING —
SCALE: 50mV/DIVISION] 50mV

TIME SCALE: 5ms/DIVISION 5ms

Table 5.4

Comparison of measurements with calculations for the large search winding.

(a) field .325 weber/m^2.

Time ms	Calculated signal mv/A	Measured signal mv/A
9.2	.99	.9
27.6	-.70	-.7

(b) field .487 weber/m^2.

Time ms	Calculated signal mv/A	Measured signal mv/A
6.1	1.62	1.5
18.4	-1.30	-1.2
30.7	.98	.9

(c) field .650 weber/m^2.

Time ms	Calculated signal mv/A	Measured signal mv/A
4.6	2.27	2.2
13.8	-1.93	-1.9
23.0	1.57	1.4

In both the tests using the small search winding and the tests using the large search winding the maximum disagreement between the measurements and the calculations was thus at about the limit of the observational error due to pick-up or ripple. Apart from ignoring the effects of viscosity and of the conducting walls the calculations were subject to the same errors in the assumed properties of sodium and the assumed magnetic field as the calculations for the steady state experiments.

With sharp wave fronts the casing of the small search coil might cause a disruption by interfering with the current sheets, but with well dispersed fronts it should not have caused a serious disturbance. The e.m.f. from the small search winding must have contained a component from the area enclosed by its leads inside the supporting stalk, which would reverse at each reflection of the waves, causing a small deflection of the oscilloscope beam at these instants. It is not likely however that any of these errors was as great as the observational error, which therefore probably masked the others.

CHAPTER 6.

EPILOGUE.

Magnetohydrodynamic waves can, then, be demonstrated. Without a demonstration it would be rash to assume too quickly that the waves can be found — when there is no damping the governing equations are wave equations, but the presence of terms representing resistive and viscous damping changes the order, and consequently the mathematical nature, of these equations.

The conclusions of a detailed analysis of the equations in situations where the state is steady are:-

1) There are two solutions of the equations, a wave mode and a boundary layer mode (3.2, page 18).

2) When λ and ν are sufficiently small the damping of the wave mode is determined by the sum $\lambda+\nu$. The higher resonances are more heavily damped than the fundamental. A first harmonic resonance is only possible if $\Lambda+N = \frac{\lambda+\nu}{cd} \sim .05$ or less (3.3, figures 3.3-3.7).

3) The nature of the resonant behaviour is critically affected by the ratio $\frac{\nu}{\lambda}$, which determines the relative amplitudes of the wave and boundary layer modes. With magnetic excitation magnification is only possible if $\lambda > \nu$, and is limited to at most $\frac{1}{2} = (\frac{\lambda}{\nu})^{\frac{1}{2}}$. In this case although ν may play a negligible part in the damping it is still liable to be important through its

effect on the excitation. If $\nu > \lambda$ there is diminution and the resonant frequencies are displaced. (3.3, figures 3.3 and 3.4). With mechanical excitation λ and ν exchange their roles.

4) When ν or $\lambda = 0$ the boundary layer mode disappears and the behaviour is truly wavelike (3.3, pages 22-23).

5) When $\lambda = \nu$ there is no resonance (3.3, pages 23-24). The varying amount of power taken in as the phase changes is then absorbed by the varying amplitude of the boundary layer mode. As $\lambda \rightarrow 0$ the boundary layer gets thinner so that the shear in it is sharper and the power absorbed is constant (3.4, page 32). The lack of a resonance even when $\lambda \rightarrow 0$ illustrates the way in which the presence of both types of damping completely alters the nature of the equations.

6) When there are side walls there is a region of shear of the transverse field and velocity near each side wall which is a source of additional damping. There is a sharp deterioration in performance if the ratio E of the section width to depth falls below 1 (3.7, page 44, figures 3.8 and 3.9). At resonance the regions of shear expand towards the centre (3.7, pages 44, 46, 47, figures 3.10 and 3.11).

7) In an axial system the ratio of external to internal radius has little importance (3.7, page 44, figures 3.12 and 3.13).

In transient situations it is difficult to obtain manageable mathematical expressions to represent the solution, there being difficulties of convergence except when ν or $\lambda = 0$. When ν or $\lambda = 0$ a series solution can be obtained in which each term has the form of a damped propagating wave (4.2, page 68). When $\lambda = \nu$ the series obtained is one in which the terms do not have this form (4.2, page 73). Again this illustrates the way in which the presence of both damping terms alters the nature of the equations.

The necessary conditions for a demonstration of the waves are:-

1) The right method of excitation must be used.

2) The total damping must be small enough.

3) The apparatus must have the right shape — Lehnert's apparatus did not.

Using an apparatus carefully designed to give optimum conditions the waves have been demonstrated with $\Lambda + N$ in the range .1 to .05. In steady state experiments the transverse field which would have been obtained in

empty space was found to be magnified by as much as 9 times at the fundamental resonance, and by as much as 1.5 times at the first harmonic resonance. In transient experiments a direct indication of the wave speed was obtained, and wave reflection was exhibited.

APPENDIX 1.

NUMERICAL CALCULATIONS.

Numerical calculations were carried out on the electronic calculating machine at the Mathematical Laboratory. Originally the decision was taken to use the machine because of the complexity of the formulae for plane and axial systems. However, the use of the machine in calculations for one-dimensional systems in a steady state also resulted in a considerable saving in time and increase in accuracy.

In the calculations for one-dimensional systems in a steady state the machine was simply programmed to calculate the analytical formulae exactly for given values of Λ, ν, X and P. This process required a few seconds, the answer being printed out correct to 5 figures.

In the calculations for plane and axial systems in a steady state the machine was programmed to sum the first 20 terms of the series expansion for each case. The advice of experts was that this would be quicker and more accurate than the use of a direct numerical method. In the calculations for axial systems it was necessary first to prepare a subroutine for the computation of the

Bessel functions $J_1(x)$ and $Y_1(x)$. Since the power series for these converge very slowly when x is large, the subroutine was arranged to switch to the use of asymptotic series when $x > 8$. The eigenvalues N were found as the zeros of $\mathcal{E}(Y_2)$ by trial and error, this requiring about 30 seconds. From this point the calculation of H and U for given values of $\wedge$, $\curlyvee$, X and Y could be repeated for a new frequency as often as was wanted in about 7 seconds for each calculation. For plane systems the sine terms were eliminated by taking $Y = 0$ as the centre line, and the first 20 cosine terms were summed. Calculation of the e.m.f. induced in the large search winding required knowledge of the average value of the transverse field through the section and this was obtained by summing the first 20 terms of the series, integrated term by term analytically.

As an indication of accuracy, the sum of the first 20 terms of the expansion

$$I = \sum \bar{I}_\epsilon \mathcal{E}_\epsilon$$

for a unit square wave in a plane case is accurate to 3.4% at the centre, and the sum of the first 20 cosine terms is accurate to 1.7%. Near resonance the rate of convergence of the full solution is greater than the

rate for I and the accuracy correspondingly greater. The programmes were checked by seeing that the answers satisfied the boundary conditions.

For calculations on transient waves in one-dimensional systems, again the first 20 terms of the series expansion were summed for each case.

For plane and axial systems, the double expansion was summed as far as the 20^{th} term of each component, making 400 terms in all. Calculation of the e.m.f. induced in the small and large search windings required knowledge of the time derivatives of both the transverse field at the centre and the average transverse field. To obtain the average the machine was programmed as in the steady state calculations to sum the series integrated term by term analytically, as far as the 20^{th} term of each component. Differentiation, however, created a difficulty, because term by term differentiation reduces the rates of convergence of the series, and they do not converge at all when $t = 0$. Results of calculations by summing the differentiated series were compared at the instants of peak e.m.f. with results obtained by differentiating the series numerically after summing them, and it was found that at the second and third peaks these agreed within 5%, but that at the

first peak there were discrepancies of up to about 15%. Numerical differentiation everywhere would have required calculation at an excessive number of points, so the curves presented were drawn from the results of calculations by summing the differentiated series, corrected at the peaks to the values given by numerical differentiation.

APPENDIX 2.

MEASUREMENTS RECORDED IN THE STEADY STATE TESTS.

Tables A 2.1 - A 2.3 give the results of the tests using the small search winding. Tables A 2.4 - A 2.6 give the results of the tests using the large search winding.

Table A 2.1

Field .325 weber/m^2; $\wedge + \vee$ = .099; small search winding.

Frequency c/s	Coupling mH	Phase difference o
19	195	75
22	265	62
24	345	42
25	395	30
26	410	15
27	410	0
28	390	-15
29	365	-30
30	310	-42
32	240	-57
34	190	-68
37	145	-77
40	115	-82
50	71	-92
60	64	-105
70	60	-140
81	55	-170
100	30	-400
120	18	-440

Table A 2.2

Field .487 weber/m^2; $\Lambda+N$ = .066; small search winding

Frequency	Coupling	Phase difference
c/s	mH	°
25	155	85
30	245	80
34	350	70
36	440	50
38	545	25
40	570	0
42	515	-25
44	405	-45
46	310	-60
50	205	-75
60	100	-85
80	72	-90
100	77	-120
110	88	-140
120	85	-170
130	68	-195
140	51	-215
160	33	-250
200	22	-315

Table A 2.3

Field .650 weber/m^2; $\Lambda+N$ = .0495; small search winding

Frequency	Coupling	Phase difference
c/s	mH	°
30	120	84
40	210	75
45	320	67
50	565	45
52	670	25
54	660	-3
56	590	-30
58	450	-52
60	330	-67
70	150	-80
100	69	-92
120	66	-105
146	95	-135
162	100	-173
178	70	-210
200	47	-245

Table A 2.4

Field .325 weber/m^2; $\Lambda+N = .099$; large search winding

Frequency c/s	Coupling μH	Phase difference o
19	25.0	75
22	27.1	68
24	29.2	55
25	30.9	47
26	32.0	37
27	31.5	25
28	30.4	12
29	26.6	0
30	21.2	-6
32	15.5	-10
34	11.1	-5
37	8.3	7
40	6.9	20
50	5.9	45
60	6.5	55
70	6.8	55
76	6.8	55
84	6.4	52
92	5.6	50
100	5.2	50
120	5.1	52
150	4.9	58

Table A 2.5

Field .487 weber/m^2; $\Lambda+N = .066$; large search winding

Frequency	Coupling	Phase difference
c/s	μH	o
25	22.2	85
30	25.1	75
38	40.7	40
40	41.6	20
44	28.8	-15
50	11.1	-25
60	5.1	10
80	5.2	55
100	6.5	60
120	6.8	50
130	5.8	42
140	5.1	45
160	4.7	52
200	4.35	55

Table A 2.6

Field .650 weber/m^2; $\Lambda+N$ = .0495; Large search winding

Frequency	Coupling	Phase difference
c/s	μH	o
30	20.5	85
40	26.8	78
45	34.8	70
50	43.6	48
52	48.0	33
54	49.2	13
56	44.6	-1
58	32.7	-25
60	24.4	-30
65	12.8	-33
70	7.3	-27
80	4.5	3
90	4.4	38
100	4.5	55
120	5.6	62
140	7.1	58
154	7.2	43
162	6.6	40
170	5.8	35
200	4.3	50

APPENDIX 3.

GENERAL ANALYSIS OF MAGNET DESIGN.

The factors underlying the design of an optimum magnet will here be considered. The magnets discussed will be assumed to have relatively deep air gaps $\sim \frac{1}{10}$, say, of the iron path, so that with a permeability ~ 1000, the reluctance of the iron path can be neglected compared with that of the air gap. The magnets will also be assumed to have uncooled coils and to be required to produce fields of such strength that, with the coil current density limited by the permissable rate of temperature rise, the coils will have considerable width. Then the iron shell size will be determined by the need to carry the waste flux across the coil width as well as the pole flux, and in order to restrict the coil width it is desirable that the coil should have the maximum possible height. This leads us to consider magnets with the configuration illustrated in figure A 3.1, in which the coil occupies the full depth between the shell bridge pieces, completely enclosing the air gap, and the analysis here will be confined to magnets of this type, though it could easily be extended to other configurations. The object will be to discover how the specific cost/unit volume of air gap depends on the geometry of the magnet, the overall size,

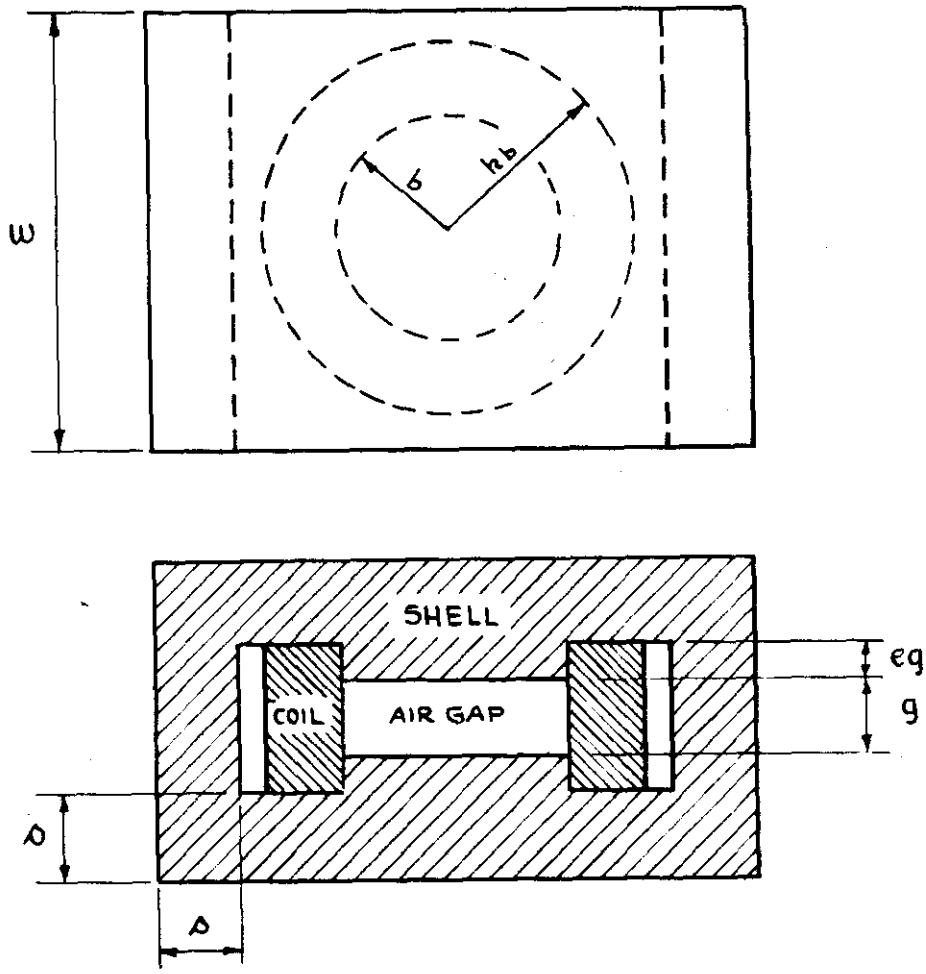

FIG. A.3.1 MAGNET SHAPE.

and the choice of material.

Let g be the gap depth and $b = cg$ be the gap radius to the inner face of the coil. Also let the outer radius of the coil be kb, and the saliency of the poles be eg, so that the total height of the coil is $(1 + 2e)g$, figure A 3.1. Then neglecting the iron reluctance, if H_a is the air gap field, j the mean current density through the coil area,

$$H_a g = j(k-1)b(1+2e)g$$

Also the air gap volume is

$$V_a = \pi b^2 g = \frac{\pi b^3}{c}$$

so

$$k-1 = \frac{1}{1+2e}\left(\frac{\pi}{c}\right)^{\frac{1}{2}} \frac{H_a}{V_a^{\frac{1}{3}} j}$$

The coil shape is thus determined by the parameters $\frac{H_a}{V_a^{\frac{1}{3}} j}$, c, and e, representing the current density, the gap shape, and the pole saliency respectively. If we consider a magnet to produce a field $B \sim 1$ weber/m^2 through a volume $\sim .05\ m^3$ with a current density $\sim 3\ 10^6$ A/m^2 corresponding to the requirements of this application

$$\frac{H_a}{V_a^{\frac{1}{3}} j} \sim .8 .$$

Next the ratio of the total flux to the pole flux, assuming the field declines linearly across the width

of the coil, figure A 3.2, is found by integration

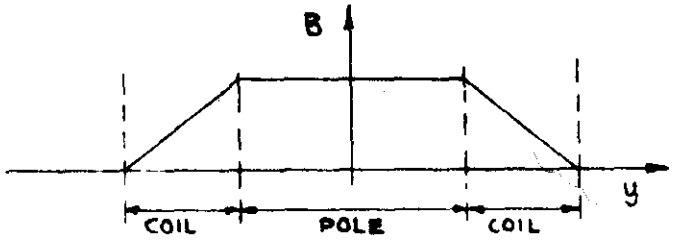

Fig. A 3.2

to be

$$n = \frac{k^2 + k + 1}{3} .$$

Now choose the iron shell section area to be just large enough to cause no flux concentration. Then if s is the shell thickness, ω its width,

$$2s\omega \geq n\pi b^2 ,$$

since the flux divides between the two sides.

Also where the flux lines bend as they come out of the pole face, figure A 3.3, it is necessary that the cylindrical area $2\pi sb$ through which they pass shall be not less than the pole area πb^2, or that

$$2s \geq b$$

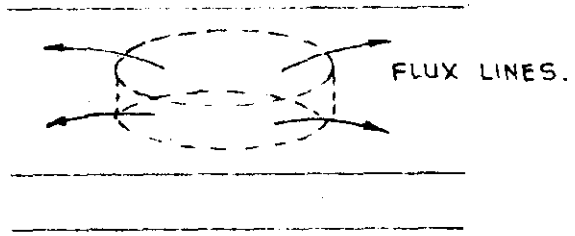

Fig. A 3.3

Take

$$s = .75\ b, \quad \omega = \frac{n\pi b}{1.5} = 2.09\ nb\ .$$

Then since

$$\frac{k}{n} < 1$$

$$\omega > 2.09\ kb$$

and the shell is always wide enough to cover the coil. Finally choose a length for the bridge pieces of $2(k+1)b$, leaving a clearance each side of $.25\ b$, since $s = .75\ b$, round which the outside flux lines should be able to turn quite easily. The magnets will now be geometrically similar not only in their coils but also in their shells for given values of $\frac{H_a}{V_a^{\frac{1}{3}} j}$, c, and e.

The winding and shell volumes can accordingly be expressed in terms of the air gap volume.

The winding volume is

$$V_\omega = \pi(k^2-1)b^2(1+2e)g$$

so

$$\frac{V_\omega}{V_a} = (k^2-1)(1+2e)$$

The shell volume, allowing for the projecting poles, is

$$V_s = (2\pi(1+2e) + 4(k+1)b)\ s\omega + 2eV_a$$

so

$$\frac{V_s}{V_a} = (1 + 2e + 2e(k+1))\ n + 2e$$

It is now possible to determine the cost for a given air gap volume simply by multiplying the winding and shell volumes by the price/unit volume of whatever materials may be used. The results are presented in Tables A 3.1-A 3.3 of calculations on these principles for a family of magnets. The shell material is taken as ordinary mild steel at a cost of £.05/kg, or £.39/1000 cm^3. For the winding both copper at a price of £.5/kg or £4.45/1000 cm^3, and aluminium at a price of £.5/kg or £1.35/1000 cm^3, are considered. The ratio of the actual volume of conductor to the total winding volume is assumed to be .75. The tables each show, for a particular value of the pole saliency parameter e, how the winding radius ratio k, the ratio of total to used flux n, the ratio of winding volume to air gap volume, the ratio of shell volume to air gap volume, and the cost/unit volume of air gap either with a copper or with an aluminium winding, depend on the current density parameter $\frac{H_a}{V_a^{\frac{1}{3}} j}$ and the gap shape parameter c. The rapid increase of cost as the value of $\frac{H_a}{V_a^{\frac{1}{3}} j}$ is increased, or the value of j decreased, is obvious. The gap shape, on the other hand, is comparatively unimportant, the smaller coil volume resulting from the use of a flat shape being balanced by the larger shell size required.

The use of increasing saliency reduces the cost by allowing a narrower coil with less waste flux. However,

Table A 3.1 : e = 0.

Values of k for values of c and $\frac{H_a}{V_a^{\frac{1}{3}} j}$:

(c) \ $\frac{H_a}{V_a^{\frac{1}{3}} j}$	.5	1	1.5
1	1.73	2.47	3.20
1.5	1.64	2.28	2.92
2	1.58	2.16	2.74

Values of n:

c \ $\frac{H_a}{V_a^{\frac{1}{3}} j}$	.5	1	1.5
1	1.91	3.17	4.80
1.5	1.79	2.80	4.14
2	1.70	2.59	3.75

Values of $\frac{V_w}{V_a}$:

c \ $\frac{H_a}{V_a^{\frac{1}{3}} j}$	.5	1	1.5
1	1.98	5.08	9.20
1.5	1.68	4.08	7.50
2	1.48	3.65	6.48

Values of $\frac{V_s}{V_a}$:

c \ $\frac{H_a}{V_a^{\frac{1}{3}} j}$	.5	1	1.5
1	12.3	24.8	45.2
1.5	15.9	30.3	53.2
2	19.2	35.4	59.8

Values of $\frac{cost}{V_a}$, £/1000 cm^3 — copper:

c \ $\frac{H_a}{V_a^{\frac{1}{3}} j}$	.5	1	1.5
1	10.9	26.8	48.9
1.5	11.8	26.2	46.3
2	12.5	26.4	43.6

Values of $\frac{cost}{V_a}$, £/1000 cm^3 — aluminium:

c \ $\frac{H_a}{V_a^{\frac{1}{3}} j}$	.5	1	1.5
1	6.9	15.0	27.5
1.5	7.9	16.2	28.8
2	9.2	17.9	30.5

Table A 3.2 ; e = .25.

Values of k:

(c) \ $\left(\frac{H_a}{V_a^{\frac{1}{3}}}\right)$	.5	1	1.5
1	1.49	1.98	2.47
1.5	1.43	1.86	2.29
2	1.39	1.78	2.17

Values of m:

(c)	.5	1	1.5
1	1.58	2.30	3.17
1.5	1.50	2.11	2.82
2	1.44	1.99	2.61

Values of $\frac{V_w}{V_a}$:

(c)	.5	1	1.5
1	1.82	4.38	7.64
1.5	1.56	3.67	6.33
2	1.39	3.22	5.55

Values of $\frac{V_s}{V_a}$:

(c)	.5	1	1.5
1	10.7	17.6	27.3
1.5	13.6	21.7	32.6
2	16.4	25.6	37.5

Values of $\frac{cost}{V_a}$,
£/1000 cm^3 — copper:

(c)	.5	1	1.5
1	10.4	21.5	36.5
1.5	10.6	21.0	34.2
2	11.2	21.0	33.5

Values of $\frac{cost}{V_a}$,
£/1000 cm^3 — aluminium:

(c)	.5	1	1.5
1	6.2	11.4	18.6
1.5	7.1	12.3	19.4
2	8.1	13.5	20.5

Table A 3.3 : e = .5.

Values of k:

(c) \ $(\frac{H_a}{V_a^{\frac{1}{3}}})$	.5	1	1.5
1	1.37	1.73	2.09
1.5	1.32	1.64	1.96
2	1.29	1.58	1.87
2.5	1.27	1.54	1.81

Values of n:

	.5	1	1.5
1	1.41	1.91	2.49
1.5	1.36	1.79	2.26
2	1.32	1.70	2.12
2.5	1.29	1.65	2.02

Values of $\frac{V_w}{V_a}$:

	.5	1	1.5
1	1.74	3.96	6.75
1.5	1.48	3.36	5.66
2	1.32	2.98	4.98
2.5	1.21	2.72	4.52

Values of $\frac{V_s}{V_a}$:

	.5	1	1.5
1	10.5	15.3	21.3
1.5	13.2	18.8	25.6
2	15.7	21.9	29.5
2.5	18.2	24.9	33.4

Values of $\frac{cost}{V_a}$, £/1000 cm^3 — copper:

	.5	1	1.5
1	10.1	19.4	31.1
1.5	10.3	18.8	29.2
2	11.3	19.2	28.4
2.5	11.3	19.2	28.4

Values of $\frac{cost}{V_a}$, £/1000 cm^3 — aluminium:

	.5	1	1.5
1	5.9	10.1	15.2
1.5	6.7	10.8	16.0
2	7.5	11.6	16.8
2.5	8.5	12.6	17.7

since refraction causes the lines of force to leave the iron almost at right angles, with a completely flat face the field will be everywhere vertical as if the coil were a slice of a long solenoid, with the field correspondingly uniform. With a salient pole on the other hand, there will be fringing, with a consequent loss of uniformity of the field. To make a true comparison therefore, it is necessary to find the true usable volume under the pole faces. An analysis by Carter[12] for a two dimensional case using a Schwarz Christoffel transformation, suggests that the field will start to fall off more than about 1.5% at a distance of about one gap width in from the edge of a very salient pole, or at a distance about equal to the saliency for a slightly salient pole. Taking it that this degree of uniformity is desired, so that only the region inside this limit can be used, the usable volume is

$$V_u = V_a \left(\frac{b-e}{b}\right)^2 = V_a \left(1 - \frac{e}{c}\right)^2.$$

Tables A 3.4 and A 3.5 show the costs of magnets with salient poles re-expressed in terms of this usable volume for different values of the shape parameter $c-e$ of the usable region. It can now be seen that the advantage lies with the flat faced design, which is also the simplest. For example with $\frac{H_a}{V_a \frac{1}{2} J} = 1.0$, $c = 1.5$ the costs/1000 cm^3.

Table A 3.4 : e = .25.

Values of $\frac{cost}{V_u}$, £/1000 cm^3 — copper:

(c-e) \ $(\frac{H_s}{V_a^{\frac{1}{3}}})$	.5	1	1.5
.75	18.5	37.4	65.0
1.25	15.3	30.2	49.1
1.75	14.3	26.9	43.6

Values of $\frac{cost}{V_u}$, £/1000 cm^3 — aluminium:

(c-e) \ $(\frac{H_s}{V_a^{\frac{1}{3}}})$	.5	1	1.5
.75	10.8	20.3	33.1
1.25	10.1	17.9	27.7
1.75	10.2	17.2	26.4

Table A 3.5 : e = .5.

Values of $\frac{cost}{V_u}$, £/1000 cm^3 — copper:

	.5	1	1.5
1	23.2	42.4	65.6
1.5	19.0	33.3	50.5
2	17.6	30.0	44.3

Values of $\frac{cost}{V_u}$, £/1000 cm^3 — aluminium:

	.5	1	1.5
1	15.1	24.3	36.0
1.5	13.3	20.7	29.9
2	13.2	19.6	27.8

with copper windings for $\epsilon = 0$, .25 and .5 are about £26, £28 and £33. If a less strictly uniform field were required or the current density was lower, the conclusion would be different.

Finally there remains the question of whether to use copper or aluminium for the winding. For a valid comparison the current densities must be chosen to give equal rates of heating. Now the resistivity of copper at 20°C is $1.73\ 10^{-8}$m, and its specific heat $3.40\ 10^{6}$ Joules/m^3 °C, whereas the resistivity of aluminium is $2.75\ 10^{-8}$m and its specific heat $2.45\ 10^{6}$ Joules/m^3 °C. For copper at a current density j A/m^2 for the whole coil, allowing a ratio of conductor area to total area of .75, the heating rate at 20°C is therefore

$$\theta = 1.21\ 10^{-14}\ j^2\ ^{\circ}C/s$$

and for aluminium the rate is

$$\theta = 2.1\ 10^{-14}\ j^2\ ^{\circ}C/s.$$

For each material similar magnets are obtained for the same value of $\frac{H_a}{V_a^{\frac{1}{3}}\ j}$, and therefore for the same value of $\frac{\theta\ V_a^{\frac{1}{3}}}{H_a^2}$. Figure A 3.4 shows how the cost and the heating rate expressed as $\frac{\theta\ V_a^{\frac{1}{3}}}{H_a}$ vary with $\frac{H_a}{V_a^{\frac{1}{3}}\ j}$ for a flat faced magnet with a gap radius 1.5 times the gap depth. For

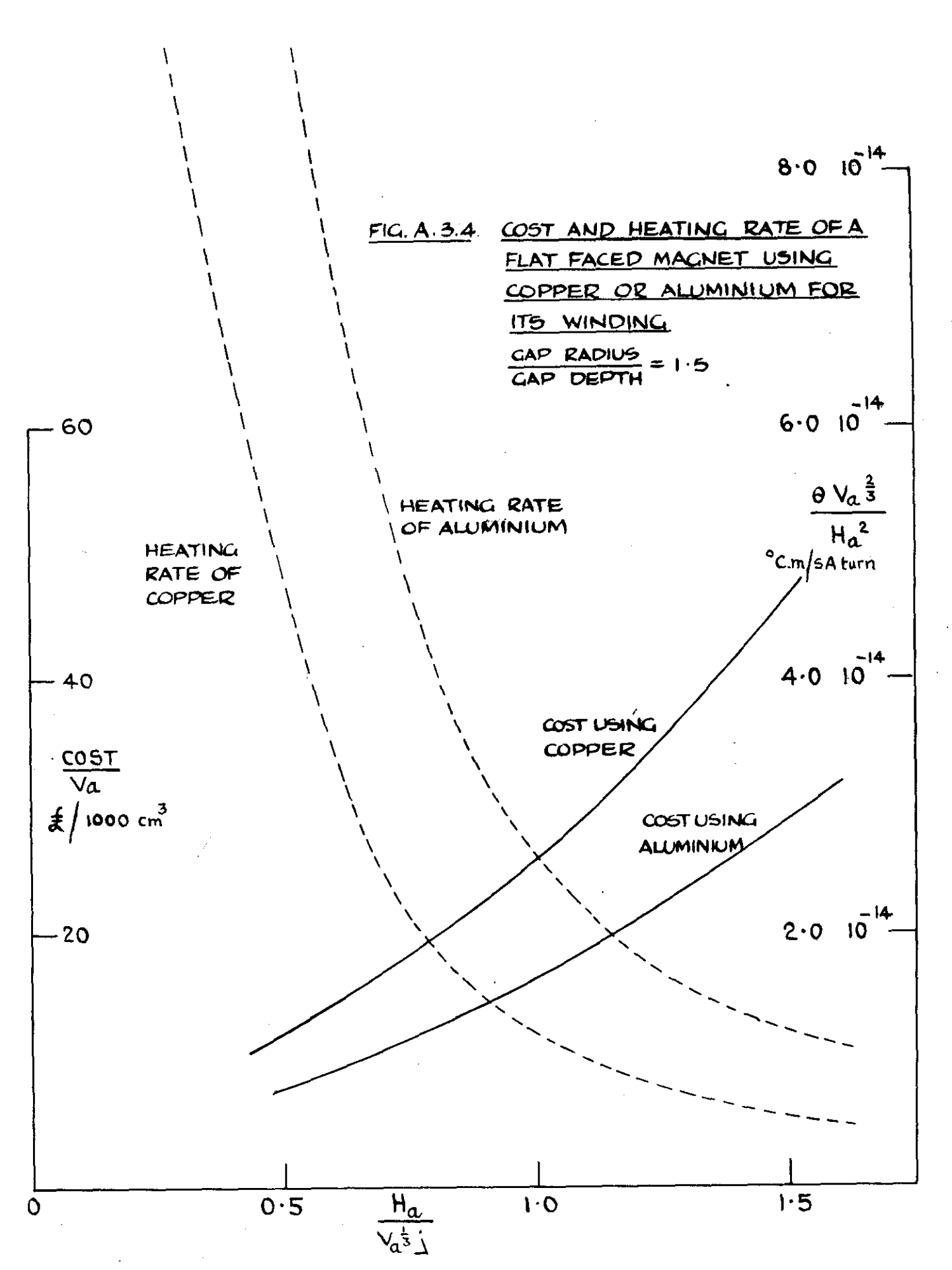

FIG. A.3.4 COST AND HEATING RATE OF A FLAT FACED MAGNET USING COPPER OR ALUMINIUM FOR ITS WINDING

$\frac{\text{GAP RADIUS}}{\text{GAP DEPTH}} = 1.5$

equal heating rates it can be seen that the costs of magnets with copper and aluminium windings are almost equal.